Self-Similar Rupture of Thin Liquid Films with Slippage

DISSERTATION

zur Erlangung des akademischen Grades
doctor rerum naturalium
(Dr. rer. nat.)
im Fach Mathematik

eingereicht an der
Mathematisch-Naturwissenschaftlichen Fakultät II
Humboldt-Universität zu Berlin

von
Herrn Dirk Peschka
geboren am 21.11.1977 in Zossen

Präsident der Humboldt-Universität zu Berlin:
Prof. Dr. Christoph Markschies

Dekan der Mathematisch-Naturwissenschaftlichen Fakultät II:
Prof. Dr. Wolfgang Coy

Gutachter:

1. Priv. Doz. Dr. Andreas Münch
2. Prof. Dr. Barbara Niethammer
3. Priv. Doz. Dr. Lutz Recke

Tag der mündlichen Prüfung: 30. Oktober 2008

Danksagung

Ich bedanke mich sehr herzlich bei Andreas Münch und Barbara Niethammer für die Möglichkeit, mit einem sehr interessanten Thema in der angewandten Analysis Fuss zu fassen. Ihre hilfreichen Bemerkungen und kritischen Anmerkungen haben mir oft weitergeholfen.

Mein Dank gilt auch allen Studenten und allen Mitgliedern des Graduiertenkollegs *Analysis, Numerics, and Optimization of Multiphase Problems*, die für eine angenehme und produktive Arbeitsatmosphäre gesorgt haben. Insbesondere möchte ich mich bei Sebastian Heinz, Thomas Surowiec und Georgy Kitavtsev für unsere vielen wissenschaftlichen Diskussionen bedanken.

Weiterhin danke ich Konstantina Kostourou and Ralf Seemann für die sehr gute wissenschaftliche Zusammenarbeit und für die Tatsache, dass ich einige ihrer experimentellen Ergebnisse in meiner Arbeit zeigen darf.

Nicht zuletzt gilt mein Dank der Deutschen Forschungsgemeinschaft, durch deren finanzielle Unterstützung diese Arbeit ermöglicht wurde.

Abstract

In this dissertation the formation of interfacial singularities of fluid surfaces is studied. Starting with a discussion of the most important physical effects, a two-dimensional model, which includes physical effects such as surface tension, intermolecular forces, and Navier-slip boundary conditions, is constructed. By applying symmetry assumptions and a reduction formalism[1] this model can be simplified into the following set of partial differential equations:

$$\begin{aligned}\partial_t h + (hu)_x &= 0,\\ \Re(\partial_t u + uu_x) &= \frac{4}{h}(hu_x)_x - (\varphi(h) - h_{xx})_x - \frac{1}{b}\,\frac{u}{h},\end{aligned}$$

the so-called strong-slip equations (SSE). The function h in that equation describes the thickness of the thin liquid film and u is the averaged velocity. These equations non-dimensional slip-length b as one parameter.

Slip refers to the possibility that the continuous velocity field of the fluid still has a non-zero value at a fluid–solid interface, i.e., fluid particles do not get stuck on the interface. Deviations from the no-slip condition, where the velocity at the interface is set to zero, are usually observed in microfluidic experiments on hydrophobic substrates at length scales of several hundred nanometers (Lauga et al. 2006).

In this thesis the onset of singularities is studied in different ways. First a linearization of the SSE is computed and a long-wavelength instability is found. Then a numerical scheme, which is used to study the non-linear behavior of solutions to the SSE, is proposed and discussed in some detail. A characteristic feature of the numerical finite-difference scheme is the high spatial resolution due to the non-uniformity of the computational meshes. This property allows us tracking of solutions close to a singularity. Similar studies have been performed without slip by Miksis (1996) and Vaynblat (2001).

Finally the SSE is further simplified and important properties of the rupture process are proven for a simplified equation. The procedure employed here is similar to previous work by Papageorgiou (1995) or Renardy (2001). Their results are generalized.

The simplification procedure mentioned before allows us to establish a connection to LSW models of Ostwald ripening and to study properties of self-similar solutions such as the non-existence proof in the paper by Niethammer and Pego (1999).

---

[1] Namely, the long-wavelength approximation also known as the lubrication approximation or the slender-body theory.

The main results found in this thesis are:

- The effect of slippage is studied systematically with respect to singularity formation and transient self-similar solutions.
- A numerical scheme that allows following the growth of physical singularities over many orders of magintude (in h) is developed.
- The singularity formation is studied in a rigorous mathematical way. For example it is proven that singularities form within a finite time, their shape is characterized, and convergence to self-similar solutions is proven.

Zusammenfassung

In der vorliegenden Arbeit wird das Entstehen von Singularitäten an Oberflächen von dünnen Flüssigkeitsfilmen studiert. Unter einer Singularität versteht man hier das plötzliche und schnelle Aufreißen einer Flüssigkeitsoberfläche.

Nach einer Diskussion wichtiger physikalischer Phänomene, wird ein zweidimensionales Modell zur Beschreibung von Flüssigkeitsfilmen hergeleitet. Dieses Modell beinhaltet neben der allgemeinen Dynamik von Flüssigkeiten weiterhin die Oberflächenspannung von Grenzflächen, van der Waals Kräfte zwischen Flüssigkeit und einem Trägersubstrat und die Navier-slip Randbedingung (Schlupf-Randbedingung) zwischen Substrat und Flüssigkeit. Auf dieses Modell wendet man einen Reduktionsformalismus an (dt. Schmierfilmmodelle) und erhält die Differentialgleichungen

$$\begin{aligned} \partial_t h + (hu)_x &= 0, \\ \Re(\partial_t u + u u_x) &= \frac{4}{h}(h u_x)_x - (\varphi(h) - h_{xx})_x - \frac{1}{b}\,\frac{u}{h}. \end{aligned}$$

Sie sind unter dem Namen *strong-slip* Gleichungen (SSG) bekannt (siehe z.B. Münch et al. 2005, *J. Eng. Math.*). Die Gleichungen beschreiben die zeit- und ortsabhängige Dicke eines dünnen Filmes h und eine mittlere Geschwindigkeit von Flüssigkeitspartikeln u. Das Modell SSG enthält unter anderem die Schlupf-Länge (*slip-length*) b als Parameter.

Unter *Schlupf* versteht man in diesem Kontext, dass die Flüssigkeit am Rand zum Substrat eine von Null verschiedene Geschwindigkeit hat, d.h. sie haftet *nicht* an der Grenzfläche zum Substrat. Abweichungen von der *no-slip* Bedingung — hier haftet die Flüssigkeit am Substrat — werden zumeist im Nano- und Mikrometerbereich bei Experimenten mit Flüssigkeiten auf hydrophoben Oberflächen beobachtet (Lauga et al. 2006, *Handbook of Experimental Fluid Mechanics*).

In dieser Dissertation werden verschiedene Ansätze verfolgt, um die Singularität der Flüssigkeitsoberfläche zu beschreiben. Der Entstehungsprozess der Singularität wird durch die Linearisierung der Gleichung SSG beschrieben. Da die Linearisierung schnell ihre Gültigkeit verliert, wird das nichtlineare Verhalten der Singularität mit einem numerischen Verfahren beschrieben. Das dazu hier konstruierte Finite-Differenzen-Schema besitzt eine hohe räumliche und zeitliche Genauigkeit. Dadurch kann das Verhalten der Singularität über viele Größenordnungen beschrieben werden. Für verwandte Modelle existieren ähnliche Untersuchungen von Miksis et al. (1996, *Appl. Math. Lett.*) und Vaynblat et al. (2001, *European J. Appl. Math.*), jedoch unter Vernachlässigung von Schlupf.

Im zweiten Teil der Arbeit wird die Gleichung SSG weiter vereinfacht, was es uns erlaubt qualitative Eigenschaften der Singularitätsentstehung zu beweisen. Bei der Analyse der Singularitäten gehen wir wie Papageorgiou (1995, *Phys. Fluids*) und Renardy (2001, *Z. Angew. Math. Phys.*) vor, verallgemeinern jedoch deren Ansatz von Flüssigjets auf dünne Filme. Die Vereinfachung von SSG erlaubt es weiterhin eine Verbindung zu Modellen der Ostwald-Reifung herzustellen und Untersuchungen zu selbstähnlichen Lösungen wie im Paper von Niethammer und Pego (1999, *J. Statist. Phys.*) durchzuführen.

Die neuen Ergebnisse der vorliegenden Forschungsarbeit sind vor allem ...

- die systematische Studie, wie Schlupf (Navier-slip Bedingung) die Singularitätenbildung beeinflusst. Das wird detailliert am Beispiel der *strong-slip Gleichung* SSG diskutiert.
- die Entwicklung eines numerischen Verfahrens, mit dem Singularitäten über viele Größenordnungen verfolgt werden können. Das Verfahren erlaubt, gezielt Übergänge zwischen verschiedenen Regimen selbstähnlicher Lösungen zu untersuchen.
- eine mathematisch strenge Untersuchung der Entstehung von Singularitäten anhand eines vereinfachten Modells. Es wird bewiesen, dass die Singularitäten in endlicher Zeit entstehen und für geeignete Anfangsdaten gegen selbstähnliche Lösungen konvergieren.

Contents

List of Figures **xi**

List of Tables **xiii**

1 Introduction **1**
- 1.1 Applications and Experiments in Microfluidics 2
- 1.2 Liquid Films on Substrates, Liquid Jets, and Free Liquid Films 4
- 1.3 Outline of the Thesis 8

2 Modeling **11**
- 2.1 Equations in the Fluid 12
- 2.2 Discussion of Boundary Conditions 15
- 2.3 Role of Slippage 16
- 2.4 London–van der Waals Interaction 20
- 2.5 Full Model 22
- 2.6 Lubrication Models and Scalings 23
- 2.7 Lubrication Model with Cylindrical Symmetry 27

3 Numerical Analysis of Thin-Film Rupture **33**
- 3.1 Motivation 34
- 3.2 Strong-Slip Equation with Finite Differences 35
- 3.3 Solver for the Nonlinear Equation 38
- 3.4 Linear Stability of the Flat State 42
- 3.5 Numerical Solutions and Self-Similarity 45
- 3.6 Reduction to Ordinary Differential Equations 59
- 3.7 Summary 63

4 Analysis of a Simplified Thin-Film Model **67**
- 4.1 Simple Examples and Properties 68
- 4.2 Thin-Film Rupture after Finite Time 74
- 4.3 Jet Pinch-Off after a Finite Time 78
- 4.4 Definition of Similarity Solutions 80
- 4.5 Similarity Equations and Solutions 84
- 4.6 Exact Self-Similar Solution 86

4.7 Convergence to Self-Similar Solutions 99
4.8 Summary 110
4.9 Motivation 111
4.10 Simplification of the Strong-Slip Model 112

5 Summary and Outlook 117
5.1 Summary 118
5.2 Thin Films on Elastic Substrates 119
5.3 Extension to LSW Models 130

Bibliography 135

List of Figures

1.1 Experimental dewetting patterns 3
1.2 Sketch of the thin film geometry 5
1.3 Experimental dewetting dynamics 6
1.4 Sketch of a liquid jet 7

2.1 Detailed sketch of thin-film geometry 12
2.2 Idealized flow profiles near boundary 18
2.3 Experimental mass flows 20
2.4 Layered dielectric system 21
2.5 Sketch of domain with cylindrical symmetry 28

3.1 Sketch of a staggered grid 36
3.2 Difference star for the strong-slip equation 39
3.3 Numerical solution on a uniform mesh 40
3.4 Numerical solution on a non-uniform fixed mesh 41
3.5 Comparison with linearization 45
3.6 Numerical solution on adaptive mesh 46
3.7 Dynamics of $\min_x h(t,x)$ 47
3.8 Different numerical solution of strong-slip eqn. 54
3.9 Rescaled solution of strong-slip eqn. 55
3.10 Solution of strong-slip eqn. with $\Re = 10^{-5}$, $b = 10^{-8}$ 56
3.11 Similarity scales for $\Re = 0$ 58
3.12 $H_0 - \beta$ phase plane 63

4.1 Numerical solutions of integro-differential eqn. 70
4.2 Comparison of self-similar solution with exact sol. 90
4.3 K^* as a function of K 91
4.4 K^* hyperplane as a function of K and γ 97
4.5 Cantor-function 107
4.6 Scale transformation for Cantor-function 108
4.7 No convergence for Cantor-function 109
4.8 Illustration of Eulerian/Lagrangian coordinates 113

5.1 Sketch of experiment with viscoelastic substrate 120

5.2 Stability analysis with viscoelastic substrate 125
5.3 Rupture on viscoelastic substrate 126
5.4 Dynamics of rupture on viscoelastic substrate 127
5.5 Dewetting dynamics with repulsive forces 127
5.6 Droplet on viscoelastic substrate 128
5.7 Droplet on viscoelastic substrate (experiment) 129
5.8 Droplet on viscoelastic substrate (experiment) 129
5.9 Dewetting rims (experiment) 130

List of Tables

3.1 All possible similarity scales 52
3.2 Similarity scales from PDE computations 53
3.3 Different similarity scales of strong-slip eqn. 56
3.4 Similarity scales for $\Re = 0$ 57
3.5 Similarity scales for different L, initial data, parameter 59
3.6 Exponents for different self-similar solution 64

Chapter 1

Introduction

1.1 Applications and Experiments in Microfluidics

Nano- and microfluidics are branches of applied sciences that combine topics from physics, biology, medicine, chemistry, material sciences, and mathematical modeling. Scientists and engineers from these fields seek to understand and control fluids that are bound to microscopically small devices in domains with typical extensions between $10^{-9}\,m$ and $10^{-3}\,m$.

The perception of a macroscopic fluid, which can be described by the incompressible Navier-Stokes equations with gravitational force and no-slip boundary condition at solid–liquid interfaces only, is usually inadequate on microscopic length scales. Nevertheless, it is often assumed that the fluid can be approximated as a continuous medium with complex properties.

For example, one finds that the fluid exhibits complex rheological properties like shear thinning, shear thickening, more complex intermolecular interactions, or slippage at liquid–solid interfaces. Popular examples for the so-called *complex fluids* are polymer melts[1], liquid crystals, emulsions, and liquid metals.

Modern applications, such as the development of Lab-on-a-chip devices, fuel cells, and liquid crystal displays, have drawn much attention to microfluidics [1, 2]. Many recent advances in this field are due to the refinement of experimental methods and measuring devices for microscopic length scales, e.g., the invention of the atomic force microscope and the development of new materials. Applications and experiments in microfluidics are often performed with fluids that have freely movable interfaces. We shortly examine two examples from engineering and science which show how important it is to understand and control these moving interfaces.

First, consider the engineering of a thin film by the spin-coating method[2] where small amounts of liquid are placed on the center of a flat rotating substrate and are distributed by centrifugal forces. When the average thickness of the liquid has decreased down to a certain desired value, typically several nano- or micrometers, the spinning is stopped. The goal of this procedure is to spread the liquid material uniformly such that the thickness of the fluid film is constant across the substrate. Similar applications appear in coating, printing, painting, and lubrication processes and in most cases it is imperative to prevent thin liquid films from rupturing. The term *rupture* denotes a change of the topology of the domain occupied by the liquid, e.g., formation of holes or separation into several parts. In order to control this process one has to understand the hydrodynamic stability of fluids and the stability of their free interfaces.

The second example is from the paper *Spinodal Dewetting in Liquid Crystal and Liquid Metal Films* [4] of Herminghaus et al. In their experiment

---

[1] such as polymethylmethacrylate (PMMA), polystyrene (PS), polydimethylsiloxane (PDMS)

[2] For a review on the theory of spin-coating see Oron et al. [3] in Chapter II.K.

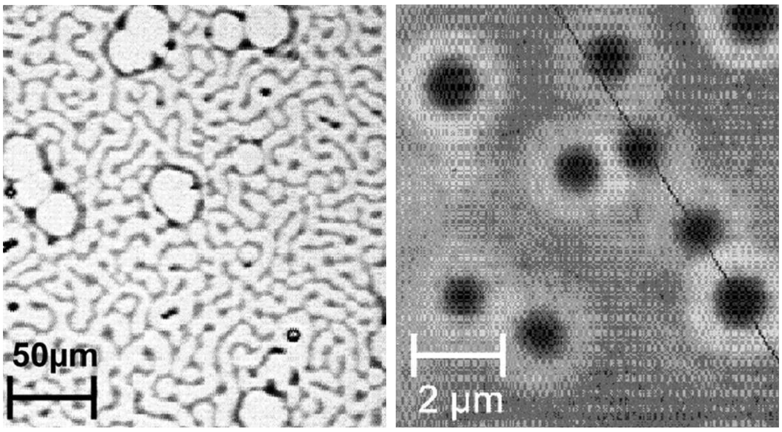

Figure 1.1: (left) This picture shows dewetting patterns of a liquid crystal (avg. thickness of $40\,nm$) above a silicon substrate (covered with oxide layer) at room temperature. Darker regions of the picture indicate that the thickness of the fluid film changes. Bigger holes correspond to nucleation from defects while the smaller regular patterns show the existence of a critical unstable wave-length (undulation mode) for which the flat liquid crystal film is unstable. (right) Surface topography (close-up) of a dewetting gold film obtained with a scanning force microscope. A correlation between holes is proven using Minkowski functionals. This indicates that the liquid film ruptures by spinodal dewetting rather than by heterogenous nucleation. (Reprinted with permission of Herminghaus [4])

liquid crystals were transferred onto cleaned silicon wafers. Subsequently, two different mechanisms by which surface instabilities grow were observed, namely: spontaneous nucleation at random defects, e.g., dust or enclosed gases; and spinodal dewetting by growth of wavy unstable perturbations, so-called undulation modes. In their experiment the flat surface of the liquid crystal was unstable and patters, like those shown in Figure 1.1, emerged. Nucleation is easily triggered by impurities and hence it is usually the dominating effect. Nonetheless, experiments such as [4] in clean environments suppress such impurities and spinodal dewetting is observed. Herminhaus et al. argue that this distinction is not always apparent in an experiment, however, in our numerics the onset of singularities is triggered by spinodal dewetting, i.e., singularities develop from a critical unstable mode of the linearized system.

Both examples, spin-coating and experiments with dewetting liquids, show that it is important to understand the dynamics of free interfaces. The major challenge in the description of liquids on microscopic scales is the complexity and the large number of interactions and forces that might influence thin liquid films. In their review, Oron et al. [3] considered models including combinations of shear stress, viscosity, surface tension, intermolecular interactions (van der Waals forces), effects related to temperature variations (heat conduction), non-uniformities of solid substrates, evaporation and surfactants appearing in different geometries (domains with different symmetries and dimensions) for thin liquid films. Owing to the large number of physical effects and material properties, there exists a wide variety of thin film models. Therefore a short overview of the literature on thin film rupturing shall be given first. Although we focus on thin films on substrates, a short review of known results on free liquid films and liquid jets is given as well in order to inform the reader of the existing mathematical theory and numerical analysis.

In this thesis we discuss the impact of wall slippage on the rupture of thin films on solid substrates. The instability leading to rupture of the interface is driven by attractive intermolecular van der Waals forces. We will investigate how to implement slippage into various models of thin films. A numerical analysis of our model reveals that interface rupture of thin liquid films evolves in a self-similar manner. The influence of slippage on self-similar solutions is analyzed and a rigorous theory showing features of self-similarity is built.

1.2 Liquid Films on Substrates, Liquid Jets, and Free Liquid Films

The literature survey is divided according to the three main geometries considered in thin film modeling: liquid films on flat solid substrates, cylindrically symmetric liquid jets, and freely suspended films. While only the first is of main concern for this thesis, the latter two are mentioned because the mathematical theory of thin film rupture is very similar for all three geometries. Finally we mention some rigorous mathematical studies.

Liquid films on flat solid substrates

In the context of nano- and microfluidics, the discussion of thin films on solid substrates and the boundary condition between the liquid and the substrate has regained some attention during the $1990s$. This is mainly because experiments suggested a deviation from the no-slip condition [5]; deviations from the no-slip condition are mainly found for hydrophobic interfaces on length scales $\sim 100\,nm$ or below.

In 1994 Bertozzi et al. [6] provided a numerical analysis of thin film rupture including a discussion of terms related to slippage [3]. They ended up with a fourth-order degenerate parabolic equation for which they showed blow-up and prove existence of (weak) solutions. Their existence proof is based on earlier work by Bernis et al. [7] (1990). More up-to-date experimental evidence concerning slippage at microscales have appeared, as recapitulated

---

[3] Due to choice of scales, we will later refer to their equation as the weak-slip equation.

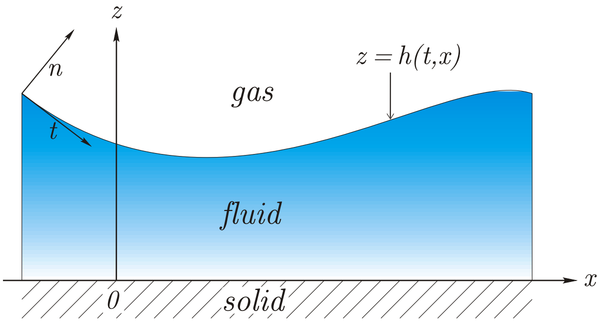

Figure 1.2: Geometry of a thin liquid film on a solid substrate in 2-dimensional space $\Omega(t) = \{(x, z) : 0 \leq z \leq h(t, x)\}$; Experiments suggest that the boundary condition at $z = 0$, i.e., the choice of the fluids' velocity at the liquid-solid interface, differs from the no-slip condition, i.e., the velocity at the interface is zero, when microfluidic experiments are performed with complex fluids on hydrophobic substrates.

by Lauga et al. [8] (2006). Therefore one should have a closer look at thin-film models with wall slippage. For a review of different models including slippage in the context of contact line motion see Münch et al. [9] or in the special case of the strong-slip equation also López et al. [10] (1995).

Up until now, no extensive analysis of self-similar rupture in the strong-slip model was performed. Figure 1.1 suggests that the proper geometry for rupture should be either rotational symmetric (for nucleation) or fully 3-dimensional (in order to describe the complex patterns of spinodal dewetting). However, for simplicity we only consider rupture with translational symmetry along one axis. Due to the underlying symmetry, this process is also called line rupture Figure 1.2. Using only attractive van der Waals forces, flat films are usually linearly unstable and hence the rupture mechanism is spinodal dewetting.

Many investigations consider rupture of thin films on a solid substrate to be the first stage of a more complex dewetting process, consisting of rupture and hole formation, growth of holes which coalesce and build liquid fronts. These fronts recede and create a polygonal network of fluid that finally decays into single droplets, as it can be observed for example in the pioneering work of Reiter et al. [11, 12] (1992,1996) or in experiments by Seemann et al. (Figure 1.3). A common approach to model the motion of contact lines (or points) between liquid–solid–gaseous phase is to introduce a wet precursor layer on the solid, on which the droplet can slide [13].

Liquid jets

A liquid jet is a rotationally symmetric thread of liquid like it is sketched in Figure 1.4. Already in the 19*th* century, physicists such as Rayleigh realized that surface tension alone suffices to destabilize the cylindrical interface of

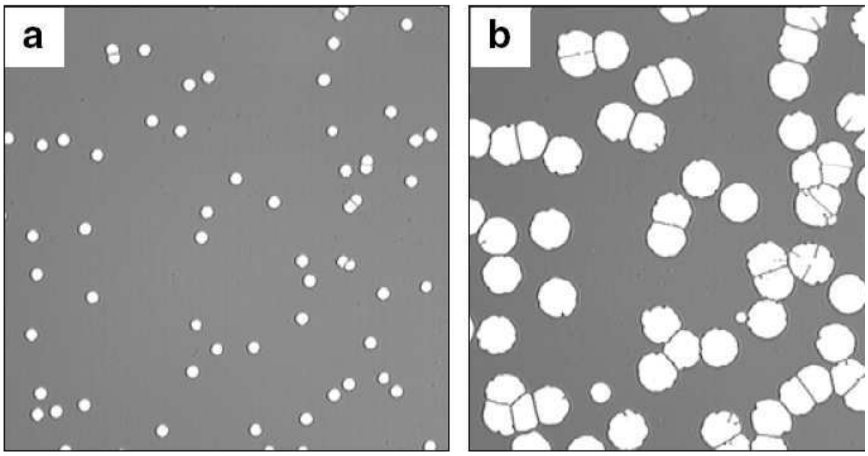

Figure 1.3: Dewetting polystyrene film with average thickness of 80 nm on a hydrophilic silicone substrate after a) 2 min, b) 18 min, c) 100 min. One can clearly distinguish the initial phase a) with rupture and hole formation, the second phase b) with coalescence of holes, and the last phase c), where the polygonal liquid network decays into single droplets. (Picture from Seemann et al. [14])

a jet. This instability ultimately leads to rupture of the jet, a phenomenon called *jet pinch-off*. One typically wishes to understand the formation of drops from pinching jets and the dynamics of pinch-off. A combination of the history and new developments in the mathematical theory and experiments of jet pinch-off is given in the review article *Nonlinear dynamics and breakup of free-surface flows* by Eggers [15] (1997) or also in the recent review by Eggers and Fontelos [16].

Eggers [17] (1993) and Bertozzi[4] et al. [6] (1994) considered pinch-off of liquid jets and found that it evolves self-similarly. For many years, only the linear theory of jet pinch-off was discussed [18]. Many current studies employ symmetry assumptions together with a long-wavelength approximation in order to reduce the set of 3-dimensional Navier-Stokes equations into a simpler system of partial differential equations. Using the so-called "slender jet approximation" Papageorgiou [19] (1995) applied this simplification to inertialess jet pinch-off and studied its similarity structure in great detail. In particular he found that similarity solutions are of the second kind[5].

The work on similarity solutions of Eggers and Papageorgiou was extended by Brenner et al. [21] (1996), where they found an infinite family

---

[4] They consider an interface between two immiscible liquids and not liquid and gas.

[5] For an extensive introduction into the general notion of self-similarity of first and second kind and scalings including application to fluid dynamics the book by Barenblatt [20] is recommended. Even though we discuss a definition of self-similarity, this is adapted to our special model of film rupture.

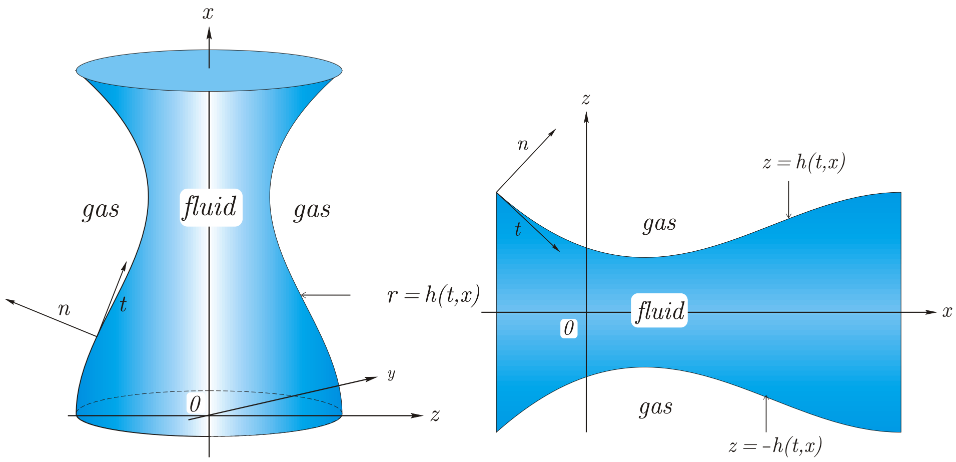

Figure 1.4: rotationally symmetric liquid jet with a non-uniform thickness (left) and the symmetric squeezing mode of a free liquid film (right); The boundaries of both domains are given implicitly by $\{z = h\}$ or $\{r = h\}$, where h represents the thickness of the liquid film/jet at some point. The thickness h depends on time and the residual spatial coordinate(s). The symmetric squeezing mode has a symmetric (fluid) velocity field, with effective boundary conditions imposed at $\{z = 0\}$.

of similarity solutions that are all unstable. Because it has least curvature, only the solution previously found by Eggers and Papageorgious is stable.

For a simpler model of surface tension driven jet pinch-off Renardy proved that the pinch-off already happens after a finite time [22] and started to analyze exact similarity solutions [23] of inertialess jet pinch-off.

Free liquid films

Free liquid films have no supporting substrate, and they are extended infinitely in two spatial directions. We assume that the fluid film is initially flat and that the introduction of perturbations only leads to variations of its thickness, i.e., the midplane of the squeezed liquid layer stays the $\{z = 0\}$ plane. The nonlinear rupture of free films was initially studied by Prévost [24] (1986). Like in derivation of nonlinear jet pinch-off models, the Navier-Stokes equations were simplified by a long-wavelength approximation and it was assumed that the dominant dynamical behavior can be described by a squeezing mode, i.e., the two opposite moving interfaces remain symmetric about the half-plane $\{z = 0\}$ of the liquid, like it is depicted in Figure 1.4.

The work of Prévost was extended by Erneux et al. [25] (1993), who derived a set of equations for which they employed a weakly nonlinear analysis to show that rupture occurs after a finite time. In particular, rupture evolves much faster than the linear stability analysis suggests. Miksis et al. [26] (1996) analyzed the nonlinear evolution of thin film rupture by numerical methods and also found that it evolves self-similarly. They resolved the self-similarity of the film thickness h by a numerical analysis. Unfortunately, their results were dominated by transient self-similar solutions, which made it impossible to fully resolve the true similarity structure. Their work was revisited by Vaynblat et al. [27] (2001), who determined the symmetry properties of similarity structure and found an infinite set of similarity solutions. Their model contains a continuous parameter that allows them to switch between jet pinch-off models and rupture models. This clearly shows that the structure of thin film rupture is related to the structure of jet pinch-off and vice versa.

In some models of thin film and jet dynamics, the thickness of the liquid film h is the solution of a degenerate higher-order parabolic equation such as

$$\partial_t h = \nabla \cdot \big[m(h)(\nabla \Delta h + A h^n \nabla h)\big]. \tag{1.1}$$

The parameter A is the relative strength of van der Waals forces with respect to surface tension, while Δh is the approximate curvature of the interface. The mobility function $m(h)$ is affected by boundary conditions — for a thin film on a solid non-slipping interface $m(h) = h^3$, while $m(h) = h^2$ or $m(h) = h^3 + bh^2$ on interfaces with intermediate-slip or weak-slip condition [9]. There exist some analytical studies that, following ideas of Bernis and Friedman [7], prove analytic properties like positivity of solutions and rupture in finite time [6, 28–30]. Those analytic properties are related to long-time existence of classical solution and crucially depend on the power law m of the mobility $m(h) = h^m$ and on n, i.e., in a certain range of m and n solutions are positive for all times, and another range one can prove that h approaches zero after a finite time. There exist analytical studies that concentrate on the finite speed of propagation [31], which were also started by the work of Bernis and Friedman. For example, one can find a rigorous analysis for self-similar solutions of Equation (1.1) in the work by Slepčev and Pugh [32] (2005) and references therein.

1.3 Outline of the Thesis

In this thesis the topic of singularity formation for special thin-film models is addressed. A numerical analysis is employed to study non-linear properties of interface singularities and a mathematical framework, which allows to prove some important properties, is developed.

For this purpose the thesis is divided into five parts. In the second chapter we discuss the physical origin of intermolecular forces and the reason to implement slippage. We state the mathematical problem of the evolution of an incompressible liquid with a free interface and extend the usual Navier-Stokes equation by intermolecular forces and Navier-slip boundary conditions. This model can be simplified and, depending on the choice of scales, one obtains different thin-film models.

The derivation of lubrication models is similar to the procedure of Münch et al. [9]. In the same manner we derive a strong-slip model where cylindrical symmetry of the solution is assumed. This procedure is straight-forward but was not performed so far. We introduce this model for completeness because it provides a more realistic setup of 3-dimensional interface rupture[6].

Within the third chapter the numerical algorithm that is designed to solve the lubrication equation close to the interfacial singularity will be constructed and discussed. It should be pointed out, that a high numerical precision is required in order to fully resolve the onset of the interfacial singularity and to distinguish the singularity from the transient behavior. The computation of similarity solutions follows the usual strategy, e.g., the one employed by Vaynblat et al. [27]. The lubrication model that we study is a system of two coupled partial differential equations which describe transport of mass and dissipation of kinetic energy. The numerical algorithm allows us to study self-similar rupture in great detail, for example we can study transitions between different self-similar solutions of first and second kind, which was not done so far. Neglecting inertia and surface tension, the thin film model can be simplified to an integro-differential equation. Such a transformation has been applied to jet pinch-off models but not to rupture models.

In the fourth chapter properties of the integro-differential equation will be studied in great detail. Most importantly, notice that this model is similar to the jet pinch-off model studied by Renardy [22, 23] and Papageorgiou [19]. We rather follow the approach of Renardy and not the classical approach for equations like (1.1) because it is observed that the higher order surface tension term plays a minor role near the singularity.

For this equation we prove that rupture occurs after a finite time. Even though our approach is similar to the one of Renardy[22], the present proof is more explicit and does not require the regularity assumptions on initial data. Furthermore, a formal notion of convergence to self-similar solutions will be introduced. Results regarding convergence to self-similar solutions will be given. The first parts of this chapter follow ideas by Renardy [22, 23] and later parts follow the work by Pego and Niethammer [33]. The fact that self-similar solutions are of second kind and that they are defined on unbounded intervals makes the convergence proof more involved. Such a rigorous analysis has not been performed for any of the liquid film geometries before.

There exists an analogy between our simplified model for thin film rupture and LSW models[7] (Lifshitz, Slyozov [34] and Wagner [35]) which makes the fourth chapter even applicable to a wider class of problems. The possibility of second kind self-similarity has not been discussed for LSW-like models yet.

---

[6] Usually thin films rupture at points (cylindrical symmetry) and not along lines (translational symmetry).

[7] The LSW model describes the long-time evolution of a particle size. Under certain conditions the blow-up of the distribution evolves self-similarly.

In the fifth chapter we summarize our results and give an outlook to future work. We present a model of a thin film on an elastic substrate and show some numerical results regarding the short- and long-time behavior. This study is a part of a project in the DFG Priority Program SPP 1164 Nano- and Microfluidics[36].

Chapter 2

Modeling

2.1 Equations in the Fluid

Mathematical models of fluids with a freely movable interface, so-called *free boundary problems*, are important in many applications. As an example spin-coating of a thin liquid film onto a solid substrate was mentioned in the introduction. In all our models we assume that the fluid is a continuous medium and that its dynamical behavior is solely characterized by a set of equations that describe the transport fluid mass, dissipation of kinetic energy, and the evolution of the free boundary of the fluid. The model should incorporate boundary conditions at liquid–solid interface and forces which originate from intermolecular interactions between fluid particles and the solid substrate.

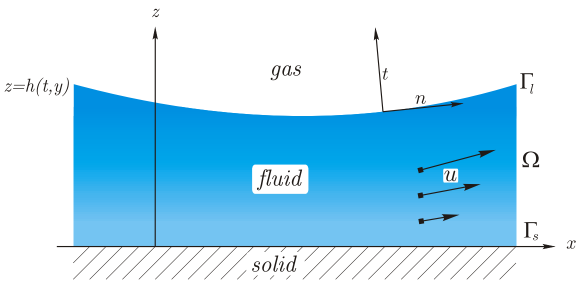

Figure 2.1: The fluid velocity at point $(x, z) \in \mathbb{R}^2$ and time t is denoted by $\mathbf{u}(t, x, z)$, where x runs parallel to the substrate and z runs perpendicular to the substrate interface. The fluid–air interface is parametrized by $z = h(t, x)$, where $\mathbf{n}$ and $\mathbf{t}$ are the corresponding normal and tangential vectors.

Thus the fundamental degrees of freedom of the model are the time-dependent domain $\Omega(t) \subset \mathbb{R}^d$, i.e., the subset of the d-dimensional space that is occupied by fluid particles, and the velocity of fluid particles $\mathbf{u}(t, \mathbf{x})$ at time t for every point inside $\Omega(t)$. Density fluctuations and transport of energy are not taken into consideration. The fluid is placed on a flat solid substrate $\Omega(t) \subset \mathbb{R}^{d-1} \times \mathbb{R}^+$ where the fluid–substrate interface Γ_s is located at $(x_1, x_2, ..., x_{d-1}, 0)$.

It is assumed that the free interface between the liquid and the gaseous phase Γ_l can be parametrized by $x_d = h(t, x_1, \ldots, x_{d-1})$. Initially this is not a serious restriction since we study the evolution starting from flat liquid films where $h(t_0, x_1, ..., x_d)$ is close to or equal to a positive constant.

In the numerical computation of the next chapter we will restrict to liquid films that are confined to a finite box $\Omega(t) \subset [0, L]^{d-1} \times \mathbb{R}^+$. In Figure 2.1 a sketch of a typical 2-dimensional domain $\Omega(t)$ at some time t is shown. An example for more complex geometries is presented in the last chapter, where we study a model of a thin liquid film resting on a viscoelastic solid. There the interface between the fluid and solid is elastic and freely movable as well.

Throughout the whole work we assume that the velocity field $\mathbf{u}(t, \mathbf{x})$ of an incompressible, viscous fluid with typical extensions of several micrometers can be described by the Navier-Stokes equations

$$\rho \frac{D\mathbf{u}}{Dt} = \nabla \cdot \boldsymbol{\sigma} + \mathbf{f}_{\text{ext}}, \tag{2.1a}$$

$$\nabla \cdot \mathbf{u} = 0, \tag{2.1b}$$

which hold for every point in the bulk of the domain $\Omega(t)$. By ρ we denote the mass density of the liquid, $\mathbf{f}_{\text{ext}}$ is an external force density, and $\boldsymbol{\sigma}$ is the stress tensor of the liquid that one obtains by virtue of Cauchy's Theorem (e.g. for a proof see [37]). By $D\mathbf{u}/Dt := \dot{\mathbf{u}} + \mathbf{u} \cdot \nabla \mathbf{u}$ we denote the material derivative of the velocity with respect to time, i.e., the acceleration of particles. The notion $\nabla\cdot$ refers to the divergence of a tensor field, $\mathbf{u} \cdot \nabla$ is the directional derivative along $\mathbf{u}$, and an upper dot like in $\dot{\mathbf{u}}$ always refers to the (partial) derivative with respect to time. Both equations express dissipation of energy and incompressibility of the fluid respectively.

For most parts of this work we restrict to 2-dimensional systems $d = 2$ and with the notion $x_1 = x$ and $x_2 = z$. In order to make the Navier-Stokes equation a well-posed problem, we have to add boundary conditions that express

- the geometrical evolution of the free boundary,
- equilibrium of forces,
- and conservation of mass.

In the 2-dimensional domain $\Omega(t)$ occupied by the fluid

$$\Omega(t) = \left\{ \left(x, z\right) \in \mathbb{R}^2 | x \in \mathbb{R}, 0 \le z \le h(t, x) \right\}$$

we would like to have conservation of total mass

$$M(t) = \rho \int_{\Omega(t)} dx.$$

The local mass flow is conserved because the continuity equation $\dot{\rho} + \text{div}(\rho\mathbf{u}) = 0$ is automatically fulfilled with a constant density $\rho(t, \mathbf{x}) \equiv \rho$ and $\text{div}\mathbf{u} = 0$. Before we check conservation of mass in $\Omega(t)$, we define the so-called kinematic boundary condition, which states that the normal components of velocity of the interface and the velocity of fluid particles on the interface are equal. By $\mathbf{v}_\Gamma$ we denote the velocity of the interface. The kinematic boundary condition reads

$$(\mathbf{u} - \mathbf{v}_\Gamma) \cdot \mathbf{n} = 0 \qquad \text{on } \Gamma_l.$$

One possibility to define the interfacial velocity is $\mathbf{v}_\Gamma := \mathbf{e}_z\,\dot{h}(t,x)$. Then, using the velocity components $\mathbf{u}(t,x,z) = u(t,x,z)\,\mathbf{e}_x + v(t,x,z)\,\mathbf{e}_z$, the kinematic condition reads

$$\dot{h}(t,x) = \big(v(t,x,z) - h_x(t,x)u(t,x,z)\big)_{z=h(t,x)} \quad .$$

Note again that only the normal component of $\mathbf{u}$ enters in the computation of $\dot{h}$. If the velocity of the interface $\mathbf{v}_\Gamma$ is purely tangential, then the shape of the interface Γ_l *does not change* at all.

We can safely set $\mathbf{v}_\Gamma = \mathbf{u}$ and define $\mathbf{v}_\Gamma$ also inside $\Omega(t)$. For any point $\mathbf{x}_0$ in $\Omega(0)$ define its trajectory by $\dot{\mathbf{x}}(t) = \mathbf{u}\big(t,\mathbf{x}(t)\big)$ with $\mathbf{x}(0) = \mathbf{x}_0$. For $\Omega(t)$ being the set of all these points at a given time t, Reynold's transport theorem states

$$\dot{M}(t) = \rho\frac{d}{dt}\int_{\Omega(t)} dx = \rho\int_{\Omega(t)} \operatorname{div}(\mathbf{v}_\Gamma)\,dx = 0,$$

which of course implies conservation of mass. For a setup with in- and outflow conditions ($\mathbf{u}\cdot n \neq 0$) defined on $\Gamma \subset \partial\Omega(t) \setminus \big(\Gamma_l(t)\cup\Gamma_s\big)$ the total mass changes according to

$$\dot{M}(t) = -\rho\int_\Gamma (\mathbf{u}\cdot n)\,dS,$$

where $\mathbf{n}$ is the outer normal on Γ. However, we use (generalized) impermeability conditions $\mathbf{n}\cdot(u - v_\Gamma) = 0$ on the hole boundaries of $\Omega(t)$.

We have to add a constitutive relation for the stress tensor $\boldsymbol{\sigma}$. By virtue of Cauchy's theorem contact forces like pressure or friction can be put into a stress tensor $\boldsymbol{\sigma}$. Basically one has to assume that the contact forces between adjacent test-volumes are continuous function of the normal vector that connects both volumes. Then one shows, using balance of momenta, that the force depends linearly on $\mathbf{n}$. Thus the total contact force that the surrounding fluid exerts onto a piece of volume V is computed by

$$\int_{\partial V} \boldsymbol{\sigma}\cdot\mathbf{n}\,dS,$$

where $\mathbf{n}$ is the outer normal onto V.

The stress tensor itself is usually defined by a constitutive relation. Here we assume that the fluid under consideration is *Newtonian*, i.e., the Cauchy stress tensor is a linear function of the velocity gradient $\nabla\mathbf{u}(t,x,z)$ in the following way

$$\boldsymbol{\sigma}(p,\nabla\mathbf{u}) = -p\,\mathbb{I}_d + \mu\,D\mathbf{u}. \tag{2.2}$$

The Newtonian Cauchy stress tensor contains the internal pressure $p(t,x,z)$, the deformation tensor $D\mathbf{u} := \big(\nabla\mathbf{u} + \nabla\mathbf{u}^\top\big)$, $\mathbb{I}_d$ is the d-by-d identity matrix, and μ denotes the viscosity of the fluid. Real fluids obey $\mu > 0$, contrary to perfect fluids for which $\mu = 0$. In isotropic non-Newtonian fluids the viscosity is a function of the strain rate[1]

$$\mu = \mu(\gamma) \qquad \text{with} \qquad \gamma = \sqrt{\tfrac{1}{2} D\mathbf{u} : D\mathbf{u}}.$$

The only complex properties of the fluid that we consider are intermolecular interactions $\mathbf{f}_{\text{ext}}$ and complex boundary conditions at the liquid–solid interface Γ_s. Now that the equations in the bulk phase and the kinematic condition at the free interface are defined, let us examine the remaining boundary conditions on Γ_s and Γ_l.

2.2 Discussion of Boundary Conditions

In order to close the system of equations we have to add boundary conditions. For the fixed boundaries the velocity at the boundary must be prescribed, whereas on the free boundary, in addition to the kinematic condition, equilibrium of forces must hold. We have three different types of boundaries:

(1) the free capillary surface between fluid and gas $\Gamma_l(t)$,

(2) an artificial boundary at $\Gamma(t) = \big\{(x,z) \in \Omega(t) : x = 0 \text{ or } x = L\big\}$,

(3) and the fixed interface between fluid and solid Γ_s.

(1) For moderatly fast motions of the liquid it is a good approximation to neglect tangential shear forces, which the gaseous phase exerts on the fluid. In addition it is assumed that the outer pressure of the gaseous phase is constant. In the notation we introduced before, the free interface of the liquid is implicitly defined by

$$\Gamma_{\mathrm{l}}(t) = \big\{(x,z) \in \mathbb{R}^2 | f(t,x,z) = 0, x \in \mathbb{R}\big\}$$

with $f(t,x,z) = z - h(t,x)$. Tangential vector and outer normal vector are given by

$$\mathbf{t} = (1 + h_x^2)^{-1/2} \begin{pmatrix} 1 \\ h_x(t,x) \end{pmatrix}, \qquad \mathbf{n} = (1 + h_x^2)^{-1/2} \begin{pmatrix} -h_x(t,x) \\ 1 \end{pmatrix}.$$

It is well known that whenever a smooth $d-1$ dimensional interface is defined implicitly by $\{\mathbf{x} \in \mathbb{R}^d : f(\mathbf{x}) = 0\}$ and f has some regularity, then a normal vector field can be computed by $\mathbf{n} = \nabla f \cdot \|\nabla f\|^{-1}$ and the corresponding mean curvature of the interface is given by $\kappa = |\nabla \cdot \mathbf{n}|$. Using the outer normal $\mathbf{n}$ from above the obtain the mean curvature

---

[1] A free boundary problem with non-Newtonian fluids can be found for example in [38].

$$\kappa = \frac{|h_{xx}|}{(1+h_x^2)^{3/2}}.$$

If we chose the sign of $\mathbf{n}$ such that it points outward some volume, then the signed mean curvature leading to surface tension forces onto that volume is given by $\kappa = -\nabla \cdot \mathbf{n}$. For example, the signed mean curvature of a fluid ball of radius r is $\kappa = -1/r$. Then the force balance on the free capillary surface reads

$$\boldsymbol{\sigma}\mathbf{n} = \gamma_l \kappa\, \mathbf{n} \tag{2.3}$$

with γ_l being the surface tension associated with the interface. As this notion indicates, there are no tangential forces acting on the interface and the outer pressure of the gaseous phase is set to zero.

(2) Though one can consider the Navier-Stokes equation in unbounded domains $\Omega(t)$ ($x \in \mathbb{R}$), for the purpose of numerical implementation it is better to restrict to finite boxes, i.e., $x \in [0, L]$. Thus, on the level of the Navier-Stokes equations one has to define boundary conditions on

$$\Gamma = \big\{(x,z) \in \mathbb{R}^d : x \in \{0, L\}, 0 \le z \le h(t,x)\big\}$$

as well. In- or outflow of mass is not needed so that we can set Γ to be an impermeable wall, i.e., using the velocity $\mathbf{u}(t,x,z) = u(t,x,z)\,\mathbf{e}_x + v(t,x,z)\,\mathbf{e}_z$ we have $u(t,x,z) = 0$ on Γ. There are two standard choices for the tangential part of $\mathbf{u}$, namely

- (2a) the no-slip condition $v(t,x,z) = 0$ on Γ,
- (2b) or the free-slip condition $\partial_x v(t,x,z) = 0$ on Γ.

Both equations have a different impact on the evolution of the free interface Γ_l at the points $\mathbf{x}_\pm = \big(\pm L, h(t, \pm L)\big)$. For example (2a) implies $\dot{h} = 0$ (no movement of the free surface at $\mathbf{x}_\pm$, whereas (2b) implies $\dot{h} = v$ and $\partial_x \dot{h} = h_x v_z$ at $\mathbf{x}_\pm$ (contact angle changes with time). For the moment the Navier-Stokes equations are considered in the unbounded domain with $x \in \mathbb{R}$, later on, when we introduce the simplification of the Navier-Stokes equation, we will use the boundary condition (2b). What remains is to discuss boundary condition (3).

2.3 Role of Slippage

(3) In this section we discuss different possibilities to model the liquid–solid interface using various boundary conditions. Impermeability of the interface

implies that the flow of liquid particles is tangential $\mathbf{u} \cdot \mathbf{n} = 0$. This is generally the case for our models.

In no additional tangential forces act on an interface, then one can conclude that the following relation

$$\mathbf{t} \cdot \boldsymbol{\sigma} \mathbf{n} = 0 \tag{2.4}$$

holds for any tangential vector $\mathbf{t}$. Together with the impermeability condition this is called the *free-slip* or *perfect-slip* boundary condition, because the fluid can move freely and without any resistance (or frictional forces) along the interface. While this assumption is plausible for interfaces such as between gas and liquid, it seems hardly realistic for solid–liquid interfaces, where one would expect larger contact forces between solid and fluid phase.

One usually observes that the flow profile $\mathbf{u}$ near the interface has a non-vanishing shear, which is to say that the tangential component of the strain tensor $(D\mathbf{u}) \cdot n$ is nonzero. This immediately implies that there are also tangential forces that the fluid exerts on the solid, which in turn are equal to the forces that the solid exerts on the fluid. In case the friction is strong, a detailed description of the solid-liquid interaction can be circumvented by assuming that fluid particles are stuck on the interface, i.e.,

$$\mathbf{u} = 0. \tag{2.5}$$

This is the well-known *no-slip* boundary condition. The drag force at the liquid–solid interface is proprotional to the product of viscosity and the tangential part of the shear rate but independent of the properties of the solid or the liquid–solid interface.

There is no (physically) strict reason that the tangential velocity $\mathbf{u}_{||} = (\mathbb{I}_d - \mathbf{n} n^\top)\mathbf{u}$ is always zero. A first approximation of a relation between drag force and shearing is a linear ration; in this case the drag force is a linear function of the tangential velocity of $\mathbf{u}_{||}$ and points in the opposite direction of $\mathbf{u}_{||}$. One writes

$$\mathbf{t} \cdot \boldsymbol{\sigma} \mathbf{n} = \mu E \, \mathbf{t} \cdot \mathbf{u}_{||}. \tag{2.6}$$

for any tangential vector $\mathbf{t}$. This condition is the *Navier-slip* boundary condition [39].

The debate on the validity of the last two boundary conditions (no-slip and Navier-slip condition) has a long standing history, with two famous participants being Claude Louis Marie Henri Navier and George Gabriel Stokes. Navier proposed condition (2.6) first in his 1823 paper [39]. Considering experimental finding, Stokes stated in his *Report on Recent Researches in Hydrodynamics* [40] that

> ...the condition to be assumed in the case of a fluid in contact with a solid is that the fluid does not move relatively to the solid. This condition will be included in M. Navier's, if we supposed the

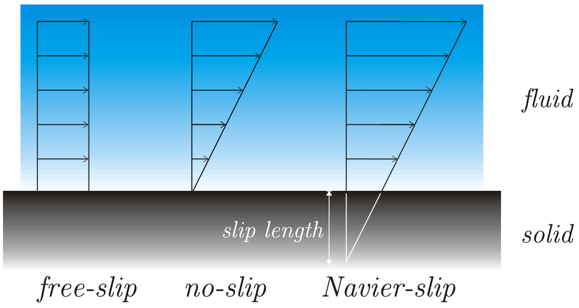

Figure 2.2: Idealized flow profiles near the solid-liquid interface for the free-slip, no-slip, and Navier-slip boundary condition

> coefficient of the velocity when M. Navier's condition is expressed analytically, which he denotes by E, becomes infinite.

Here he refers to experiments of Du Buat and Coulomb which show that fluid particles adhere to slowly moving solid walls, and that the friction between a oscillating metallic disc and a fluid does not depend on the coating of the surface (Coulomb). He also refers to experiments by Girard with narrow capillary tubes which indicate that

> ... the condition to be satisfied at the surface of fluid in contact with a solid is different according as the fluid does or does not moisten the surface of the solid.

Furthermore he states

> If we adopt Navier's explanation, we may reconcile it with the experiments of Coulomb by supposing the E is very large, so that unless the fluid is confined in a very narrow pipe, the results will depend mainly on A^2, being sensible the same as they would be if E was infinite.

which coincides with findings of modern experiments. The expression E he is referring to is basically the same one as in (2.6) and has the dimension 1/length. The quotations show that scientists first struggled to accept the Navier-slip boundary condition. The main problem today is that due to the smallness of the effect slippage is difficult to measure and that there is no clear correlation between properties of the interface and the value of E. Still, slippage is a useful parameter to explain typical patterns observed in dewetting of liquid films [13].

For the planar interface Γ_s at $z = 0$ with our 2-dimensional flow $\mathbf{u} = u\,\mathbf{e}_x + v\,\mathbf{e}_z$ the Navier-slip boundary condition reads

---

[2] viscosity of the fluid

$$E\,u(t,x,0) = \partial_z u(t,x,0),$$

Figure 2.2 illustrates that the slip-length $1/E$ represents a virtual distance below the interface, where the no-slip condition holds. In what follows we refer to $1/E$ as the *slip-length*, which will be denoted by the symbol b. For $b \to 0$ the no-slip condition is reproduced, where it can be seen in (2.6) that $b \to \infty$ or equivalently $E \to 0$ implies the absence of tangential forces $\mathbf{t} \cdot \boldsymbol{\sigma}\mathbf{n} = 0$ on the interface.

Recent experimental results regarding the breakdown of the no-slip boundary condition in microfluidic systems are summarized in the review by Lauga, Brenner and Stone [8]. They distinguish three different types of slippage:

- *Molecular slip*: Molecules can move along the interface if the shear forces are sufficiently large. This depends much on the microscopic details of the system.
- *Apparent slip*: Slippage is observed on a mesoscopic scale even though the no-slip condition is valid on a microscopic scale. This is possible due to boundary layers.
- *Effective slip*: Certain macroscopic measurements can be explained by theoretical predictions of models that include Navier-slip boundary conditions.

A standard experiment is measurement of a flow rate $Q_{\text{exp}} = \int_A (\mathbf{u} \cdot \mathbf{n})\, dS$ through the cross section A of a microchannel at a given applied pressure p. The actual flow rate can be compared with the flow-rate with no-slip condition. For a cylindrical tube of radius h and length l the Hagen-Poiseuille-law (no-slip) gives

$$Q_{\text{ns}} = \frac{\pi h^4}{8\mu} \frac{p}{l}$$

where the general expression with Navier-slip is easily seen to be

$$Q_{\text{slip}} = \frac{\pi h^3}{8\mu} \frac{p}{l} (4b + h).$$

We obtain the slip-length b by measuring the ratio

$$\frac{Q_{\text{exp}}}{Q_{\text{ns}}} = \frac{h + 4b}{h}.$$

As this is an indirect measurement, one determines the effective slip. Another technique is measurement of resistance between liquid and solid bodies, such as spheres, in a given simple flow. Similarly there exist direct measurements to determine apparent slip. Results of such an experiment [41] are shown in Figure 2.3.

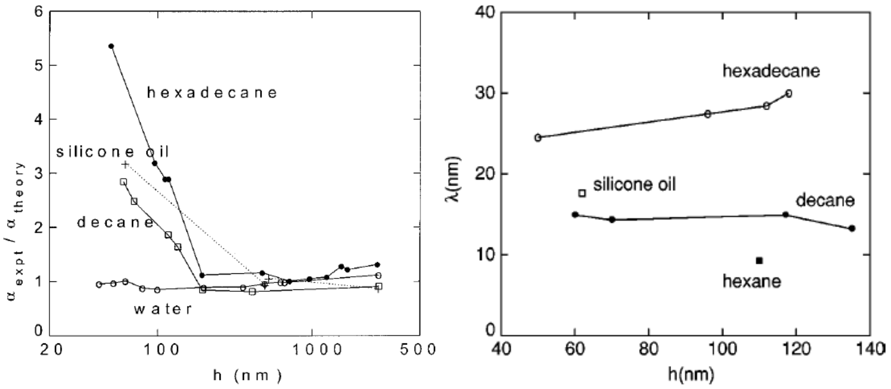

Figure 2.3: (left) excess mass flow $Q_{\text{exp}}/Q_{\text{ns}}$ versus microchannel radius (left); (right) slip-length $\lambda(= b)$ versus channel size h; (Cheng et al. [41])

We shortly summarize the status of experiments according to Lauga et al. [8].

Experimental status

It is found that the slip-length depends on surface roughness, air bubbles in the liquid, wetting properties of the surface, electric properties of the liquid , shear rate (Navier-slip becomes non-linear) and pressure.

Similarly to the free interface where a free-slip boundary condition is imposed, air bubbles on the interface generate some apparent slip even on no-slip boundaries.

There is the tendency that slip increases with larger contact angles, but so far no good correlation between contact angle and slip-length has been proven experimentally. Molecular dynamics is employed to model microscopic behavior and molecular slip theoretically. However, there are many open questions how to measure molecular slip in experiments.

This makes it desirable to relate measurements of the effective slip-length in microfluidic flows to models which include the Navier-slip boundary condition.

2.4 London–van der Waals Interaction

On smaller length scales electrodynamic properties of the liquid become more and more important. The dewetting process of a liquid on a solid substrate depends sensibly on the (intermolecular) interaction[3] between fluid and solid. Such an interaction is usually implemented by defining an external volume force $\mathbf{f}_{\text{ext}}$.

Fundamental molecular interaction forces are summarized in terms of the so-called London–van der Waals forces and have various physical origins, e.g., dipole-dipole forces, induced dipole forces or so-called dispersion forces. The *dipole-dipole force* goes back to *Keesom* [42], who established the following classical, statistical expression for the interaction between two dipoles

---

[3] Intermolecular interactions/van der Waals forces are long ranged forces, not to be confused with friction which is a short ranged (contact) force.

$$-C\frac{\beta}{r^6}.$$

Due to the Boltzmann factor $\beta = 1/(kT)$ this interaction is negligible at high temperatures. By r we denote the distance between two such dipoles. Assuming that the molecules have polarizabilities α, *Debye* [43] derived the *induction force*

$$-C\frac{\alpha}{r^6}.$$

However, the attractive interaction between molecules of rare gases could not by explained by any of those interactions. Therefore, *London* and *Wang* [44, 45] established an interaction which is of quantum mechanical origin, i.e., an attractive interaction between non-polar, neutral atoms. Their so-called *dispersion force* has the form

$$-C\frac{\hbar\nu}{r^6},$$

where $\hbar$ is the Planck constant and ν is a typical frequency of the system. All forces are attractive and decay equally fast as $r \to \infty$.

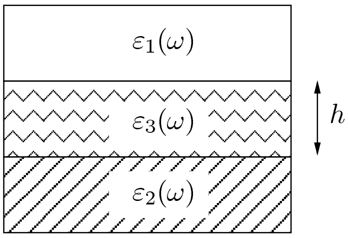

Figure 2.4: system of 3 dielectric layers: gas ε_1, fluid ε_3, solid phase ε_2, thickness of fluid layer h

Based on the dispersion force, Dzyaloshinskii, Lifshitz, and Pitaevskii [46] developed the general theory of van der Waals forces for macroscopic bodies, which allows the computation of van der Waals forces for solids or fluids, or in general for a 3-layered system of dielectric substances with (complex) relative permittivity $\varepsilon_i(\omega)$ $(i = 1, 2, 3)$ like the one shown in Figure 2.4. Assuming that the gaseous phase has permittivity $\epsilon_2 = 1$, their general leading order expression for the interaction force (per area) without dilatation effects is

$$F(h) = \frac{\hbar\bar{\omega}}{8\pi^2 h^3}, \qquad \bar{\omega} = \int_0^\infty \frac{\big(\varepsilon_3(i\chi) - \varepsilon_1(i\chi)\big)\big(\varepsilon_3(i\chi) - 1\big)}{\big(\varepsilon_3(i\chi) + \varepsilon_1(i\chi)\big)\big(\varepsilon_3(i\chi) + 1\big)}\, d\chi.$$

for a small thickness $h \ll \xi$ (ξ is a characteristic electromagnetic absorbtion length) and the permittivities ε_i are evaluated at imaginary frequencies $i\chi$. For a larger thickness h dilatation effects become important and the force is proportional $F(h) \propto h^{-4}$ where the factor in front of the power-law is again some integral over the complex permittivities.

Commonly, in thin film the long range contribution into a volume force $\mathbf{f}_{\text{ext}} = -\nabla\Phi$, where the interaction potential is parametrized by

$$\Phi(h) = \frac{A}{6\pi\, h^3}. \tag{2.7}$$

Oron et al. [3] review different interactions including disjoining pressures, e.g.,

$$\Phi(h) = \frac{A}{6\pi\, h^3} - \frac{A'}{h^4}.$$

With $A, A' > 0$ this force is attractive for large h and repulsive for small h. The material constant A is the so-called Hamaker constant and has typical values between $10^{-18}\, J$ and $10^{-20} J$.

With the goal to study the onset and nonlinear behavior of thin film rupture, we study the destabilization of a thin liquid film by purely attractive forces of the form (2.7). Even though it is clear that the empirical law of the van der Waals interaction by [46] does not apply for large deformations, we still use (2.7) beyond the region where it is stricly valid.

2.5 Full Model

The motion of an incompressible liquid film on a solid substrate with empirical van der Waals potential $\phi(h) = A/h^3$, slippage at the fluid–solid interface Γ_s, and capillary forces at the free gas–fluid interface Γ_l is described by

$$\rho\big(\dot{\mathbf{u}} + \mathbf{u}\cdot\nabla\mathbf{u}\big) = \nabla\cdot\boldsymbol{\sigma} - \nabla\phi(h) \qquad \text{in } \Omega(t) \tag{2.8a}$$

$$\operatorname{div}\mathbf{u} = 0 \qquad \text{in } \Omega(t) \tag{2.8b}$$

$$\boldsymbol{\sigma}\mathbf{n} = \gamma_l \kappa\, \mathbf{n} \qquad \text{on } \Gamma_l(t) \tag{2.8c}$$

$$\mathbf{n}\cdot(\mathbf{u} - \mathbf{v}_\Gamma) = 0 \qquad \text{on } \Gamma_l(t) \tag{2.8d}$$

$$\boldsymbol{\sigma}\mathbf{n} = \frac{\mu}{b}\mathbf{u} \qquad \text{on } \Gamma_s \tag{2.8e}$$

$$\mathbf{n}\cdot\mathbf{u} = 0 \qquad \text{on } \Gamma_s \tag{2.8f}$$

in the layered domain $\Omega(t) = \{(x,z) \in \mathbb{R}^2 : 0 \leq z \leq h(t,x)\}$ with $\Gamma_s = \mathbb{R} \times 0$, and $\Gamma_l(t) = \{(x,z) \in \mathbb{R}^2 : z = h(t,x)\}$ such that $\partial\Omega(t) = \Gamma_l(t) \cup \Gamma_s$. By $\mathbf{v}_\Gamma$ we denote the velocity of the interface $\Gamma_l(t)$, e.g., $\mathbf{v}_\Gamma = \dot{h}\,\mathbf{e}_z$. As it was done before, the domain $\Omega(t)$ is parametrized by $h(t,x)$. The stress tensor of the fluid is

$$\boldsymbol{\sigma} = -\mathbb{I}_2\, p(t,x,z) + \mu\, D\mathbf{u}(t,x,z).$$

and the signed mean curvature of the free interface in the point $\big(x, h(t,x)\big) \in \Gamma_l$ is given by $\kappa(t,x) = h_{xx}(t,x)/(1 + h_x(t,x)^2)^{3/2}$.

For given initial data $\big(h_0(x), \mathbf{u}_0(x,z)\big)$ and using the compatibility condition $\operatorname{div}\mathbf{u}_0(x,z) = 0$ and $h_0(x) > 0$ we call a triple

$$\begin{aligned}
&h : [0,t^*) \times \mathbb{R} \to \mathbb{R}^+\\
&p : \{(t,x,z) : t \in [0,t^*), x \in \mathbb{R}, 0 \leq z \leq h(t,x)\} \to \mathbb{R}\\
&\mathbf{u} : \{(t,x,z) : t \in [0,t^*), x \in \mathbb{R}, 0 \leq z \leq h(t,x)\} \to \mathbb{R}^2
\end{aligned}$$

a solution of (2.8), if $(h, p, \mathbf{u})$ are sufficiently regular, solve (2.8) for some time interval $[0,t^*)$, and fulfill the initial conditions $h(0,x) = h_0(x)$, and $\mathbf{u}(0,x,z) = \mathbf{u}_0(x,z)$. Since the potential energy $\phi(h)$ is unbounded as h approaches zero, one can only expect local existence of solutions in the general case. Note that when h_x becomes infinite, the parametrization of $\Omega(t)$ becomes infeasible.

Regarding existence of solutions for such models, with and without surface tension, for short and long times, but in any case without van der Waals interaction, consider Beale [47, 48] (1981,1983) (and references therein).

Example 2.1. A particularly simple global solution ($t^* = \infty$) is the flat film

$$\begin{aligned}
h(t,x) &= h_0,\\
\mathbf{u}(t,x,z) &= \mathbf{0},\\
p(t,x,z) &= 0.
\end{aligned}$$

We will show that this solution is linearly unstable with respect to long-wavelength perturbations. ♢

2.6 Lubrication Models and Scalings

The free boundary problem presented before contains scalar parameters $(\rho, \mu, b, \gamma_l, A)$, the solution $\big(h, p, \mathbf{u} = (u,v)\big)$, and independent measures of time t and length (x,z). Each of those quantities carries a physical scale, which is a certain integer power of the fundament units of length L, time T, and mass M. All dimensional parameters that occur in this thesis are expressed in SI units, thus $[M] = 1\,kg$, $[L] = 1\,m$, and $[T] = 1\,s$. For example, the physical dimension of the mass density ρ is $[\rho] = [M] \cdot [L]^{-3} = kg \cdot m^{-3}$.

For the purpose of the non-dimensionalization procedure, we use uppercase letters for the solution $\big(H, P, \mathbf{U} = (U, V)\big)$, and the coordinates (T, X, Z). Each of these quantities is decomposed into its numerical value, which we denote by the lower case letter, and a typical physical scale, which we denote by the same symbol with a tilde, e.g., $H(T, X) = h(t, x)\,\widetilde{H}$ and so on. For the parameters we use the notation $(\rho, \mu, B, \gamma_l, A)$.

In the next step solutions of the non-dimensionalized model will be expanded in terms of the small parameter $\epsilon = \widetilde{Z}/\widetilde{X}$. By assuming the solution is basically given by the leading order term of this expansion, we can reduce system of 2-dimensional Navier-Stokes equations to a set of partial equations in one spatial dimension, the so-called *lubrication equations.*

We seek $\big(H, P, \mathbf{U} = (U, V)\big)$ such that

$$\begin{aligned} \rho(U_T + UU_X + VU_Z) &= \mu\Delta U - (P + F)_X, && \text{(2.9a)}\\ \rho(V_T + VV_X + VV_Z) &= \mu\Delta V - P_Z, && \text{(2.9b)}\\ U_X + V_Z &= 0, && \text{(2.9c)} \end{aligned}$$

in the bulk phase $\Omega(t) = \big\{(X, Z) \in \mathbb{R}^2 : 0 \le Z \le H(T, X)\big\}$. As described before, all quantities are decomposed into their numerical value and their physical scale as follows:

$$\begin{aligned} &Z = \widetilde{H}\,z, && H = \widetilde{H}\,h, && B = \widetilde{H}\,b, && X = \widetilde{L}\,x, \\ &U = \widetilde{U}\,u, && V = \widetilde{V}\,v, && T = \widetilde{H}\widetilde{V}^{-1}\,t, && P + F = \widetilde{P}p, \qquad F = \widetilde{P}\phi. \end{aligned}$$

In this definition it is already assumed that some quantities share the same (typical) scale, e.g., H, B, and Z are all measured with respect to $\widetilde{H}$. Using these definitions one can rewrite the boundary conditions in a similar manner. For the physical scales we basically have $[\widetilde{H}] = [\widetilde{L}] = [L]$, $[\widetilde{U}] = [\widetilde{V}] = [L/T]$, $[\widetilde{T}] = [T]$, $[\widetilde{P}] = [M] \cdot [L]^{-1} \cdot [T]^{-2}$.

At this point the choice of units is completely arbitrary. However, if we employ the the lubrication approximation, where we assume that the solution can be written in terms of the asymptotic expansion

$$\begin{aligned} \widetilde{U}^{-1} \cdot U(T, X, Z) &= u(t, x, z) = u_0(t, x, z) + \epsilon^2 u_1(t, x, z) + \mathcal{O}(\epsilon^4),\\ \widetilde{V}^{-1} \cdot V(T, X, Z) &= v(t, x, z) = v_0(t, x, z) + \epsilon^2 v_1(t, x, z) + \mathcal{O}(\epsilon^4),\\ \widetilde{P}^{-1} \cdot P(T, X, Z) &= p(t, x, z) = p_0(t, x, z) + \epsilon^2 p_1(t, x, z) + \mathcal{O}(\epsilon^4),\\ \widetilde{H}^{-1} \cdot H(T, X) &= h(t, x) = h_0(t, x) + \epsilon^2 h_1(t, x) + \mathcal{O}(\epsilon^4), \end{aligned}$$

then the leading order term of that expansion depends on the choice of the scales. The smallness of the parameter

$$\epsilon = \frac{\widetilde{H}}{\widetilde{L}} = \frac{\widetilde{V}}{\widetilde{U}}$$

expresses that the film is flat and the mass flux is mainly into the $\mathbf{e}_x$ direction. It will be useful to write the relative magnitude of the slip by $b = \widetilde{b}\epsilon^r$, because it allows us to study different classes of lubrication equations. Different values of r yield different expansion of the Navier-Stokes equation (2.9) and every choice produces a different partial differential equation as the leading order in the asymptotic expansion.

Here the so-called strong-slip equation with $r = 2$ is used. With the scales

$$\Re := \frac{\rho\sigma\widetilde{H}}{\mu^2}, \qquad \widetilde{U} = \epsilon\,\frac{\sigma}{\mu} \qquad \widetilde{P} = \epsilon\,\frac{\mu\widetilde{U}}{\widetilde{H}}$$

the non-dimensionalized problem reads

$$\begin{aligned}
\epsilon^2\Re(u_t + uu_x + vu_z) &= -\,\epsilon^2 p_x + \epsilon^2 u_{xx} + u_{zz},\\
\epsilon^2\Re(v_t + uv_x + vv_z) &= -\,p_z + \epsilon^2 v_{xx} + v_{zz},\\
u_x + v_z &= 0,
\end{aligned}$$

in the bulk phase $\Omega(t)$. The boundary conditions at $z = h(t, x)$ are

$$\begin{aligned}
h_t - v + uh_x &= 0,\\
(u_z + \epsilon^2 v_x)(1 - \epsilon^2(h_x)^2) + 2\epsilon^2 h_x(v_z + u_x) &= 0,\\
p - \phi(h) - 2\frac{(1 - \epsilon^2(h_x)^2)v_z - h_x(u_z + \epsilon^2 v_x)}{1 + \epsilon^2(h_x)^2} + \frac{h_{xx}}{(1 + \epsilon^2(h_x)^2)^{3/2}} &= 0,
\end{aligned}$$

and at $z = 0$ there holds an impermeability and a Navier-slip condition

$$v = 0 \qquad \text{and} \qquad u = \widetilde{b}u_z.$$

We skip a detailed derivation of the lowest order equation, because it can be found in [9]. Instead we perform a more detailed derivation of the strong-slip lubrication model with cylindrical symmetry. Anyways, these equations can be integrated and the lowest order of the asymptotic expansion is determined by the *strong-slip equation*

$$h_t^0 + (h^0u^0)_x = 0, \tag{2.10a}$$

$$\Re(u_t^0 + u^0u_x^0) = \frac{4}{h^0}(h^0u_x^0)_x + \left(h_{xx}^0 - \phi(h^0)\right)_x - \widetilde{b}^{-1}\frac{u^0}{h^0}. \tag{2.10b}$$

For readability we drop the superscript "0" and the tilde over the b in the future. There are three additional important models which we will just mention but not derive. The first model is the so-called *intermediate-slip equation*

$$h_t = -\beta \left[h^2(h_{xx} - h^{-3})_x\right]_x . \tag{2.11}$$

To act naive[4], we can obtain the intermediate-slip equation from the strong-slip equation Equation (2.10) by a suitable scaling in terms of b and then letting $b \to 0$, i.e., solutions of the intermediate-slip equation might be limiting solutions of the strong-slip equation. Of course it can be also recovered from the asymptotic expansion by use of the scales

$$\Re = \epsilon^{\gamma-1}\frac{\rho\sigma\widetilde{H}}{\mu^2}, \qquad \widetilde{U} = \epsilon^{2-\gamma}\,\frac{\sigma}{\mu} \qquad \widetilde{P} = \epsilon^{2-\gamma}\,\frac{\mu\widetilde{U}}{\widetilde{H}},$$

for any $-1 < \gamma < 1$ and with the slip length scaled as $\beta = \widetilde{b}/\epsilon^{\gamma+1}$. The second model is the so called *weak-slip equation*

$$h_t = -\left[\left(\frac{h^3}{3} + \tilde{b}h^2\right)\left(h_{xx} - h^{-3}\right)_x\right]_x . \tag{2.12}$$

The connection between (2.12) and (2.11) is that the latter can be obtained in the limit $\tilde{b} \to \infty$ with the scaling $t = \tilde{t}/\tilde{b}$ and $u = \tilde{b}\tilde{u}$ for $h = O(1)$. Both differ in the definition of the so-called mobility $m(h)$ in

$$h_t = -\left[m(h)\Big(h_{xx} - \phi(h)\Big)_x\right]_x$$

where $m(h) = h^2$ in Equation (2.11) while $m(h) = h^3/3 + \tilde{b}h^2$ in Equation (2.12). Basic techniques to prove existence and uniqueness for such degenerate parabolic equations are due to Bernis and Friedman [7], the singular van der Waals potential leads to finite time singularities and renders strong solutions meaningless at some point. Note that we use the abbreviation $\phi(h)_x = \phi'(h) \cdot \partial_x h$. Even without the strongly singular interaction $\phi(h) = 1/h^3$, Bernis and Friedman find that positivity of such equations strongly depends on the behavior of the mobility function $m(h)$ close to zero.

On the other hand, if we send the slip-length in (2.10) to infinity we obtain the equation corresponding to perfect slip at the solid-liquid interface, i.e., $U_Z = 0$. The problem corresponds to the dynamics of a free film or liquid sheet, where both sides of the interface attract each other due to intermolecular forces. The model can be written

---

[4] Naive because it is not obvious why a solution h_ϵ, u_ϵ should converge to a solution of the weak-slip equation.

$$h_t + (hu)_x = 0, \tag{2.13a}$$

$$\Re(u_t + uu_x) = \frac{4}{h}(hu_x)_x + \left(h_{xx} - h^{-3}\right)_x. \tag{2.13b}$$

Vaynblat et al. [49] consider this equation and study symmetry of self-similar solutions when $\min_x h(t,x)$ approaches zero. In addition to their work, we study the dependence on the Reynolds number $\Re$ and the slip length b. In particular we also consider $\Re = 0$ and compute solutions of the strong-slip equation for small b and small $\Re$.

For completeness the strong-slip equation for a cylindrically symmetric flow is derived. Even though the procedure is simple and analogous to the derivation of the strong-slip equation in two dimensions, we show the detailed derivation for this special case in three dimensions. From stability analysis one would expect that in three dimensions rupture of a liquid film produces circular holes in the liquid films, that is to say the proper symmetry is cylindric symmetry. Nonetheless we will restrict to the 2-dimensional setup corresponding to rupture along a line later.

2.7 Lubrication Model with Cylindrical Symmetry

In this section the lubrication model with strong slippage and with cylindrical symmetry will be derived. We follow the usual approach previously applied to free-slip, weak-slip, intermediate-slip, and the strong-slip equation. The cylindrical symmetric domain is defined by

$$\Omega_c(T) = \left\{ (R,\varphi,Z) \in \mathbb{R}^3 : \begin{array}{l} 0 \le Z \le H(T,R) \\ 0 \le R \\ 0 \le \phi < 2\pi \end{array} \right\}.$$

By writing $H(T,R)$ it is already assumed that the domain is cylindrically symmetric. The boundary of $\Omega_c(T)$ has the two parts

$$\Gamma_s = \left\{(R,\varphi,Z) \in \mathbb{R}^3 : Z = 0; 0 \le \varphi < 2\pi\right\},$$
$$\Gamma_l = \left\{(R,\varphi,Z) \in \mathbb{R}^3 : Z = H(T,R); 0 \le \varphi < 2\pi\right\},$$

which are the liquid–solid and the (free) liquid–gas interface respectively. The sketch of the domain $\Omega_c(T)$ is shown in the figure below.

Furthermore suppose the 3-dimensional velocity field $\mathbf{U} = (U,V,W)$ (radial, angular, cylindrical direction) has no angular component. We assume this symmetry holds for all times and by transforming the usual 3-dimensional

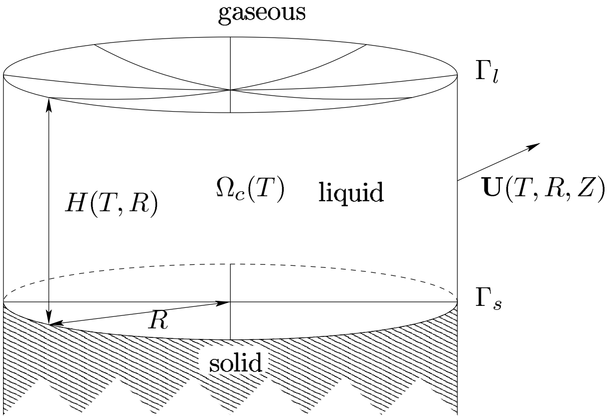

Figure 2.5: Sketch of domain with cylindrical symmetry

Navier-Stokes equation to cylindrical coordinates we obtain the following set of equations. The momentum equation

$$\rho(U_T + UU_R + WU_Z) = -\,P_R + \mu\left(\Delta_r U - \frac{U}{R^2}\right), \tag{2.14a}$$

$$\rho(W_T + UW_R + WW_Z) = -\,P_Z + \mu\Delta_r W, \tag{2.14b}$$

where the Laplace operator for scalar functions $\Delta_x = \partial_X^2 + \partial_Y^2 + \partial_Z^2$ reduces to

$$\Delta_r F = \frac{(RF_R)_R}{R} + F_{ZZ}$$

if F does not depend on φ. Conservation of mass in can be written as

$$\mathrm{div}_r U + W_Z = 0 \tag{2.14c}$$

where the radial divergence is defined as $\mathrm{div}_r U := (RU)_R/R$. All these equations hold inside the fluid phase, i.e., for small times $0 < T < T^*$ and for all points inside $\Omega_c(T)$.

On the liquid–solid and liquid–gas interface the following boundary conditions are needed. The kinematic boundary condition

$$H_T = W - UH_R \tag{2.14d}$$

specifies the evolution of the free interface Γ_l, whereas equilibrium of normal and tangential forces on that interface implies

$$\begin{aligned} -P + \Phi(H) + \frac{2\mu}{1+H_R^2}\left[W_Z + U_R H_R^2 - (W_R + U_Z)H_R\right] = \\ \gamma\,\mathrm{div}_r\left(H_R\Big/\sqrt{1+H_R^2}\right), \end{aligned} \tag{2.14e}$$

$$2(W_Z - U_R)H_R + (W_R + U_Z)(1 - H_R^2) = W, \tag{2.14f}$$

where we included the van der Waals force into the boundary condition from the beginning. This is possible by substituting all expressions containing the pressure by $P(T,X,Z)-\Phi\big(H(T,X)\big)$. The impermeability and Navier-slip condition at the solid–fluid interface are

$$W = 0, \tag{2.14g}$$

$$U = BU_Z. \tag{2.14h}$$

The system (2.14) contains all physical scales before simplification. For completeness note that the components of the fluid stress-tensor are

$$\begin{aligned}
&\sigma_{RR} = -P + 2\mu U_R, && \sigma_{R\varphi} = 0, && \sigma_{\varphi\varphi} = -P + 2\mu\frac{U}{R},\\
&\sigma_{\varphi Z} = 0, && \sigma_{ZZ} = -P + 2\mu W_Z, && \sigma_{ZR} = \mu(W_R + U_Z),
\end{aligned}$$

if we assume that the velocity field is cylindrical symmetric. As for the 2-dimensional model, we introduce physical scales and a small parameter $\epsilon = \widetilde{H}/\widetilde{R}$ as follows

$$\begin{aligned}
&Z = \widetilde{H}\,z, && H = \widetilde{H}\,h, && B = \widetilde{H}\,b, && R = \widetilde{R}\,r = \epsilon^{-1}\widetilde{H}\,r,\\
&U = \widetilde{U}\,u, && W = \epsilon\widetilde{U}\,w, && T = \widetilde{H}(\epsilon\widetilde{U})^{-1}\,t, && P = \widetilde{P}p.
\end{aligned}$$

The rescaled version of the van der Waals potential Φ is ϕ. Since we are interested in the strong-slip model in 3-dimensions with cylindrical symmetry, we use the scales analogous to the 2-dimensional strong-slip model, i.e.,

$$\begin{aligned}
\frac{\rho U H}{\mu} &= \epsilon\,\Re,\\
\frac{PH}{\mu U} &= \epsilon,\\
\frac{U\mu}{\sigma} &= \epsilon.
\end{aligned}$$

In a compact notation we end up with the following model: Conservation of momentum in the fluid phase $\Omega_c(t)$:

$$\epsilon^2\Re(u_t + uu_r + wu_z) = -\epsilon^2 p_r + u_{zz} + \epsilon^2\left(\mathrm{div}_r u_r - \frac{u}{r^2}\right), \tag{2.15a}$$

$$\epsilon^2\Re(w_t + uw_r + ww_z) = -p_z + w_{zz} + \epsilon^2\mathrm{div}_r w_r, \tag{2.15b}$$

and conservation of mass in the fluid phase $\Omega_c(t)$:

$$\mathrm{div}_r u + w_z = 0. \tag{2.15c}$$

The kinematic boundary condition on the air-liquid interface $z = h(r,t)$:

$$h_t + uh_r - w = 0, \tag{2.15d}$$

and conservation of momentum on the air-liquid interface:

$$-p+\phi+\frac{2}{1+\epsilon^2 h_r^2}\left[w_z+\epsilon^2 u_r h_r^2-(\epsilon^2 w_r+u_z)h_r\right]=\mathrm{div}_r\frac{h_r}{\sqrt{1+\epsilon^2 h_r^2}}, \tag{2.15e}$$

$$2\epsilon^2(w_z-u_r)h_r+(\epsilon^2 w_r+u_z)(1-h_r^2)=0. \tag{2.15f}$$

And finally we have impermeability and the Navier-slip condition on the solid-liquid interface at $z=0$:

$$w=0, \tag{2.15g}$$

$$u=bu_z. \tag{2.15h}$$

As usual, we assume that solutions (u,w,h,p) of the Navier-Stokes equation in non-dimensional form (2.15) can be decomposed into an asymptotic series of the form

$$\begin{aligned} u(t,r,z;\epsilon) &= u^0(t,r,z)+\epsilon^2 u^1(t,r,z)+O(\epsilon^4),\\ w(t,r,z;\epsilon) &= w^0(t,r,z)+\epsilon^2 w^1(t,r,z)+O(\epsilon^4),\\ h(t,r;\epsilon) &= h^0(t,r)+\epsilon^2 h^1(t,r)+O(\epsilon^4), \end{aligned}$$

such that as $\epsilon\to 0$ each term in the decomposed solution is asymptotically smaller then the next order. In what follows we will be only interested in the solution of the lowest order problem (u^0,w^0,h^0,p^0). Hence, for reasons of readability, we drop the superscript for the lowest order, and obtain to leading order the following set of partial differential equation: In the bulk phase $\Omega_c(t)$ we have

$$u_{zz}=0, \tag{2.16a}$$

$$-p_z+w_{zz}=0, \tag{2.16b}$$

$$\frac{(ru)_r}{r}+w_z=0, \tag{2.16c}$$

whereas on the free boundary Γ_l we have

$$h_t-w+uh_r=0, \tag{2.16d}$$

$$-p+\phi+2(w_z-u_z h_r)=\frac{(rh_r)_r}{r}, \tag{2.16e}$$

$$u_z=0. \tag{2.16f}$$

The the solid–fluid interface Γ_s the Navier-slip and the impermeability condition hold

$$w=0 \tag{2.16g}$$

$$u=bu_z \tag{2.16h}$$

The different terms in (2.16) originate from the terms in (2.14) and (2.15) with the corresponding index (a-h).

The leading order bulk equations of (2.16) clearly show that the leading order u and p are solely functions of r and t and independent from z, hence we can integrate the leading order equations in the following way

$$\begin{aligned} w(r,z,t) &= -z\,\operatorname{div}_r u, && (2.17\text{a})\\ -p(r,t) &= \operatorname{div}_r h_r - \phi + 2\,\operatorname{div}_r u, && (2.17\text{b})\\ h_t + \operatorname{div}_r hu &= 0. && (2.17\text{c}) \end{aligned}$$

Yet, system (2.17) provides insufficient information in order to determine $u(t,r)$ and $h(t,r)$ for given initial data. Therefore we have to check higher order terms u^1, etc., of the asymptotic expansion in order to have a well posed lowest order problem. We defined u^1 to be the $O(\epsilon^2)$ term in the asymptotic expansion. All we will need from the next order are the two equations

$$\Re(u_t + uu_r) = -\epsilon^2 p_r + u^1_{zz} + \left(\frac{(ru_r)_r}{r} - \frac{u}{r^2}\right) \tag{2.18}$$

in $\Omega_c(t)$ and at the air-liquid interface

$$2(w_z - u_r)h_r + w_r + u^1_z = 0. \tag{2.19}$$

The first equation can be integrated over z and the latter equation is used to fix the constant of integration. We divide by h and obtain

$$\begin{aligned} \Re(u_t + uu_r) &= -\,p_r + \left.\frac{u^1_z}{h}\right|_{z=0}^{z=h} + \left(\frac{(ru_r)_r}{r} - \frac{u}{r^2}\right),\\ &= \left(\operatorname{div}_r(h_r + 2u) - \phi\right)_r + \left(\operatorname{div}_r u_r - \frac{u}{r^2}\right) + \left.\frac{u^1_z}{h}\right|_{z=0}^{z=h} \qquad, \end{aligned}$$

with the u^1_z

$$\begin{aligned} u^1_z(z=h) =& (-w_r - 2h_r(w_z - u_r))_{z=h} = h\left(\operatorname{div}_r u\right)_r + 2h_r\left(\operatorname{div}_r u + u_r\right),\\ u^1_z(z=0) =& \frac{u}{b}. \end{aligned}$$

Finally, the *strong-slip equation* with *cylindrical symmetry* is given by

$$h_t + \operatorname{div}_r hu = 0, \tag{2.20a}$$

$$\Re(u_t + uu_r) = \left(\operatorname{div}_r(h_r + 3u) - \phi\right)_r + \Delta_r u + \frac{2h_r}{h}(\operatorname{div}_r u + u_r) - b^{-1}\frac{u}{h}. \tag{2.20b}$$

What remains to be done is to specify boundary conditions for $h(t,r)$ and $u(t,r)$ at $r = 0$, and, in case we want to compute solutions in a finite box, at some maximal radius R. Where the latter depends very much on the experimental setup which one would like to describe, regularity of the liquid interface and symmetry of the setup imply

$$u(t,0) = 0, \tag{2.20c}$$

$$h_r(t,0) = 0. \tag{2.20d}$$

Chapter 3

Numerical Analysis of Thin-Film Rupture

3.1 Motivation

In the previous chapter different thin film models containing slipppage were presented. The main reasons that we only analyze the strong-slip equation[1]

$$h_t + (hu)_x = 0, \tag{3.1a}$$

$$\Re(u_t + uu_x) = \frac{4}{h}(hu_x)_x + (3h_{xx} - h^{-3})_x - b^{-1}\frac{u}{h} \tag{3.1b}$$

are these: First, in the limit $b \to \infty$ and $b \to 0$ the strong-slip equation corresponds to the free-slip model and the intermediate-slip model respectively, and, as we will see in our numerics, one can reproduce the corresponding (self-similar) solutions. This makes that strong-slip model an excellent model to study the impact of the slip-length b on the onset and nonlinear behavior of interfacial singularities.

Second, if inertia is neglected in the strong-slip equation, i.e., $\Re = 0$, we observe novel similarity solutions of so-called *second kind*[2]. There are only a few studies which consider interface singularities of thin liquid films, where the singularity evolves self-similarly and is of the second kind [19, 23]. Finally, a rigorous mathematical approach showing properties like convergence to self-similar solutions is still missing — for self-similar solutions that are of first *and* of second kind.

Within this chapter we employ a numerical analysis to seek self-similar solutions for various parameters and initial conditions. Afterwards, in the next chapter, we provide a rigorous analysis in a simplified setting. This chapter contains three main parts. In the beginning we explain the numerical algorithm that is used to solve the strong-slip equation. We direct the reader's attention to the high desired precision of the algorithm together with the necessary stability of the method. We achieved both goals by combining an implicit scheme in time with an adaptive discretization on a staggered spatial grid. This algorithm is the prerequisite of the next sections. Then we perform a stability analysis of the strong-slip model, which reveals that small perturbations of a flat film profile $h(t,x) = 1$ and $u(t,x) = 0$ are linearly unstable. Nonlinearities in the model even accelerate the rupture in such a way that the speed at which h goes to zero becomes infinite.

Afterwards we introduce the notion of self-similarity of *first* and *second kind*. Our numerical solutions converge self-similar solutions for various choices of parameters and initial data. We provide parameters and initial data for which we observe up to three different approximate scaling regimes in a single solution, out of which two are transient regimes and only one is stable. A detailed study of those solutions and transitions between different self-similar solutions will be presented.

---

[1] For consistency with previous computations a factor 3 is introduced in front of the surface tension.

[2] For an introduction to self-similarity of first and second kind we refer to the book by Barenblatt[20]

Finally, we set $\Re = 0$ and observe a novel similarity regime and calculate properties of the similarity solutions with high numerical precision. In order to simplify the strong-slip equation we perform the standard reduction to ordinary differential equation. A similarity solution is characterized by its shape and similarity scales, i.e., for the strong-slip equation the scales are three real numbers. For second-kind similarity solutions, however, the similarity scales are not a priori known, and, therefore, it is not obvious straight away how to reduce the strong-slip equation to an ordinary differential equation.

We will derive the missing condition to determine all similarity scales, analogous to Papageorgiou [19], who studied self-similar solutions of second kind for jet pinch-off. The results from the reduced ordinary differential equation are in excellent agreement with the results from the strong-slip equation.

3.2 Strong-Slip Equation with Finite Differences

A prerequisite to study the nonlinear evolution of rupture is a stable numerical algorithm that provides a high spatial and temporal resolution near the singularity. This can be achieved by disrectizing the strong-slip equation on a staggered spatial grid and using an implicit Euler scheme to solve the time-dependence. An additional adaptive refinement of the spatial grid provides an improved spatial resolution of the solution close to the singularity. The time-step is automatically refined using standard step-size bisection, where a given tolerance for the relative error ensures that the time-step decreases as the singular time t^* is approached. This technique allows us to resolve the height $h(t,x)$ and the velocity $u(t,x)$ for about 20 orders of magnitude, and therefore we can study solutions that undergo transitions between different regimes with different self-similar behavior. Similar numerical methods are applied by Vaynblat et al. [27].

Even though we do not prove convergence of the method, which is non-trivial when the solution approaches a singularity and the equation degenerates, we observed that solutions are stable and compared to other methods, such as explicit time-stepping and Keller's box-schemes to discretize the spatial derivatives, the present method proved to be quite efficient. Quantitative properties of the numerical solution the strong-slip equation agree very well with results obtained by other methods, e.g., the similarity scale of the partial differential equation and the limiting ordinary differential equation agree with a relative precision of about 10^{-5}.

As usual we store the solution for the height $h(t,x)$ and for the velocity $u(t,x)$ only at certain discrete mesh points x_i, where i is from a finite index set $\mathcal{I}$. We use a staggered grid, where h and u are stored at different mesh points; values of the height are stored at positions denoted by integer i, and the velocity is stored at points with indices denoted by $i+1/2$. We have $\hat{h}_i(t) = h(t, x_i)$ and $\hat{u}_{i+1/2} = u(t, x_{i+1/2})$. The index set is composed of both integer and non-integer indices $\mathcal{I} = (-1, -1/2, \dots N-1/2, N)$ and ordered according to the ordering of points $x_i < x_j$ if $i < j$ for $i, j \in \mathcal{I}$. Similarly, the evaluation of a solution at different discrete times $t = t^n$ is denoted by an upper index n, e.g., $\hat{h}_i^n = h(t^n, x_i)$ and so on. The locations x_i and $x_{i+1/2}$ fulfill the relation $x_{i+1/2} = \frac{1}{2}(x_i + x_{i+1})$. For simplicity we arrange the discrete solution in a vector

$$\hat{w} = \big(\hat{h}_{-1}, \hat{u}_{-1/2}, \hat{h}_0, \hat{u}_{1/2}, \dots, \hat{u}_{N-3/2}, \hat{h}_{N-1}, \hat{u}_{N-1/2}, \hat{h}_N\big)^\top \in \mathbb{R}^{2N+3}.$$

This construction of the staggered mesh is illustrated in Figure 3.1.

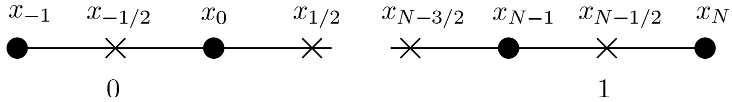

Figure 3.1: Staggered grid with h_i located on circles, and $u_{i+1/2}$ on crosses. We consider the strong-slip equation only in the domain $\Omega = [0,1]$. The positions $x_{-1/2} = 0$ and $x_{N-1/2} = 1$ represent the boundaries of Ω so that the (ghost) points x_{-1} and x_N lie outside Ω.

One does not seek the exact solution $\hat{w}$ but approximate solutions $w \approx \hat{w}$ that converge to $\hat{w}$ as the staggered grid and the time step $\tau = t^n - t^{n-1}$ are refined. While the original solution h and u solve a partial differential equation, the approximate solution w solves a ordinary differential equation, where the spatial derivatives are replaced by finite difference formulas that one can obtain by Taylor expansions. The ordinary differential equation is discretized as well such that the approximate discrete solution w at time t^n and t^{n-1} solve a system of nonlinear equations $\mathrm{Res} : \mathbb{R}^{2N+3} \times \mathbb{R}^{2N+3} \times \mathbb{R} \to \mathbb{R}^{2N+3}$ that can be written like

$$0 = \mathrm{Res}\left(w^n, w^{n-1}, \tau\right)$$

In addition to the given variables, the function $\mathrm{Res} : \mathbb{R}^{2N+3} \times \mathbb{R}^{2N+3} \times \mathbb{R} \to \mathbb{R}^{2N+3}$ depends only the mesh $\{x_i\}_{i \in \mathcal{I}}$. We begin with a discussion of the finite difference scheme for the staggered grid. Notice that the staggered formulation implies that terms in the $\dot{h}$ equation are discretized at x_i, while the terms in the $\dot{u}$ equation are discretized at $x_{i+1/2}$. To shorten expressions slightly, define $a = x_i - x_{i-1}$, $b = x_{i+1} - x_i$, $c = x_{i+2} - x_{i+1}$, the interpolation of h onto $x_{i+1/2}$ by $h_{i+1/2} = \frac{1}{2}\big(h_{i+1} + h_i\big)$, and the interpolation of u onto x_i correspondingly by $u_i = \frac{1}{2}\big(u_{i+1/2} + u_{i-1/2}\big)$.

Then, the divergence term in the transport equation reads

$$\Big[(hu)_x\Big](x_i) = \frac{h_{i+1/2}\, u_{i+1/2} - h_{i-1/2}\, u_{i-1/2}}{(a+b)/2} + \mathcal{O}\big(|b-a| + a^2\big), \tag{3.2a}$$

where the $\mathcal{O}$ term is the usual higher order term from the Taylor expansion. On uniform grids ($a = b$) the scheme is of second order. The other terms are material derivative

$$\Big[uu_x\Big](x_{i+1/2}) = u_{i+1/2}\frac{u_{i+1} - u_i}{b} + \mathcal{O}\big(|c-a| + a^2\big), \tag{3.2b}$$

surface tension

$$\begin{aligned}\Big[h_{xxx}\Big](x_{i+1/2}) = {} & \frac{6h_{i+2}}{c(c+b)(a+b+c)} - \frac{6h_{i+1}}{bc(a+b)} + \frac{6h_i}{ab(b+c)} \\ & - \frac{6h_{i-1}}{a(a+b)(a+b+c)} + \mathcal{O}\big(|c-a| + a^2\big),\end{aligned} \tag{3.2c}$$

van der Waals potential

$$\Big[\phi(h)_x\Big](x_{i+1/2}) = \frac{\phi(h_{i+1}) - \phi(h_i)}{b} + \mathcal{O}(a^2), \tag{3.2d}$$

and finally the (Trouton) viscosity term

$$\begin{aligned}&\Big[(hu_x)_x\Big](x_{i+1/2}) = \mathcal{O}\big(|c-a| + a^2\big) \\ &+\frac{2}{b}\Bigg[h_{i+1}\Big(\frac{u_{i+3/2}\,(a+3b)}{(b+c)(a+2b+c)} - \frac{u_{i+1/2}\,(a+2b-c)}{(a+b)(b+c)} + \frac{u_{i-1/2}\,(b-c)}{(a+b)(a+2b+c)}\Big) \\ &\qquad -h_i\Big(\frac{u_{i+3/2}\,(a-b)}{(a+2b+c)(b+c)} + \frac{u_{i+1/2}\,(2b+c-a)}{(a+b)(b+c)} - \frac{u_{i-1/2}\,(3b+c)}{(a+b)(a+2b+c)}\Big)\Bigg].\end{aligned} \tag{3.2e}$$

The factor $4/h$ in front of the viscosity is simply discretized as $4/h_{i+1/2}$, where $h_{i+1/2}$ is the projection of h that was described before. From the Taylor expansion we see that the staggered spatial discretization scheme (3.2) has the consistency order

$$\mathcal{O}\big(|c-a| + |b-a| + a^2 + b^2\big),$$

whereas the scheme becomes second order if the mesh is uniform or sufficiently smooth, e.g., $|b-a| = \mathcal{O}(a^2 + b^2)$ and so on.

For ease of the numerical computation we use the boundary conditions $u(t,x) = 0$ and $h_x(t,x) = 0$ at $x = 0$ and $x = L$. This choice does not affect our later results but makes the Jacobian matrix

$$d\mathrm{Res} = \frac{\partial\big(\mathrm{Res}\,(w^n, w^{n-1}, \tau)\big)}{\partial(w^n)}$$

of the nonlinear system of equations banded. The mesh points $\{x_i\}_{i\in\mathcal{I}}$ are chosen such that the boundary points $x = 0$ and $x = 1$ correspond to the points $x_{-1/2}$ and $x_{N-1/2}$, which ensures that the discrete boundary conditions

$$u_{-1/2} = 0, \qquad u_{N-1/2} = 0, \qquad h_{-1} = h_0, \qquad h_N = h_{N-1},$$

have a better consistency order on smooth meshes.

3.3 Solver for the Nonlinear Equation

Basically we have to solve two types of equation: Equation (3.1b) with $\Re > 0$ and with $\Re = 0$. While the former is an initial value problem for h and u, the latter is an initial value problem for h coupled to an algebraic differential equation for u. The advantage of our formulation is that both equation can be treated similarly. The time-derivative is discretized in an implicit Euler scheme, i.e., all terms in the spatial derivatives are evaluated at time t^n. Now we simply combine all terms in the following difference scheme

$$\operatorname{Res} h_i = h_i^n - h_i^{n-1} + \tau \left[(hu)_x\right]_i^n , \tag{3.3a}$$

$$\operatorname{Res} u_{i+1/2} = \Re\big(u_{i+1/2}^n - u_{i+1/2}^{n-1}\big) - \tau \left[\frac{4}{h}(hu_x)_x - \Re u u_x + 3h_{xxx} - \phi_x\right]_{i+1/2}^n , \tag{3.3b}$$

where the boundary conditions are expressed by

$$\operatorname{Res} h_{-1} = h_1^n - h_{-1}^n, \qquad \operatorname{Res} u_{-1/2} = u_{-1/2}^n, \tag{3.3c}$$

$$\operatorname{Res} h_N = h_{N-1}^n - h_N^n, \qquad \operatorname{Res} u_{N-1/2} = u_{N-1/2}^n. \tag{3.3d}$$

To obtain a banded Jacobian define the function $\operatorname{Res}(w^n, w^{n-1}, \tau) \in \mathbb{R}^{2N+3}$ as follows

$$\operatorname{Res}(w^n, w^{n-1}, \tau) = \big(\operatorname{Res} h_{-1}, \operatorname{Res} u_{-1/2}, \ldots, \operatorname{Res} u_{N-1/2}, \operatorname{Res} h_N\big)^\top , \tag{3.4}$$

which are $2N+3$ nonlinear equations for $2N+3$ unknowns w^n. The difference star is shown in Figure 3.2.

Fixing the old solution w^{n-1}, a Newton-Raphson method is employed in order to find a new solution w^n such that $\operatorname{Res}(w^n, w^{n-1}, \tau) = 0$. A sufficiently small time-step τ ensures that the initial guess is close to the actual solution and the method converges. Given some solution w^{n-1} at the time t^{n-1}, a preliminary new solution w_j^n at the time t^n is constructed as follows:

1. Select preconditioned initial guess w_0^n, e.g., the simplest one would be $w_0^n = w^{n-1}$. For sufficiently small τ and if $\operatorname{Res}(\cdot, w^{n-1}, \tau)$ is invertible near w^{n-1}, this initial guess is arbitrarily close the solution w^n.

2. Compute a new iterate by a Newton-Raphson step

$$w_{j+1}^n = w_j^n - \left(\frac{\partial \operatorname{Res}(w_j^n, w^{n-1}, \tau)}{\partial w^n}\right)^{-1} \cdot \operatorname{Res}(w_j^n, w^{n-1}, \tau).$$

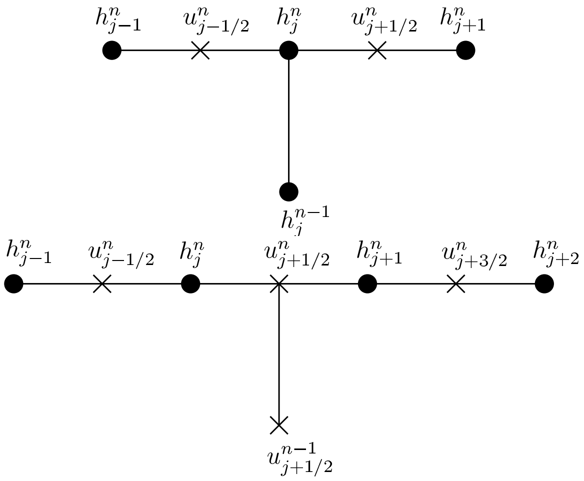

Figure 3.2: Difference scheme to compute $\dot{h}^n$ (left) and $\dot{u}^n$ (right) in the strong-slip equation. On a nonuniform mesh the spatial derivatives are consistent with $\mathcal{O}(x_{j+1} - x_{j-1})$.

3. If the relative error

   $$\epsilon = \max \left|\operatorname{Res}\,(w^n_{j+1}, w^{n-1}, \tau)\right|$$

   is larger than a predefined bound, then continue from 2 with $j+1$. If the algorithm does not converge (in a given number of steps), decrease τ and restart the algorithm.

4. Define the (approximate) new solution after the jth step: $w^n = w^n_j$

Note that due singularity of the potential $\phi(h) = h^{-3}$ at $h = 0$, the function $\operatorname{Res}\,(w^n, w^{n-1}, \tau)$ becomes singular if some h_i approaches zero and for any fixed τ the Jacobian matrix becomes ill conditioned. Thus, near the rupture convergence properties worsen, in particular smaller time steps τ are required in order to compute precise solutions.

Using step-size bisection, an error estimate for the current time-step can be obtained by comparing the solution w of $\operatorname{Res}\,(w, w^{n-1}, \tau) = 0$ with the solution $\widetilde{w}$ of the equations $\operatorname{Res}\,(\widetilde{w}, w^{1/2}, \tau/2) = 0$ and $\operatorname{Res}\,(w^{1/2}, w^{n-1}, \tau/2) = 0$. With $\Delta = w - \widetilde{w}$ and w^* the exact solution of the ordinary differential equation in we have the usual error estimate

$$w^*(t^n) - \widetilde{w} = 2\Delta + \mathcal{O}(\tau^3).$$

After each step the time-step is adjusted such that $\max |\Delta/\widetilde{w}|$ is smaller than a certain predefined precision goal[3].

---

[3] The division of vectors in this formula is understood componentwise.

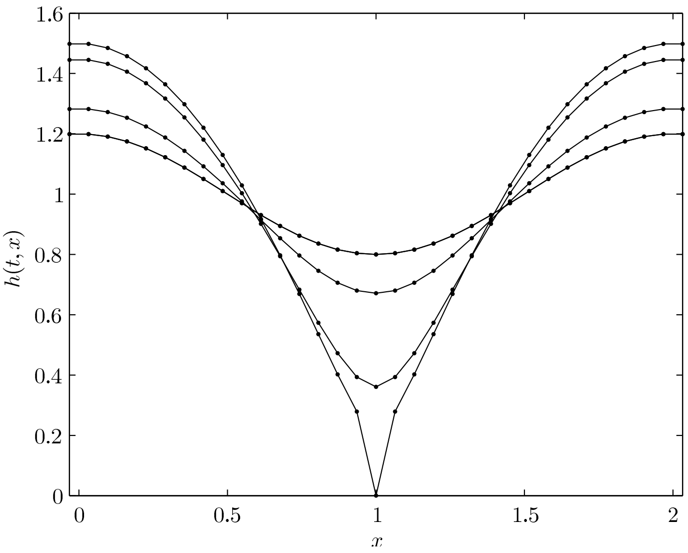

Figure 3.3: Numerical solution of the strong-slip equation on a uniform mesh with only $N = 31$ mesh points, domain $\Omega = [0, L]$ with $L = 2$, Hamaker constant $A_{\mathrm{vdw}} = 1/(2\pi^2)$, and initial data $h_0(x) = 1 + 0.2\cos(\pi x)$ and $u_0(x) = 0$; dots show the values $\{h_i\}_{i\in\{-1,0,\dots,N\}}$ at different times.

Now we are going to discuss adaptive mesh refinement as a possibility resolve the spatial dependence of the singularity as well. Figure 3.3 shows a numerical solution of the strong-slip equation, which corresponds to rupture of a liquid film on a solid substrate and is obtained on a uniform mesh with the method described before. The figure shows the height h_i at discrete mesh points connected by straight lines. Obviously, as the minimal thickness $\min_{\mathcal{I}} h_i$ approaches zero at some point $x^* = x_m$ with $m \in \mathcal{I}$, properties like higher order derivatives are less accurate near x^*. But since we are particularly interested in the behavior of the solution near x^*, we have the adapt the mesh in order to reduce such kind of inaccuracies. Even though some properties of the solution in Figure 3.3 are unreliable, notice that there are no apparent numerical instabilities, i.e., the solution does not oscillate and remains positive.

Obviously, there are many feasible methods to compute a suitable mesh; for example one can compute the local error and increase the mesh resolution where the local error is too large, or one could work on nonuniform but fixed meshes. An example for the latter approach is shown in Figure 3.4.

Observe that h_i and its derivatives can be measured for much smaller length and height scales but still this algorithm has two main drawbacks. 1) In order to observe the solution as $\min_x h(t,\cdot) \to 0$ we have to use extremely fine meshes from the start. 2) Even though one can construct such a mesh, the precision is limited due to loss of significance at points where the mesh

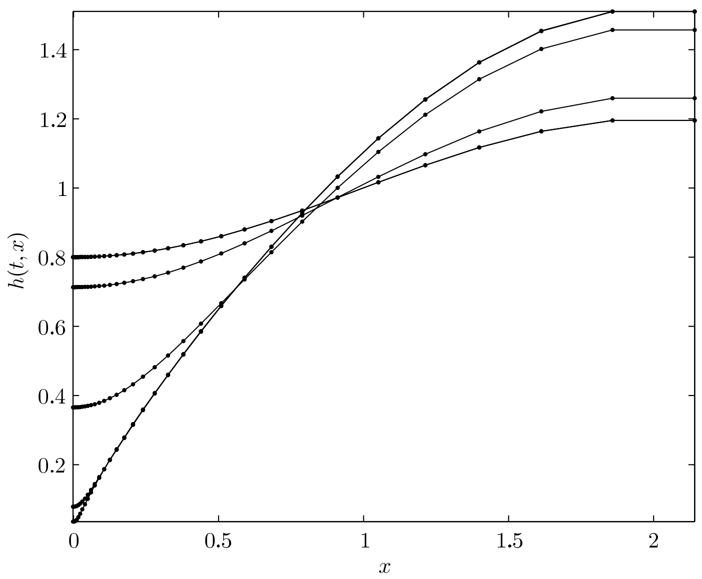

Figure 3.4: Solution of the strong-slip equation, parameters like in Figure 3.3 but with non-uniform fixed mesh and initial data $h_0(x) = 1 - 0.2\cos(\pi x/2)$.

is fine but the solution and derivatives still $\mathcal{O}(1)$. For example, the lowest order approximation of the kth derivative of a smooth $\mathcal{O}(1)$ function $f(x)$ on a uniform grid with mesh spacing Δx has the discretization error

$$\frac{\partial^k h(x)}{\partial x^k} = \Delta^h f(x) + \mathcal{O}(\Delta x) + \mathcal{O}\left(\frac{\epsilon}{(\Delta x)^k}\right),$$

where the first term is the usual finite difference approximation of a higher order derivative obtained from a Taylor expansion of f, while the second term is due to the limited precision of numbers on a computer, e.g., double precision floating point numbers have $\epsilon = 10^{-16}$. In the strong-slip equation we have $3rd$ order derivatives $k = 3$, so the error above is minimal for $\Delta x \simeq \epsilon^{1/(k+1)} \simeq 10^{-4}$.

Now suppose $h(x)$ is not $\mathcal{O}(1)$ but rescaled, such that $h(x) = b\, f\big(x/a\big)$ with some positive a and b, which are not $\mathcal{O}(1)$, and $f(x) = \mathcal{O}(1)$ as before[4]. In this case numerical derivatives of h have the same relative error like the ones of f, if the mesh size is rescaled by a factor $1/b$. This is our guiding principle to refine meshes for self-similar solutions; assume there exists a $f = \mathcal{O}(1)$ and compute the scaling factor b from the expression $\sqrt{|h/h''|} = a\sqrt{|f/f''|}$, where one replaces f/f'' by some constant $\mathcal{O}(1)$ value. This replacement is legitimate away from regions where f'' is zero or too small.

Since we have the expectation that the solution of the strong-slip equation is self-similar near the singularity, we can compute a mesh that reflects expectation. This concept has the advantage that it is simple to implement and well suited for self-similar singularities, however, the errors of the spatial discretization are not considered. Given an approximate solution h_i and u_i, the solution on the refined mesh is computed as follows:

---

[4] Assume that higher order derivatives exist and are also $\mathcal{O}(1)$.

1. A new local mesh spacing at the point x_i is given by
$$a_i = \min\left\{ e \cdot \sqrt{\frac{2\,h_i}{\max\{|[h_{xx}](x_i)|\,,1\}}}\,,\, a_{\max} \right\},$$
where $0 < e \ll 1$ is some desired precision, and $a_{\max}$ is the largest possible mesh spacing. This definition does not involve the values of the velocity $u_{i+1/2}$.
2. Define $a(x)$ for $x \in (x_i, x_{i+1})$ as the linear interpolation of a_i and a_{i+1}, and $a_{\text{new}} = a_0$.
3. Start with $\tilde{x}_{-1} = -a_{\text{new}}/2$ and $\tilde{x}_0 = a_{\text{new}}/2$
4. Set $a_{\text{old}} = a_{\text{new}}$ and for some $\alpha > 1$ define $x_{i+1} = x_i + a_{\text{new}}$ using
$$a_{new} = \begin{cases} \alpha^{-1} a_{\text{old}} & : a(\tilde{x}_i) < \alpha^{-1} a_{\text{old}} \\ \alpha\, a_{\text{old}} & : a(\tilde{x}_i) > \alpha\, a_{\text{old}} \\ a(\tilde{x}_i) & : \text{else} \end{cases}$$
and repeat this procedure until $\tilde{x}_{n+1} > L$. Then set $\widetilde{x}_{n+1}$ such that $\widetilde{x}_{n+1/2} = L$ and define $\widetilde{x}_{i+1/2} = (\widetilde{x}_i + \widetilde{x}_{i+1})/2$. If α ($\alpha > 1$) is close to 1 one gains extra regularity, but if α is too close to 1 or the number of mesh points N too small, then it might be impossible to resolve the singularity.
5. Using cubic splines with proper boundary conditions one can interpolate the old solution h_i and $u_{i+1/2}$ defined at x_i and $x_{i+1/2}$, onto the new mesh $\{\tilde{x}_j\}$ with $\tilde{h}_j$ $\tilde{u}_{j+1/2}$ at $\widetilde{x}_j$ and $\widetilde{x}_{j+1/2}$.

Then we continue the computation of the numerical solution. Since the solution does not change drastically, it suffices to compute a new mesh every 10 time steps. In the next section we make a quantitative comparison between the numerical solution and a known eigenstate of the linearized equation.

3.4 Linear Stability of the Flat State

What happens to the "flat state" solution of Example 2.1 if small perturbations are added? A linear stability analysis tells us whether the strong-slip equation with van der Waals forces predict that such a solution is linearly stable or unstable. The flat state solution

$$\bar{h}(t,x) = 1, \qquad \bar{u}(t,x) = 0 \qquad \forall t, x \in [0, L], \tag{3.5}$$

from Example 2.1 is an exact, stationary solution of the strong-slip equation. Suppose that another solution h is a small perturbation of this solution and can be written like $h = \bar{h} + \delta h$ and $u = \bar{u} + \delta u$, where δh and δu are sufficiently small. The linearization of the strong-slip equation reads

$$-\delta u_x = \delta h_t \tag{3.6}$$

$$4\delta u_{xx} + 3\delta h_{xxx} + 3\delta h_x - b^{-1}\delta u = \Re \delta u_t \tag{3.7}$$

with boundary conditions $\delta u(0) = \delta u(L) = 0$ and $\delta h_x(0) = \delta h_x(L) = 0$. This is a linear partial differential equation for the perturbations δh and δu. Using the normal-mode approach, where one computes eigenstate solutions[5] of the form

$$\delta h(t,x) = h_0 \exp(ikx + \lambda t) \quad \text{and} \quad u(t,x) = u_0 \exp(ikx + \lambda t)$$

one obtains the equation

$$\begin{aligned} (iku_0 + \lambda h_0)\exp(ikx + \lambda t) &= 0, \\ (-4k^2 u_0 - 3ik^3 h_0 + 3ikh_0 - b^{-1}u_0 - \Re\lambda u_0)\exp(ikx + \lambda t) &= 0, \end{aligned}$$

which produces the following (inverse) dispersion relation

$$\begin{aligned} \lambda_\pm(k) &= \frac{1}{2b\Re}\left(-1 - 4bk^2 \pm \sqrt{\left(1 + 4bk^2\right)^2 - 12\,\Re\, b^2\, k^2\left(k^2 - 1\right)}\right) \\ &= \begin{cases} 3bk^2 + \mathcal{O}(k^4) & \text{unstable} \\ -\frac{1}{b\,\Re} + \mathcal{O}(k^2) & \text{stable} \end{cases} \end{aligned}$$

The last line shows the behavior of long waves. For $b \to 0$ and we get

$$\lambda_+(k) = 3bk^2(1 - k^2) + \mathcal{O}(b^2) \tag{3.8}$$

There are always unstable wavelengths $k \in (0, k^*)$, such that $\lambda(k) > 0$. But we still have to account for the boundary conditions. The domain $[0, L]$ with our boundary conditions only allows $k = (\pi n)/(2L)$ for any $n \in \mathbb{N}$. The phase of u_0 is chosen purely imaginary such that the real part of δu vanishes at the boundary. The mode $k = 0$ is not allowed because of the boundary conditions for u.

---

[5] Only the real part of δh and δu contributes to a real solution of the strong-slip equation.

Thus we have a root $\lambda(k = 1) = 0$ and if L is sufficiently small, that is, $\pi/(2L) > 1$, no such eigenvector with a positive value of λ exists and the flat state is linearly stable. On sufficiently large domains the strong-slip model with van der Waals force predicts that flat liquid films are linearly unstable. The largest unstable has a finite wavelength, which is characteristic for spinodal dewetting.

The dispersion relation is also a tool to check the performance of the numerical algorithm quantitatively. One can simply compute the growth rate λ corresponding to an eigenstate of the linearized strong-slip equation and compare this with the numerical solution of the strong-slip equation.

Example 3.1. On the domain $\Omega = [0, 4]$ we solve the strong-slip problem with initial conditions

$$\begin{aligned} h(0, x) &= 1 - h_0 \cos(kx), \\ u(0, x) &= u_0 \sin(kx). \end{aligned}$$

with $k = \pi/4$, and with sufficiently small h_0 and u_0. The relative size of h_0 and u_0 is such that the real parts of $u(t, x) = u_0 e^{ikx+\lambda t}$ and $h(t, x) = 1 - h_0 e^{ikx+\lambda t}$ are solutions of the linearized strong-slip equation. With our choice of parameters $b = \Re = 1$ we obtain a growth mode with

$$\lambda = \frac{1}{16}\left(-8 - 2\pi^2 + \sqrt{64 + 80\pi^2 + \pi^4}\right) \approx 0.193670.$$

Using the same initial data and parameters, we solve the strong-slip equation numerically on a uniform grid with $N = 255$, hence, we have $\mathcal{O}(|x_{i+1} - x_i|^2)$ consistency, because the solution and derivatives are $\mathcal{O}(1)$. The internal precision of every time-step is set to a relative error of 10^{-6}. In every time-step the solution is fitted to the function $1 - h_0(t) \cos(kx)$, where the free parameter $h_0(t)$ characterizes the deviation from a flat state $h(t, x) = 1$. In Figure 3.5 it is apparent that $h_0(t)$ grows exponentially fast. The rate $\lambda = 0.193674 \pm 0.000003$ is obtained by fitting an exponential to the curve in Figure 3.5. This reproduces the value from the dispersion relation and the expected order of the error, i.e., time discretization $\mathcal{O}(10^{-6})$ and spatial discretization $\mathcal{O}(255^{-2})$, very well. ♢

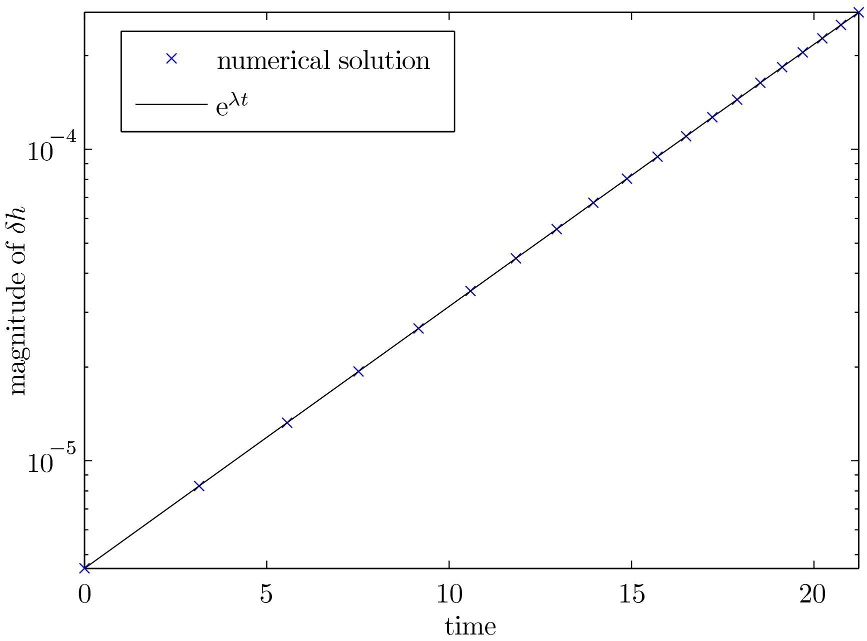

Figure 3.5: Deviation $\delta h(t) = \max_x |1 - h(t,x)|$ from a flat profile $h = 1$ as a function of time. The crosses show the numerical solution of the strong-slip equation at several selected time steps, while the full line is the prediction of the linear theory. The difference between both calculations is in agreement with the predefined error goal of the algorithm.

3.5 Numerical Solutions and Self-Similarity

We are able to construct numerical solution and we are aware of the linear instability of the flat liquid film with van der Waals forces. Now we can use the numerical algorithm to study solutions of the strong-slip equation beyond the linear theory, in particular close to a singularities.

In physical dimensions the critical wave numbers for which the linear instability is observed is proportional to $\sqrt{A/\sigma}$; stronger intermolecular interactions enlarge the region of linear instability while a larger surface tension diminishes it. Erneux and Davis [25] performed a weakly nonlinear stability analysis and showed that nonlinearities increase the speed destabilization. Their model of a free liquid film is very similar to the strong-slip model, but it does not contain terms similar to the slippage term of the strong-slip equation. Figure 3.6 shows the numerical solution of Example 3.1 beyond the validity of the linearized equation.

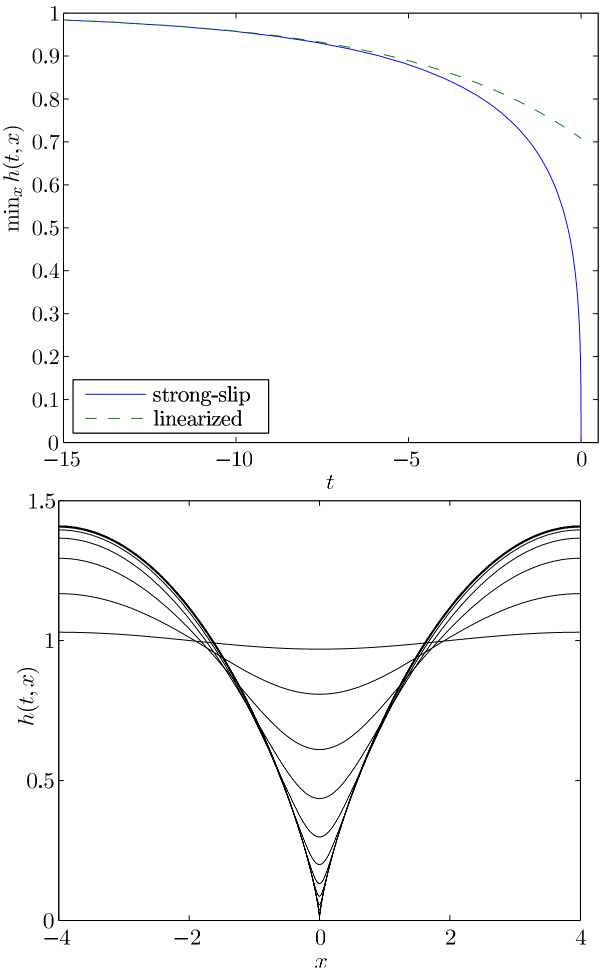

Figure 3.6: Solution of the strong-slip equation on an adaptive, nonuniform mesh starting from the linearly unstable eigenmode ($k = \pi/4$). (Left) The minimal height $\min_x h(t,x)$ as a function of time (full line) compared to the prediction of the linearization (dashed line). Time is shifted such that the rupture happens at $t = 0$. (Right) Height $h(t,x)$ at several time steps; for better visibility the solution is extended to a smooth solution on $\Omega = [-4,4]$ by reflection via $h(t,-x) = h(t,x)$.

The left panel of Figure 3.6 shows that $h(t,x)$ becomes singular much faster than the linearization, which is shown as a dashed curve, predicts. In fact $\dot{h}(t,x)$ is unbounded at $x = 0$ as $t \to 0$. In the right panel of Figure 3.6 it can be seen that the height $h(t,x)$ is not differentiable at $x = 0$ as $\min h \to 0$, the velocity $u(t,x)$ is not even continuous. The major part of the remaining thesis is devoted to answer the question:

What are main properties of the nonlinear interfacial singularity?

Can one understand and prove those properties rigorously?

We already characterized the onset of the rupture by the linear stability analysis. Basically it is the dispersion relation that governs the initial behavior of a flat film. Surface tension stabilizes the flat surface and attractive interactions between fluid and the solid destabilize the surface.

A profound property of the singularity can be discovered, if one plots $\min_x h(t,x)$ from Figure 3.6 versus the time t in a doubly logarithmical plot, as shown in Figure 3.7.

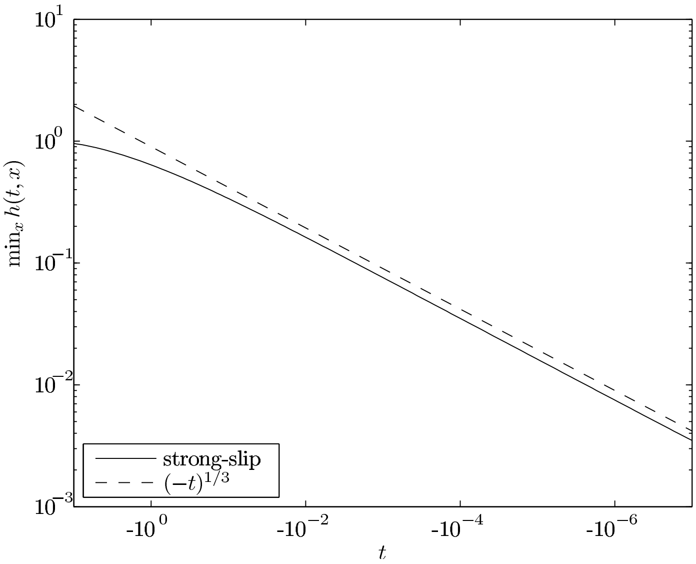

Figure 3.7: Doubly logarithmical plot of $\min_x h(t,x)$ (full line) versus the remaining time t compared to a plot of the power law $(-t)^{1/3}$ (dashed line). The slope of both curves agrees as $(-t) \to 0$.

As $\min_x\ h(t,x)$ tends to zero, its time-dependence is described by the fairly simple relation $(-t)^{1/3}\,C$. While the exact value of the constant C is unimportant for us, the exponent $1/3$ contains information about the dynamics of the singularity formation. In order to understand this statement, suppose that a solution $h(t,x)$ and $u(t,x)$ is given by the following expression

$$h(t,x) = (-t)^{\alpha} H\big((-t)^{-\beta}x\big), \tag{3.9}$$

$$u(t,x) = (-t)^{\gamma} U\big((-t)^{-\beta}x\big). \tag{3.10}$$

This expression seems to come from nowhere since we have only motivated $\alpha = 1/3$ and not why a similar property should hold for $u(t,x)$ and in the argument of some unknown functions H and U. Anyway, if such a relation holds h and u are said to evolve (exactly) *self-similarly* because the general shape of the solution is always similar to H and U and only scaled by time-dependent factors $(-t)^{\alpha}$, $(-t)^{\gamma}$, and $(-t)^{-\beta}x$. If for some α, β, γ, $H(\eta)$, and $U(\eta)$ there are solutions of the strong-slip equation of this form, then H and U solve an ordinary differential equation. This ordinary differential equation can already be deduced from the strong-slip equation, supposedly the numbers α, β, and γ are known.

In order for such a relation to hold exactly, we must either extend the strong-slip equation from $\Omega = [0, L]$ to $\Omega = \mathbb{R}$, or it can only hold in some approximate sense. Furthermore, it is not clear how to determine α, β, and γ or whether such solutions exist at all (also in an approximate sense).

For the analysis of thin-film rupture with respect to self-similar structures one has to show, whether exact self-similar solutions exist and if any solution of the strong-slip equation that becomes singular converges to one of these self-similar solutions, where convergence is defined as follows.

Definition 3.1. Let $h(t, x)$ and $u(t, x)$ be a solution of the strong-slip equation with $\min_x h(t, x) \to 0$ as $t \to 0$. The point where $h(t, x)$ first touches zero is denoted by x^*. Chose positive similarity scales $\alpha, \beta, \gamma \in \mathbb{R}$ and define $\eta = (-t)^{-\beta}(x - x^*)$, $\tau = -\log(-t)$, $H(\tau, \eta)$, and $U(\tau, \eta)$ as follows

$$\begin{aligned} H(\tau, \eta) &= h(t, x)/(-t)^{\alpha} \\ U(\tau, \eta) &= u(t, x)/(-t)^{-\gamma}. \end{aligned}$$

We say h and u *converge to a self-similar solution*, if $H(\tau, \eta)$ and $U(\tau, \eta)$ converge pointwise[6] as $\tau \to \infty$. Analogously, a solution of the strong-slip equation of the form

$$h(t, x) = (-t)^{\alpha} H(\eta) \tag{3.11}$$

$$u(t, x) = (-t)^{\gamma} U(\eta) \tag{3.12}$$

is called an *exact self-similar solution.* Though the strong-slip equation has no exact self-similar solutions on $\Omega = [0, L]$, h and u can still convergence to a self-similar solution and the limits $H(\eta)$ and $U(\eta)$ solve some relaxed problem, usually some nonlinear ordinary differential equation. In a slight abuse of notation we call these limits also *exact self-similar solutions.* ♢

In the current chapter we compute exact self-similar solutions and show that numerical solutions of the strong-slip equation that correspond to rupture evolve self-similarly, and that the limits $H(\eta)$ and $U(\eta)$ do not depend or depend only weakly on a particular choice of initial data and parameter. We investigate different types of self-similar solutions that emerge from the strong-slip equation for various parameter and $\mathcal{O}(1)$ initial data. A central question how to determine the possible α, β, γ and how to determine the limits $H(\eta)$ and $U(\eta)$.

---

[6] There exist trivial limits that should be excluded. This will be explained more precisely in the next chapter.

First of all let us recall what is known about self-similar solutions for thin film; an important paper for the full strong-slip model is the work by Vaynblat et al. [27], who study the model

$$\partial_t(h^r) + (h^r u)_x = 0, \tag{3.13a}$$

$$\Re\left(\partial_t u + u u_x\right) = \frac{1}{h^r}(h^r u_x)_x - A(h^{-p})_x. \tag{3.13b}$$

Setting $r = 1$ and $p = 3$ this model corresponds to line rupture of a free liquid film but without surface tension. For a derivation of a similar model see Erneux and Davis [25]. Even though the model (3.13) above does not contain surface tension and slippage, its similarity solutions are equivalent to certain similarity solutions of the strong-slip equation.

In general one determines α, β, γ by plugging the exact self-similar solution (3.12) into the strong-slip equation. The expressions for $h(t,x)$ and $u(t,x)$ in the strong-slip equation are replaced by $H(\eta)$ and $U(\eta)$ from and one obtains a set of ordinary differential equations for $H(\eta)$ and $U(\eta)$, the so-called similarity equation. What remains from the time-dependence in a a certain power of $(-t)$ in front of each term. Then *balancing* two terms means to set to respective exponents of those terms equal and neglect the others.

Ida and Miksis [26] argued that van der Waals forces and viscosity should be balanced, together with the mass balance. This yields $\alpha = 1/3$ and $\gamma = \beta - 1$ but leaves one similarity scale, e.g., β, undetermined. On the other hand, Vaynblat et al. performed a numerical analysis and found $\alpha = 1/3$, $\beta = 1/2$, and $\gamma = -1/2$. They argue that the self-similar solution found by Ida and Miksis is a transient solution favored by a certain choice of parameters that is unstable as $\tau \to \infty$. For this set of similarity scales they find an infinite family of self-similar solutions. They do not assume a priori that similarity solutions are symmetric $\big(H(\eta) = H(-\eta)$ and $U(\eta) = -U(-\eta)\big)$ but find it as a result of a phase plane analysis. In addition they solve (3.13) using slightly perturbed similarity solutions as initial data and find that only one solution is stable.

Let us bring forward two arguments why the leading order dependence of the strong-slip equation as $b \to 0$ is equivalent to that of the intermediate-slip equation. Rescaling the solution of the strong-slip equation by $t \to \widetilde{t}/b$ and $u \to \widetilde{u}/b$ such

$$\dot{\widetilde{h}} + (\widetilde{h}\widetilde{u})_x = 0,$$

$$\Re b^2(\dot{\widetilde{u}} + \widetilde{u}\widetilde{u}_x) = b\frac{4(\widetilde{h}\widetilde{u}_x)_x}{\widetilde{h}} + (\widetilde{h}_{xx} - \phi(\widetilde{h}))_x - \frac{\widetilde{u}}{\widetilde{h}}.$$

and then setting $b = 0$ one formally obtains

$$\dot{\widetilde{h}} + \left(\widetilde{h}^2 \left(\widetilde{h}_{xx} - \phi(\widetilde{h})\right)\right)_x = 0$$

the intermediate-slip equation. A second argument is that the leading order dependence of the dispersion relation is

$$\lambda(k) = 3bk^2(1 - k^2) + \mathcal{O}(b^2)$$

as $b \to 0$, which is obviously the dispersion relation of the intermediate-slip equation with time rescaled appropriately.

Self-similarity for degenerate higher-order models similar to the intermediate-slip equation has been studied by Witelski et al. [50] and Lister et al. [51] (jet pinch-off of liquid threads/thin liquid films on solid substrates with van der Waals force). Lister et al. performed an analysis of self-similar solution and Witelski et al.[52] added a stability analysis showing that only one solution is stable. They basically computed the eigenvalues of the linearized problem close to a self-similar solution, where one has to watch fake unstable modes corresponding to dilations in time and translations of the point where the singularity occurs.

Its also physically meaningful to determine the similarity scales of the strong-slip equation. In general it is hard to validate a model like a nonlinear partial differential equation by comparing with experimental results. Experimental results depend very much on preparation (initial data) and the physical parameters are often not know precisely. Similarity scales, on the other hand, can be measured in the experiment and are quite insensitive to changes of parameters and initial conditions. In his well known book on self-similarity[7] Barenblatt writes

> Establishing self-similarity has always represented progress for a researcher: Self-similarity has simplified computations and the representation of the properties of phenomena under investigation. In handling experimental data, self-similarity has reduced what would seem to be a random cloud of empirical points so as to lie on a single curve or surface, constructed using self-similar variables chosen in some *special way.*

With the *special way* he refers to the method used to infer the values of the similarity scales and the similarity solutions; roughly speaking self-similar solution can be divided into solutions of first and second kind as follows.

- Sometimes it is possible to compute the similarity scales without any knowledge of solutions. Balancing certain terms of the strong-slip equation suffices to determine all similarity scales, which are just rational numbers then. The resulting similarity equation determines the similarity solutions. We speak of *first kind* similarity.

---

[7] *Scaling, self-similarity, and intermediate asymptotics*, quotation from [20] page 14

- In all other cases, where we observe convergence to self-similar solutions but cannot deduce the similarity solutions that way, we speak of *second kind* similarity. An indicator for second kind similarity is that similarity scales are not rational. Then, the determination of the similarity scales is more involved, but still one does not have to solve the full (strong-slip) equation.

In order to find possible similarity scalings corresponding to *first kind* similarity solutions let us assume that self-similar solutions of the strong-slip equation given by in (3.12) exist. Then replace the expressions $h(t,x)$ and $u(t,x)$ by $H(\eta)$ and $U(\eta)$ as follows

$$\begin{aligned}
\partial_t h(t,x) =& \tau^{\alpha-1}\big(\beta\eta H'(\eta) - \alpha H(\eta)\big),\\
\partial_t u(t,x) =& \tau^{\gamma-1}\big(\beta\eta U'(\eta) - \gamma U(\eta)\big),\\
\partial_x^n h(t,x) =& \tau^{\alpha-n\beta} H^{(n)}(\eta),\\
\partial_x^n u(t,x) =& \tau^{\gamma-n\beta} U^{(n)}(\eta).
\end{aligned}$$

Now new can write the strong-slip equation as follows

$$\begin{aligned}
\tau^{\alpha-1}(\beta\eta H' - \alpha H) + \tau^{\alpha+\gamma-\beta}(HU)' =& 0, && (3.14a)\\
\Re\big(\tau^{\gamma-1}(\beta\eta U' - \gamma U) + \tau^{2\gamma-\beta} UU'\big) =& \tau^{-3\alpha-\beta}\frac{3H'}{H^4} + \tau^{\gamma-2\beta}\frac{4(HU')'}{H} && (3.14b)\\
& -\tau^{\gamma-\alpha}\,\frac{U}{bH} + \tau^{\alpha-3\beta}\,3H''' \quad .
\end{aligned}$$

Note that H and U only depend on η, so that this is not a transformed strong-slip equation but rather the equation that exact self-similar solution fulfill. Even though H and U do not depend on τ, this equation must hold for all τ.

As the solution approaches the singularity $\tau \to 0$, only the leading order terms in (3.14) remain because their respective powers of τ are dominant; subdominant terms have factors with larger powers of τ. A choice of α, β, and γ is *consistent* if either all neglected terms are subdominant, or if for some reason the term itself vanishes, e.g., because some parameter like Reynolds number vanishes or is negligible.

First, for any choice for α, β, and γ we identify the leading order terms, then we determine the corresponding solutions H and U and check whether our choice was *consistent*.

Generally we assert that the scales of $\partial_t h$ and $\partial_x(hu)$ in (3.14a) are equal and hence

$$\gamma = \beta - 1. \tag{3.15}$$

Previously we noticed that $u(t,x)$ diverges near the singular point x^* and hence $\gamma < 0$, $\beta < 1$. We also observed that higher derivatives of $h(t,x)$ with respect to x diverge at x^*, which in turn implies $\beta > 0$. In a first attempt to understand the nonlinear behavior of the rupture we also found $\alpha = 1/3$, which seems a good guess at least if all parameters and initial data are of order unity. Plugging the relations (3.15) into (3.14) we obtain

$$\beta\eta H' - \alpha H + (HU)' = 0, \tag{3.16a}$$

$$\begin{aligned} \tau^{\beta-2}\Re\big(\beta\eta U' - (\beta-1)U + UU'\big) &= \tau^{-3\alpha-\beta}\frac{3H'}{H^4} + 4\tau^{-\beta-1}\frac{(HU')'}{H} \\ &\quad - \tau^{\beta-\alpha-1}\frac{U}{bH} + \tau^{\alpha-3\beta}\,3H''', \end{aligned} \tag{3.16b}$$

Finally, we wish to fix the similarity scales and have to find two more independent conditions, or equivalently we pick out three terms of (3.16b) that supposedly have the same magnitude. There are $\binom{5}{3} = 10$ possible choices, for convenience we restrict to the $\binom{4}{2} = 6$ combinations which include van der Waals forces as the driving force. In the following table we label balances by the two terms which we include and provide the corresponding similarity scales α and β. Then γ follows from (3.15). In the last column we indicate whether the choice is consistent; if it is not the corresponding self-similar solution can still be meaningful as a transient solution, i.e., the solution is an approximate self-similar solution for intermediate times or in certain parameter ranges.

terms that balance	α	β	dominant terms
viscosity – inertia	1/3	1/2	yes
viscosity – surface tension	1/3	2/3	yes
surface tension – slippage	1/6	1/3	inertia is dominant
surface tension – inertia	2/7	4/7	viscosity is dominant
slippage – viscosity	1/3	1/6	inertia is dominant
slippage – inertia	1	−1/2	$\beta < 0$

Table 3.1: Similarity scales obtained by balancing 3 terms (the two of the first column with van der Waals force) in Equation (3.16); the remaining scale is determined by $\gamma = \beta - 1$. The *yes* in the last column means all other terms are subdominant, otherwise the dominant terms is denoted. The balance in the last row yields $\beta < 0$, which we exclude because rupture should be local. Anyway, there is only a finite number of possible similarity scales that correspond to *first kind* similarity solutions.

We determined $\alpha = 1/3$, which (possibly) corresponds to one of the three scalings in Table (3.1) that have $\alpha = 1/3$. Vaynblat et al. suggested that only the first scaling in Table (3.1), i.e., $\alpha = 1/3$, $\beta = 1/2$, and $\gamma = -1/2$, is ultimately stable. However, there are other reasonable scales, at least in terms of transient solutions. We are going to study the solutions of Vaynblat et al., but also the dependence of self-similarity on the Reynolds number $\Re$, and more importantly the dependence on the slip-length b.

We found the numerical solutions of the strong-slip equation evolve self-similar. By measuring $\max_x u(t,x)$, $\max_x h_x(t,x)$, $u_x(t,x^*)$ and $h_{xx}(t,x^*)$ and plotting those quantities versus $h(t,x^*)$ on a log − log scale one can compute the similarity scales very efficiently. Self-similar behavior will show up in (approximate) straight lines with their slopes being the following combinations of the similarity scales

$$\begin{aligned} \max_x u(t,x) &\to \frac{\gamma}{\alpha}, & \max_x h_x(t,x) &\to \frac{\alpha-\beta}{\alpha}, \\ u_x(t,x^*) &\to \frac{\gamma-\beta}{\alpha}, & h_{xx}(t,x^*) &\to \frac{\alpha-2\beta}{\alpha}. \end{aligned}$$

We start by computing similarity scales for solutions of the strong-slip equation with $\Re = b = 1$ in the domain $\Omega = [0,8]$. In order to show that self-similarity is a universal property, i.e., similarity scales and solutions do not depend on a particular choice of initial data, we study the evolution towards rupture for three different initial data. Since the symmetry of self-similar solution was been a subject of previous investigations, we study solution which are symmetric with respect to reflections at $y = L/2$. Therefore, the following three initial conditions are used

$$h(0,x) = 1 + 0.1\cos(2\pi\hat{x}) \qquad u(0,x) = 0, \tag{3.17}$$

$$h(0,x) = 1 - \hat{x}^4(1-\hat{x})^2 \qquad u(0,x) = -0.1\sin(2\pi\hat{x}), \tag{3.18}$$

$$h(0,x) = \tfrac{1}{2} + (1-2\hat{x})^4 - \tfrac{2}{3}(1-2\hat{x})^6 \qquad u(0,x) = 0, \tag{3.19}$$

with $\hat{x} = x/L$. The initial condition (3.17) is symmetric with respect to reflections at $x = 4$, whereas (3.18) is not. Initial data (3.19) is selected as an example for a higher order minimum. Snapshots of the corresponding numerical solutions and combination of the similarity scales are shown in Figure 3.8, numerical values for similarity scales are presented Table (3.2).

initial data	$(\alpha-\beta)/\alpha$	$(\gamma-\beta)/\alpha$	γ/α	$(\alpha-2\beta)/\alpha$
(3.17)	−0.4996	−2.9998	−1.5005	−1.9990
(3.18)	−0.5002	−3.0017	−1.4996	−1.9987
(3.19)	−0.4994	−3.0005	−1.4993	−1.9994

Table 3.2: Combinations of similarity scales computed from numerical solutions with initial data (3.17-3.19) give rise to $\alpha = 1/3$, $\beta = 1/2$, and $\gamma = -1/2$. Values in the table are obtained by fitting power laws (corresponding to straight lines) to the curves in Figure 3.8 (right column) for $\min h < 10^{-6}$.

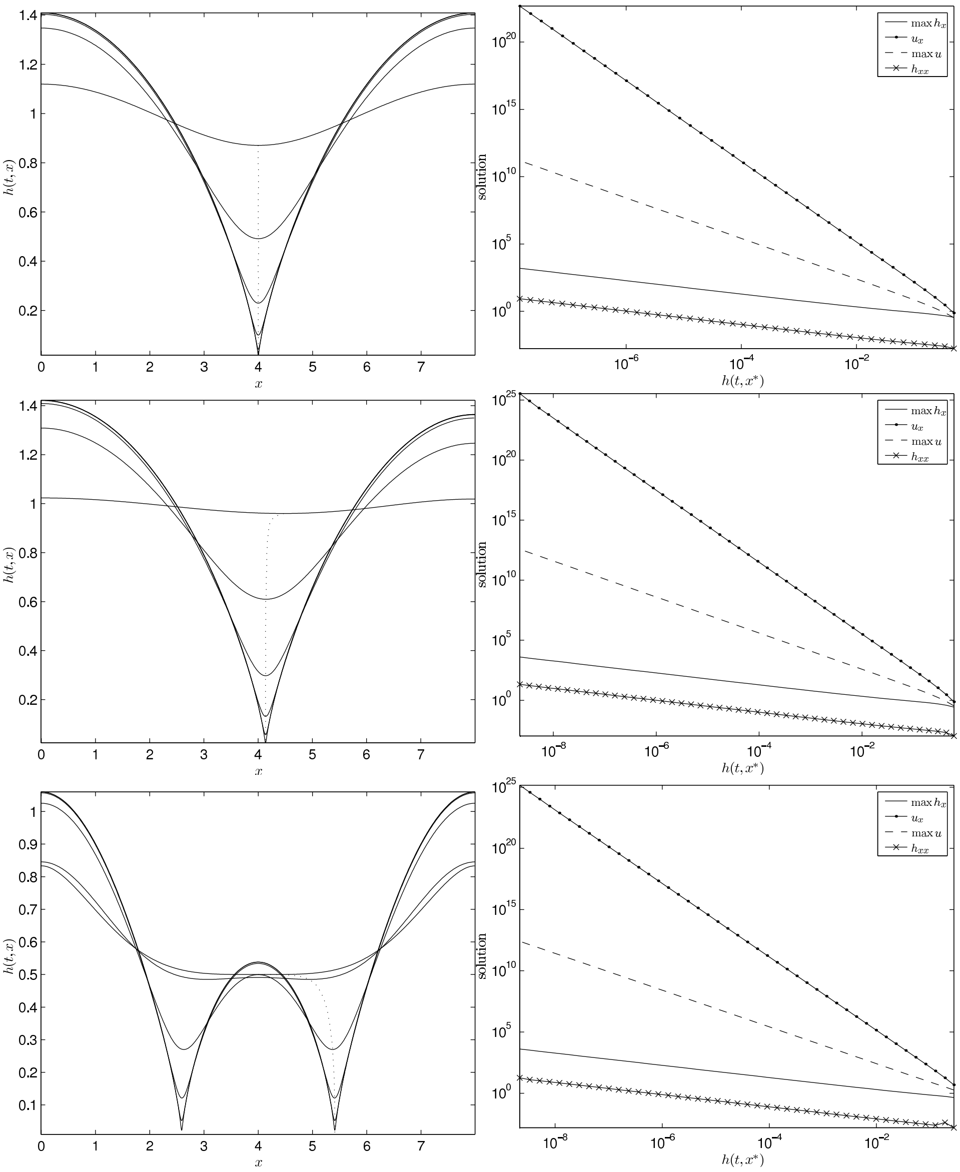

Figure 3.8: Solutions of strong-slip Eqn.: (upper row) With symmetric initial data $h(0,x) = 1 + 0.1\cos(2\pi\hat{x})$ and zero velocity; (middle row) nonsymmetric initial data $h(0,x) = 1 - \hat{x}^4(1-\hat{x})^2$ and $u(0,x) = -0.1\sin(2\pi\hat{x})$; (lower row) symmetric initial data $h(0,x) = 1/2 + (1-2\hat{x})^4 - 2/3(1-2\hat{x})^6$ and zero velocity ($\hat{x} = x/L$); (left column) Shows $h(t,x)$ at several time steps (full line). To emphasize the nonsymmetric solution, the trajectory of the minimum is shown as a dashed curve. (right column) Doubly logarithmic graphs show combinations of α, β, γ, as explained in the text.

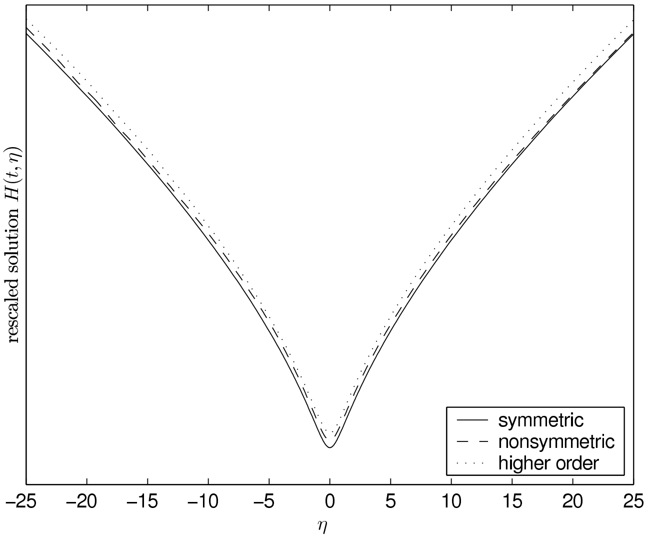

Figure 3.9: Rescaled solutions of the strong-slip equation with $\Re = b = 1$ for the different initial data. The figure shows $H(t, \eta)$ as $t \to t^*$, where the solutions are shifted along the h-axis for better visibility.

In all three cases we observe the same similarity scales; Figure 3.9 shows that even the limiting profiles $H(\eta)$ are the same. Basically this is the motivation why one studies self-similar rupture; like a dispersion relation characterizes the onset of an instability, self-similar solution characterize the nonlinear behavior near the singularity in an unambiguous way. Self-similar solutions determine the shape of the solutions near the singularity x^* and they contain information about the leading order balances, i.e., driving and inhibiting forces.

The slip term can be neglected if the slip-length is sufficiently large and the strong-slip model becomes the free-slip model (3.13). In any case, for the apparent choice of the similarity scales, the term related to slippage is smaller by a power $b^{-1}(t^* - t)^{2/3}$, and surface tension is smaller by a power $(t^* - t)^{1/3}$ then the remaining terms (inertia, viscosity, and van der Waals force). Although this is not a proof, the scaling argument persuades us that we always find the similarity scales $\alpha = 1/3$, $\beta = 1/2$, and $\gamma = -1/2$.

However, there are two limiting cases for which new similarity solutions can be expected — the limit of vanishing Reynolds number $\Re \to 0$ and small or no slip-length $b \to 0$. For sufficiently small values of $\Re$ and b it should be possible to observe transient solutions.

Therefore we choose $\Re = 10^{-5}$, $b = 10^{-8}$ and $L = 8$ (symmetric solution) as before and seek self-similar solutions. The doubly logarithmic plot of the numerical solution is shown in Figure 3.10. Interestingly, as $h(t, x*) \to 0$ $(\tau \to 0)$ there is not a single but there are 3 distinct regimes with distinct

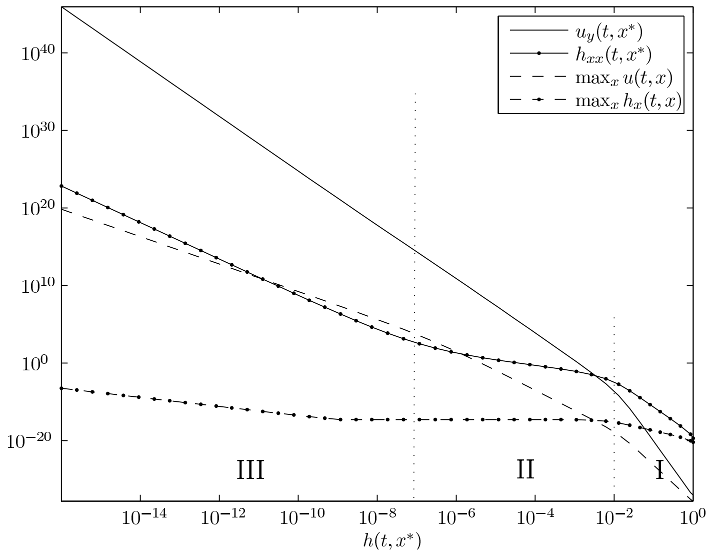

Figure 3.10: Solution of the strong-slip equation with $\mathfrak{R} = 10^{-5}$, $b = 10^{-8}$ has distinct regions I, II, III where $u_x(t,x^*)$, $h_{xx}(t,x^*)$, $\max_x u(t,x^*)$, and $\max_x h_x(t,x^*)$ evolve like a power of $(t^* - t)$.

	I	II	III
α	$1/6$	$1/3$	$1/3$
β	$1/3$	≈ 0.25	$1/2$
γ	$-2/3$	$\beta - 1$	$-1/2$

Table 3.3: Similarity scales computed from the solution of the strong-slip equation with $\mathfrak{R} = 10^{-5}$, $b = 10^{-8}$, and symmetric initial data. The similarity scales are determined by fitting power laws to the curves in the center of each regime.

similarity scales; the curves in Figure 3.10 are different slopes in region I, II, and III. Decreasing the value of b (or $\mathfrak{R}$) would shift the position of the border between region I-II (or II-III) towards smaller values of h. We chose b and $\mathfrak{R}$ such that each region is large enough to measure α, β, γ precise enough in order to compare similarity scales with Table (3.1) unambiguously.

Note that the curve $\max h_x$ versus h is horizontal in regime, i.e., it does not scale, because $h(t,x)$ has no turning point for any finite value of η but only for fixed x (as $t \to t^*$). Using the same method described before we find the similarity scales of Table (3.3) in regime I-III.

In region I and III similarity scales are determined with a relative error of order 10^{-4}, while the values $\alpha = 1/3$, $\beta \approx 0.25$ in region II are of order 10^{-2}. This is due to the slow transition between region II and III. However, with an error of order 10^{-2} we can clearly exclude any of the balances of

$(\alpha-\beta)/\alpha$	$(\gamma-\beta)/\alpha$	γ/α	$(\alpha-2\beta)/\alpha$
$< 10^{-5}$	-3.0000	-2.2532	-0.49357

Table 3.4: Combinations of similarity scales computed for $\Re = 0$ as $t \to t^*$ with relative errors being smaller than 10^{-5}. Note that the numerical simulation is computed up to $h(t, x^*) = \mathcal{O}(10^{-16})$, which produces similarity scales with errors less than 10^{-5}.

Table (3.1).

Evidently regime I and III result from a balance of van der Waals force–surface tension–slippage or van der Waals force–inertia–viscosity respectively and explain the similarity scales in Table (3.3). However, regime I and II obey $\beta < 1/2$ which renders them transient regimes and ultimately only regime III is stable; the asymptotic neglect of inertia is only justified if $\Re$ vanishes. Apparently between regime I and III exists another regime where none of the scalings in Table (3.1) applies. Our numerical results suggest that van der Waals force and Trouton-viscosity balance such that $\alpha = 1/3$. In addition numerical solutions suggest that the dynamic balance $\gamma = \beta - 1$ is also valid. No additional information about regime II are available and it's unknown how one can fix the remaining scale β.

We argued that, using a nonzero Reynolds number, regime II is only a transient self-similar regime. So we set $\Re = 0$ and $b = 10^{-8}$ and recompute the solution of the strong-slip equation *without inertia*. Note that the new equation

$$h_t + (hu)_x = 0, \tag{3.20}$$

$$\frac{4}{h}(hu_x)_x + (3h_{xx} - h^{-3})_x - b^{-1}\frac{u}{h} = 0, \tag{3.21}$$

is conservation (transport) of mass coupled to the momentum balance (algebraic equation). The implementation of the strong-slip equation without inertial is analogous to the usual strong-slip equation. We chose the initial data $h(0,x) = 1 + 0.2\cos(2\pi x/L)$ and $u(0,x)$, such that $u(0,x)$ solves the algebraic constraint. Combinations of the similarity scales, which computed from the slopes of the diverging quantities in Figure 3.11, are shown in Table (3.4).

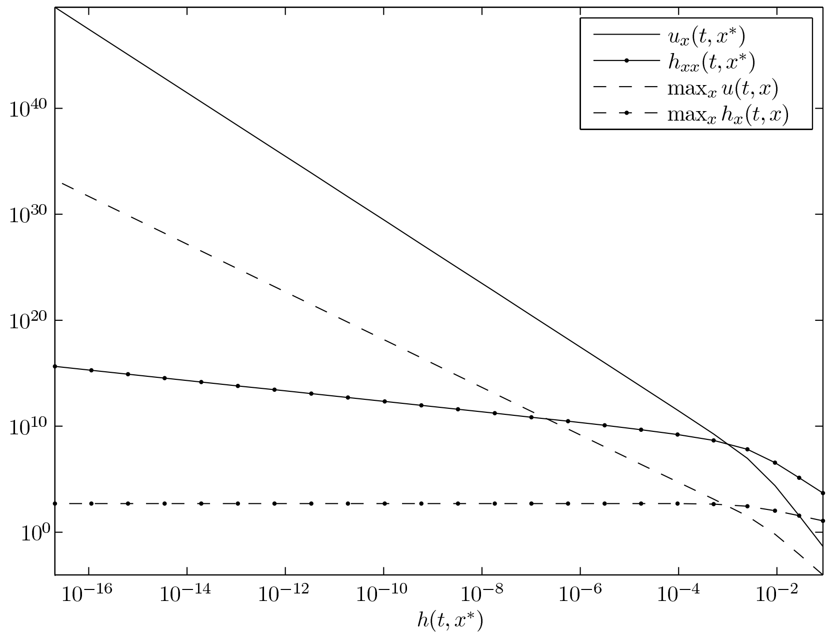

Figure 3.11: Simulation of the strong-slip equation with $\Re = 0$, $b = 10^{-8}$, and $h(0,x) = 1 + 0.2\cos(2\pi x/L)$ (initial velocity solves the momentum equation)

This way regime II is stable with scaling dimensions

$$\alpha = 1/3, \qquad \beta = 0.248930 \pm 0.000003, \qquad \text{and} \qquad \gamma = \beta - 1, \qquad (3.22)$$

which allows us to exclude any of the *first kind* similarity solutions we considered before.

To underline that similarity scales are independent of the domain, initial data, special parameters we recompute solutions of the strong-slip equation for domain sizes $L = \{4, 6, 20\}$, with slip-length $b = 1$ and without slip, and two initial conditions $h(t,x) = 1 + 0.2\cos(2\pi x/L)$ and $h(t,x) = 5/4 + 4/5\cos^6(2\pi x/L)$. To avoid influences by transient self-similar behavior, i.e., effects from regime I or III, we use $\Re = 0$ and measure the similarity scales for sufficiently small $h(t,x^*)$. For all these different parameters we extract the scaling behavior of the tentative self-similar solution. The results are shown in Table (3.5). The similarity scales in Table (3.5) coincide with a relative precision of $\mathcal{O}(10^{-6})$ which showing that the similarity scales are in fact universal. In addition we find again $\alpha = 1/3$ and $\gamma = \beta - 1$ holds true and obtain a better approximation for the remaining similarity scale β.

Let us summarize what we learned in this section. First we discovered that the evolution of the liquid film thickness is governed by the law $h(t,x^*) = C(t^* - t)^{1/3}$. An explanation of this property was given by introducing the notion of self-similar solutions, a mechanism that is usually divided into *first* and *second kind* similarity solutions.

parameters of simulation			α	β	γ
	$L = 4$	(free slip)	0.333333	0.248930	−0.751070
	$L = 4$	$b = 1$	0.333333	0.248931	−0.751069
	$L = 6$	$b = 1$	0.333333	0.248931	−0.751070
	$L = 20$	$b = 1$	0.333333	0.248931	−0.751069
(init)	$L = 4$	$b = 1$	0.333333	0.248930	−0.751070

Table 3.5: Self-similar scales for solutions of Equation (2.10) with $\Re = 0$ with different domain sizes, different slip parameter and alternative initial conditions

We listed all possible scales corresponding to *first kind* similarity solutions. In agreement with Vaynblat et al. we observed that for any choice of initial data only the first kind self-similar solution with $\alpha = 1/3$, $\beta = 1/2$, and $\gamma = -1/2$ prevails close to rupture. However, if we choose the Reynolds number sufficiently small, the slip-length ultimately decides which similarity solution we run into. For small slip-length we observe similarity solutions of the intermediate slip equation and for $1/b = \mathcal{O}(1)$ we find novel self-similar solutions which are by definition of *second kind.*

When we set $\Re = 0$ this novel regime becomes stable and prevails the first kind similarity solution of the intermediate-slip regime. The novel similarity solution is physically relevant if the transition to region III happens only at atomic length scales.

In the remaining part of this chapter we explain how we can compute β without knowing the solution of the strong-slip equation and determine β even more accurate and we discuss the similarity solutions $H(\eta)$, $U(\eta)$ of regime I and II.

3.6 Reduction to Ordinary Differential Equations

With $\mathcal{O}(1)$ initial data and $0 < b, \Re \ll 1$ we observe three different similarity regimes I,II, and III. We concentrate on the novel similarity regime II with $\alpha = 1/3$, $\gamma = \beta - 1$, and number $\beta \approx 0.24893$. We also compute the exact self-similar solution $H(\eta)$ and $U(\eta)$.

The scaling exponents of regime I suggest that the solution is of first kind with a balance of van der Waals force, surface tension and slippage. This can be seen by transforming the scales of Equation (2.10) by the rule $t \to \widetilde{t}/b$, $u \to \widetilde{u}/b$, $x \to \widetilde{x}$ and $h \to \widetilde{h}$. The strong-slip equation then reads

$$\begin{aligned} &\widetilde{h}_{\widetilde{t}} + (\widetilde{h}\widetilde{u})_{\widetilde{x}} = 0, \\ b^2\Re(\widetilde{u}_{\widetilde{t}} + \widetilde{u}\widetilde{u}_{\widetilde{x}}) &= \frac{4b}{\widetilde{h}}(\widetilde{h}\widetilde{u}_{\widetilde{x}})_{\widetilde{x}} + (3\widetilde{h}_{\widetilde{x}\widetilde{x}} - \phi(\widetilde{h}))_{\widetilde{x}} - \frac{\widetilde{u}}{\widetilde{h}}. \end{aligned}$$

For $b \to 0$ the limiting problem is the intermediate-slip equation (2.11) and similarity solutions of regime I are those of the intermediate-slip equation. An analogue problem of similarity solutions, however with the mobility $m(h) = h^3$, was discussed by Zhang and Lister [51]. Their equation turns out to be

$$\frac{1}{5}\left(H - 2\eta H'\right) = \left[\frac{H'}{H} + H^3 H'''\right]'. \tag{3.23}$$

The intermediate-slip equation has the mobility $m(h) = h^2$ and the similarity solutions of first-kind solve

$$\frac{1}{6}(H - 2\eta H') = \left[\frac{3H'}{H^2} + H^2 H'''\right]' \tag{3.24}$$

which one would also obtain by plugging the similarity scales of regime I into (3.16) and neglects terms with higher powers of $(t^* - t)$. Since Equation (3.23) and (3.24) have a similar composition it can be expected that self-similar solutions of both equations behave qualitatively the same. Therefore, we skip a detailed discussion of Equation (3.24) and refer to [51].

Solutions of III have been studied by Vaynblat et al. in [49]. They fixed the similarity scales by balancing van der Waals force, Trouton-viscosity, and inertia together with the balance $\gamma = \beta - 1$. Thereby, assume that solutions converge to similarity solutions with the exponents $\alpha = 1/3$, $\beta = 1/2$, and $\gamma = -1/2$. Then we can rewrite the strong-slip equation as follows

$$\begin{aligned} H' &= \frac{H}{2U + \eta}\left(\frac{2}{3} - \frac{R}{2}\right), \\ R' &= H_\eta\left(\frac{3}{H^4} - \frac{R}{H}\right) + \left(U + \frac{\eta}{2}\right)R + \frac{U}{2}, \\ U' &= \frac{R}{4}. \end{aligned} \tag{3.25}$$

As it turns out, in order to explain symmetry properties like $H(\eta) = H(-\eta)$ and $U(\eta) = -U(-\eta)$, one has to employ a phase plane analysis and check whether non-symmetric solutions of (3.25) are possible and meaningful. In order to answer the question whether there exist non-symmetric solutions of (3.25) Vaynblat et al. assumed that for any solution there exists a so-called stagnation point η_0 where $2U(\eta_0) + \eta_0 = 0$ holds true, consequently also $3U'(\eta_0) = 1$ holds. Any choice of the initial data $(H(\eta_0), \eta_0)$ produces a solution of Equation (3.24) as long $H(\eta_0)$ differs from certain critical values.

In order to have a meaningful self-similar solution one has to impose the asymptotic condition $\lim_{\eta\to\infty} U(\eta) = 0$. These two conditions fix the initial values of the similarity ODE and produce a countably many similarity solutions. Those solutions are parametrized by $(H(\eta_0), \eta_0)$. They find that from the infinite set the solution only the one with $\eta_0 = 0$ and the largest value of $H(\eta_0)$ is stable.

In order find the similarity scales of regime II assume that the Reynolds number is sufficiently small and that terms related to inertia can be neglected. The conditions that are needed to fix the similarity scales uniquely are similar to the procedure described by Papageorgiou in [19] for self-similar jet pinch-off of liquid threads.

Consider $\alpha = 1/3$ and the relation $\gamma = \beta - 1$ are known. Still the value of β can not be determined by scaling arguments. It depends neither on initial configuration (initial condition or domain size) nor on the slip-length etc. Suppose β is a free parameter, then the similarity equation looks as follows

$$U_\eta = \frac{3}{8H^3} + \frac{C}{H}, \tag{3.26a}$$

$$H_\eta = \frac{H}{U + \beta\eta}\left(\frac{1}{3} - \left[\frac{3}{8H^3} + \frac{C}{H}\right]\right). \tag{3.26b}$$

An unique self-similar solution of (3.26) is determined by its initial data $H(\eta_0)$, $U(\eta_0)$, the constant of integration C, the similarity scale β. Alternatively, we start the integration at a so-called stagnation point η_0, i.e., a singular point of the equation where $U(\eta_0) + \beta\eta_0 = 0$. This way we introduce a new parameter but we can eliminate $U(\eta_0)$. We are left with four unknowns, say $H(\eta_0)$, η_0, C, and the similarity scale β. Next we impose the restriction that H_η in (3.26b) is finite at η_0 and hence the constant C is determined by

$$C = \frac{H(\eta_0)}{3} - \frac{3}{8H(\eta_0)^2}, \tag{3.27}$$

which can be plugged into (3.26a) and shows $U_\eta(\eta_0) = 1/3$. Assume that the self-similar solution is symmetric, so we have the conditions $\eta_0 = 0$, $U(0) = 0$ and $H_\eta(0) = 0$ and there are still 2 free parameter left; $H(0)$ and β.

In fact, as a result of the parametrization in terms of the stagnation point we have one additional parameter. The ordinary differential equation with initial data at η_0 has no unique solution but for every solution there exists an one-dimensional family of solutions, connected to each other by the transformation

$$\begin{aligned} H(\eta) &\mapsto \tilde{H}(\eta) = H(a\,\eta), \\ U(\eta) &\mapsto \tilde{U}(\eta) = a\,U(a\,\eta). \end{aligned} \tag{3.28}$$

Transforming similarity solutions this way leaves the initial data $H(0)$, $U(0)$ invariant and has the fixed point $H(\eta) = H(0)$, $U(\eta) = \eta/3$ (limit $a \to \infty$). This fixed point solution is discarded as a self-similar solution for a simple reason; is does not obey the asymptotic condition $\lim_{\eta\to\infty} U(\eta) = 0$. The asymptotic condition, in turn, should hold because the solution of the strong-slip equation, $h(t, y)$ and $u(t, y)$, has a finite limit for every $y \neq y^*$. Hence, $H(t, \eta) = H(t, y(t^* - t)^{-\beta}) = h(t, y)(t^* - t)^{-1/3}$ tends to infinity while $U(t, \eta) = U(t, y(t^* - t)^{-\beta}) = u(t, y)(t^* - t)^{-\gamma}$ tends to zero as $t \to t^*$.

So far to the behavior at infinity. At η_0 the ordinary differential equation has a removable singularity. In order to find the condition to remove the singularity we write the solution $U(\eta)$ and $H(\eta)$ in terms of a power series in terms of the distance to the singular point η_0

$$U(\eta) = \sum_{n=0}^{\infty} U_n \eta^n \qquad , \qquad H(\eta) = \sum_{n=0}^{\infty} H_n \eta^n .$$

As a consequence of symmetry U and H contain only odd and even powers of η respectively. Plugging this expansion into (3.26), we obtain the following recursion relation for the kth power of H and $(k+1)$th power of U

$$\begin{pmatrix} H_0^3(k+1) & H_0^2 - 2CH_0 \\ 0 & H_0^2(\beta + \frac{1}{3})k - H_0^2 + 2CH_0 \end{pmatrix} \begin{pmatrix} U_{k+1} \\ H_k \end{pmatrix} = \begin{pmatrix} \alpha_k \\ \beta_k \end{pmatrix} \tag{3.29}$$

where the right hand side only depends on coefficients with lower indices and one has $\alpha_2 = \beta_2 = 0$. In the generic case the determinant of the matrix is nonzero and the expansion has only the fixed point $H(\eta) = H_0$ and $U(\eta) = \eta/3$ as a solution. Thus, in order to find a nontrivial solution of the equation that can be matched to an outer solution using the asymptotic condition $\lim_{\eta\to\infty} U(\eta) = 0$ the determinant of (3.29) must vanish at some iteration level n. Consequently we have

$$\beta = \frac{9 - 4H_0^3(n-1)}{12H_0^3 n} .$$

At this point we have exchanged the dependence on 2 continuous parameters, i.e., $H(0)$ and β, for 1 continuous parameter, say H_0, and an even natural number n. To determine H_0 for any fixed n, we have to use the asymptotic condition. For example we set $n = 2$ and have the relation

$$\beta = \frac{3}{8H_0^3} - \frac{1}{6} . \tag{3.30}$$

and the recursion formula

$$\begin{pmatrix} H_0^3(k+1) & \frac{9+4H_0^3}{12H_0} \\ 0 & \frac{9+4H_0^3}{24H_0}(k-2) \end{pmatrix} \begin{pmatrix} U_{k+1} \\ H_k \end{pmatrix} = \begin{pmatrix} \alpha_k \\ \beta_k \end{pmatrix} . \tag{3.31}$$

In the generic case the recursion depends on H_0 and n only. The coefficients H_k, U_{k+1} for $k < n$ vanish; for $k = n$ we can chose any $(H_k, U_{k+1})^\top$ from the 1-dimensional kernel of the recursion matrix. The freedom to choose the length of the vector freely corresponds to the scaling ambiguity (3.28), which persists at the level of the power expansion.

Still it is not guaranteed that the far field condition $U \to 0$ as $\eta \to \pm\infty$ is , fulfilled. Only a one parameter family of solutions in the (H_0, β) plane has the proper asymptotic behavior. In order to find numerical solutions we transform Equation (3.26a,3.26b) via $z = \log(\eta)$ and $\eta V = U$ into the autonomous system

$$V_z = -V + \frac{3}{8H^3} + \frac{C}{H}, \tag{3.32a}$$

$$H_z = \frac{H}{V+\beta}\left(\frac{1}{3} - \left[\frac{3}{8H^3} + \frac{C}{H}\right]\right). \tag{3.32b}$$

This ordinary differential equation can be solved numerically by starting an integration near the saddle-point $(1/3, H_0(\beta))$ into the direction of the unstable manifold (increasing H-direction), where $H_0(\beta)$ is the inverse of Equation (3.30). Both criteria, zero determinant and the asymptotic behavior respectively, are independent as it can be seen in Figure 3.12, where both curves in the (H_0, β) are shown. In the intersection point of both curves both criteria are simultaneously fulfilled.

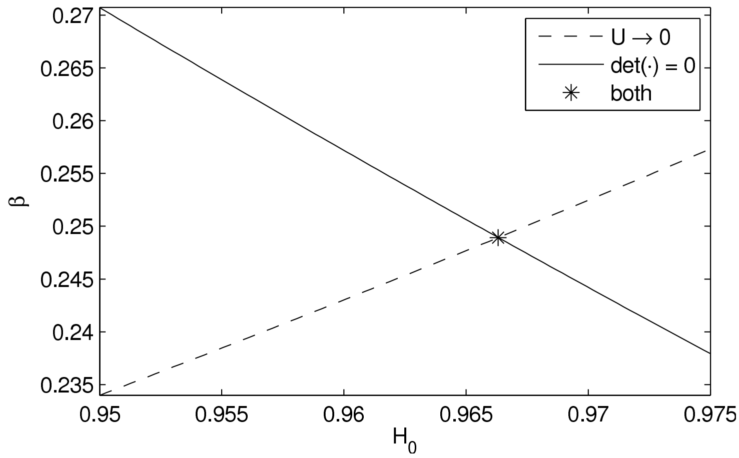

Figure 3.12: Solutions with nontrivial power expansion (full line) or proper asymptotic behavior $U \to 0$ (dashed line), both cross at $H_0 = 0.9663168$, $\beta = 0.2489306$

This is the last condition required to fix β and $H(0)$. Repeating the same procedure for larger values of n ($n = 4, 6, \ldots$) we find other solution of the similarity equation. Although the self-similar scales in Table (3.6) are observed as smooth solutions of the similarity equation with proper behavior at infinity, only the solution for $n = 2$ is realized as a self-similar solution in the strong-slip equation.

3.7 Summary

In this chapter we discussed a numerical scheme to solve the strong-slip equation. The scheme works on adaptive meshes such that the singularity

mode	α	β	H_0
$n=2$	1/3	0.2489306	0.9663168
$n=4$	1/3	0.1280401	0.7915672
$n=6$	1/3	0.0877860	0.6992785

Table 3.6: solutions for higher n with corresponding β and H_0 values

related to the rupture of the thin film can be resolved, in space and in time. Convergence of the scheme is an open question; we expect that it is a delicate question how to show convergence if the external force $\phi(h)$ is purely attractive and thus singular as $h \to 0$. Some issues that appear in the construction of numerical schemes for higher order degenerate parabolic thin-film equations are addressed in the paper by Grün et al.[53] (2000).

Flat states $h(t, y) =$ constant and $u(t, y) = 0$ are exact solutions of the strong-slip solutions but linearly unstable with respect to long-wavelength perturbations of a certain critical wavelength. For small values of b slippage increases this instability, as can be seen from the dispersion relation of the unstable mode

$$\lambda_+(k) = 3bk^2(1-k^2) + \mathcal{O}(b^2).$$

With the numerical scheme we explored the nonlinear solution corresponding to rupture of thin liquid films and found that the thickness of a liquid films evolves as

$$h(t, x^*) \sim (t^* - t)^{1/3},$$

where t^* is the time where the film finally ruptures. Velocity and typical length parameters scale in a similar fashion like $(t^*-t)^\gamma$ and $(x-x^*)(t^*-t)^{-\beta}$ respectively; we found $\beta > 0$ and $\gamma = \beta - 1 < 0$. This type of behavior suggests that the solution of the strong-slip equation evolves locally self-similar and in fact, changing parameters and initial conditions, we found up to three regimes corresponding to three different different similarity solutions.

Generally the role of the Reynolds number $\Re$ and the slip-length b is to select which similarity regimes are observed in which order. The size of the slip-length decides whether the novel similarity regime is observable before the lubrication approximation breaks down. For $\mathcal{O}(1)$ initial data and $\Re \ll 1$ and $b \ll 1$ we find three regimes I,II,III with

$$\begin{aligned} \alpha_I &= 1/6, & \beta_I &= 1/3, \\ \alpha_{II} &= 1/3, & \beta_{II} &= 0.24893..., \\ \alpha_{III} &= 1/3, & \beta_{III} &= 1/2. \end{aligned}$$

Solving a nonlinear ordinary differential equation we compute the similarity scales of regime II and find an infinite family of similarity solutions of second kind. This is similar to the approach by Papageorgiou [19].

In the next chapter we add a more sophisticated mathematical analysis of self-similar solutions and their properties. We concentrate on a simplified nonlinear model which only contains the leading order singular terms.

Chapter 4

Analysis of a Simplified Thin-Film Model

4.1 Simple Examples and Properties

Before we prove properties of the integro-differential equation, let us have a look at some numerical examples and show some basic properties of (4.51). Later in this chapter we also consider similar equations describing jet pinch-off of a liquid thread [19, 22]. For convenience define the averaged stretching by $s_0(t) = \sqrt{C(t)}$. For completeness the full problem is stated again. We seek solutions $s : [0 : t^*) \times \Omega \to \mathbb{R}^+$ of the equation

$$\dot{s}(t,x) = s(t,x)^2 \left(s(t,x)^2 - s_0^2(t) \right), \tag{4.1a}$$

$$s_0^2\,(t) = \int_\Omega s(t,x)^4 \, dx \quad \Big/ \quad \int_\Omega s(t,x)^2 \, dx, \tag{4.1b}$$

where $t \geq 0$ and with initial data

$$s(0,x) = s_i(x), \quad x \in \Omega = [0,1]. \tag{4.1c}$$

Suppose that $s_i(x)$ is non-negative, bounded and normalized in the following sense

$$\int_\Omega s_i(x) \, dx = 1. \tag{4.1d}$$

Define the abbreviation $s_{\max}(t) := \max_x s(t,x)$. Since the evolution defined by (4.1) is locally Lipschitz continuous in $C\big([0,T] \times \Omega\big)$ with $\|u\|_\infty = \sup_{[0,T]\times\Omega} |u|$, by virtue of the Picard-Lindelöf theorem, unique solutions exist and can be extended as long $s_{\max}(t)$ remains finite. At the instant when $s_{\max}(t)$ becomes infinite, say at $t = t^*$, the model becomes ill-posed anyway.

We will concentrate on the question, whether $s_{\max}(t)$ determined from (4.1) has a blow-up after a finite time and how the nonlinear behavior of this blow-up is related to rupture of thin films in the strong-slip equation.

As for the strong-slip equation, the flat liquid film $s(t,x) = 1$ is a (global) solution of the integro-differential equation. Small perturbation of the flat film $s(t,x) = 1 + \delta s(t,x)$ solve

$$\delta\dot{s}(t,x) = 2\delta s(t,x) - 2\delta s_0(t) \qquad \text{where} \qquad \delta s_0(t) = \int_0^1 \delta s(t,x) \, dx.$$

which shows that perturbations different from the average stretching $\delta s > \delta s_0$ tend to grow. Obviously, the stability depends only on the amplitude (and not on wave-lengths of perturbations) because surface tension and other higher-order terms are not considered.

4.1.1 Examples

In the beginning of this chapter we prove blow-up of solutions, in particular that blow-up occurs within a finite time. This is equivalent to property i) in the introduction, namely, the singularity of the interface occurs after a finite time.

In the following example we show that one can easily construct stationary solutions; these solutions are bounded and provide counter-examples to what we would like to show. For example consider the following class of solutions of (4.1)

$$s(t,x) = \begin{cases} \frac{1}{\delta} & \text{in } \omega \subset \Omega \\ 0 & \text{elsewhere} \end{cases} \tag{4.2}$$

where the size of the set ω such that is $|\omega| = \delta > 0$. Solutions with positive initial data that can be decomposed

$$s_i(x) = \begin{cases} s_{\max}(0) & \text{in } \omega \subset \Omega \\ s_i(x) < s_{\max}(0) & \text{elsewhere} \end{cases} \tag{4.3}$$

along with property (4.1d) and $|\omega| > 0$ are bounded in time and converge to these stationary solutions. Note that these initial data are not necessarily continuous functions $C\big([0,T] \times \Omega\big)$ for which we showed existence; though it makes perfectly sense to consider initial data in a more general sense. However, for our consideration for restrict to continuously differentiable $h(t_0, y)$ in the Eulerian formulation or equivalently a continuous $s_i(x)$.

Equation for $s(t,x)$ is derived from the strong-slip equation, which contains higher-order derivatives of h, and one might expect that initial data $s(t_0,x)$ exhibit more regularity than the examples (4.2) and (4.3); for example quadratic behavior near the global minimum $h(t_0,x) = h_{\min} + c(x - x_{\min})^2 + \mathcal{O}\big(|x - x_{\min}|^3\big)$. Supposing that initial data behave like that we are able to establish blow-up within a finite time, in fact, we only need that there exists an upper bound with quadratic (or power law) behavior.

In Figure 4.1 we show two numerical solutions of (4.1). Both solutions are computed using an explicit Euler scheme on a uniform (spatial) grid $x_i = i/N$ $(i = 0, ..., N)$

$$s(t_n + \Delta t, x_i) = s(t_n, x_i) + \Delta t \left(s(t_n, x_i)^4 - s(t_n, x_i)^2 s_0(t_n)^2 \right),$$

where average stretching s_0 is computed by the midpoint rule

$$s_0(t_n) = \sum_{i=0}^{N-1} \frac{s(t_n, x_i) + s(t_n, x_{i+1})}{2} (x_{i+1} - x_i).$$

The solution shown in the left panel of Figure 4.1 is bounded $s(t,x) < 2$ for all finite times and seemingly converges to

$$s(t,x) \to \begin{cases} 2 & x \in [0, 1/2] \\ 0 & x \in (1/2, 1] \end{cases}$$

as t goes to infinity. There is convergence to the stationary solution Equation (4.2) because the initial data are as in Equation (4.3). The solution shown in the right panel of Figure 4.1 diverges increasingly fast until the simple numerical scheme is insufficient to resolve the singularity of $s(t,x)$ at $x = 0$. Later we will analyze this type of singular solutions quantitatively. But first let us study properties of (4.1).

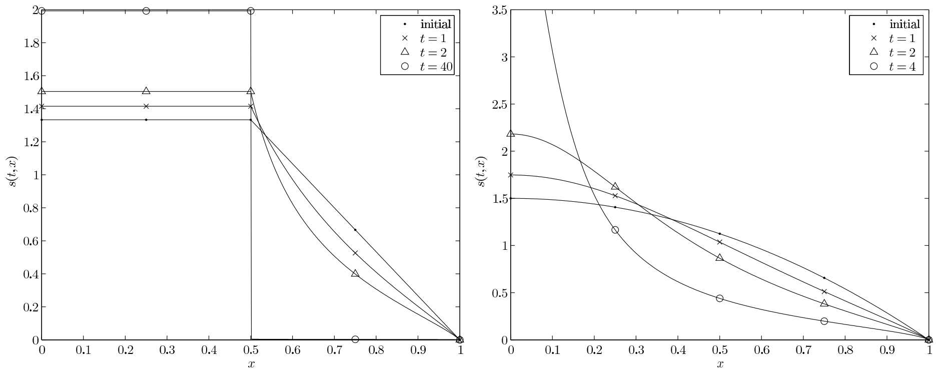

Figure 4.1: Numerical solutions of (4.1) with initial data $s_i(x) = \min\{4/3, 8/3(1-x)\}$ (left; solution is bounded $s(t,x) < 2$) and $s_i = 3/2(1-x^2)$ (right; solution is unbounded) for different times

4.1.2 Properties of Solutions

Examining properties of Equation (4.1) will be helpful to prove blow-up later. The properties proven here are generic for this type of integro-differential equation and do not depend too much on the special form of the equation.

Lemma 4.1. *(Properties of solutions) Solutions of the integro-differential equation* (4.1) *and the related functions* $s_{max}(t)$ *and* $s_0(t)$ *obey the following properties:*

1. *Volume conservation:*

$$\int_\Omega s(t,x)\,dx \equiv 1 \qquad \forall\, t \in [0, t^*). \tag{4.4a}$$

2. *Estimate from above and below:*

$$s_{max}(t) \geq s_0(t) \geq 1. \tag{4.4b}$$

3. *Monotonicity of* s_{max} *and* s_0*:*

$$\dot{s}_{max}(t) \geq 0 \quad \textit{and} \quad \dot{s}_0(t) \geq 0. \tag{4.4c}$$

4. *Maximum-property:*

$$\dot{s}_{max} \geq \dot{s}(t,x) \qquad \forall x \in \Omega, t \in [0,t^*). \tag{4.4d}$$

5. $s_0(t) = 1$ *if and only if*

$$s(t,x) = 1 \qquad a.e.\ in\ \Omega \tag{4.4e}$$

6. *For continuous solutions* $s_{max}(t) > s_0(t) > 1$ *if and only if the set*

$$M_\epsilon(t) = \big\{x \in \Omega : \epsilon < s(t,x) < s_0(t) - \epsilon\big\}$$

has strictly positive measure for some $\epsilon > 0$.

Proof.

1. Integrate (4.1a) and use (4.1b) and (4.1d).
2. The first inequality follows by applying the Cauchy-Schwarz (C.S.) $\|uv\|_1 \leq \|u\|_\infty \|v\|_1$ to $u = v = s^2$. Hence

$$\int_\Omega s^4\,dx \leq s_{\max}^2 \int_\Omega s^2\,dx.$$

Similarly one uses C.S. to find

$$s_0^2 = \frac{\int s^4\,dx}{\int s^2\,dx} \geq \int_\Omega s^2\,dx \geq \left(\int_\Omega s\,dx\right)^2 = 1. \tag{4.5}$$

3. The first inequality is a consequence of 4. For the second part we compute the time-derivative of $s_0^2(t)$

$$\begin{aligned} 2s_0\dot{s_0} &= \frac{4\int \dot{s}s^3\,dx}{\int s^2\,dx} - \frac{2\int \dot{s}s\,dx \int s^4\,dx}{(\int s^2\,dx)^2} \\ &= \left(\int_\Omega s^2\,dx\right)^{-1} \left(\quad 2s_0^4 \int_\Omega s^3\,dx - 6s_0^2 \int_\Omega s^5\,dx + 4\int_\Omega s^7\,dx \quad \right) \\ &= \left(\int_\Omega s^2\,dx\right)^{-1} \left(A\,s_0^4 + B\,s_0^2 + C\right) \end{aligned}$$

with $A = 2\int s^3\,dx$, $B = -6\int s^5\,dx$ and $C = 4\int s^7\,dx$. This expression is non-negative, if $s_0^2 \leq (-B - \sqrt{B^2 - 4AC})\,/\,2A$. Using

$$B^2 - 4AC = 36\left(\int_\Omega s^5\,dx\right)^2 - 32\int_\Omega s^3\,dx \int_\Omega s^7\,dx \overset{\text{C.S.}}{\leq} 4\left(\int_\Omega s^5\,dx\right)^2$$

one finds

$$s_0^2 \le \Big(\int_\Omega s^5\,dx\Big) \Big/ \Big(\int_\Omega s^3\,dx\Big) \quad \Leftrightarrow \quad \dot{s}_0 \ge 0.$$

The assertion follows directly from Cauchy-Schwarz inequalities

$$\begin{aligned} \Big(\int_\Omega s^4\,dx\Big)^2 &\le \int_\Omega s^5\,dx \int_\Omega s^3\,dx \qquad \text{and} \\ \Big(\int_\Omega s^3\,dx\Big)^2 &\le \int_\Omega s^4\,dx \int_\Omega s^2\,dx. \end{aligned}$$

4. The function $f(s) = s^2(s^2 - s_0^2)$ has the non-negative maximum at $s = s_{\max}$ because $f \le 0$ for $s \le s_0$ and $f(s)$ is non-negative and increasing for $s \ge s_0$.

5. By using (4.5) with $s_0 = 1$ we get $\int s^2\,dx = 1$ and therefore

$$0 = \int_0^1 s^2 - 2s + 1\,dx = \int_0^1 (s-1)^2\,dx \ge 0$$

which implies $s = 1$ almost everywhere. The reverse direction is trivial.

6. $s_0 > 1$ follows from 5. ($\Leftarrow$) Assume $s_{\max} = s_0$, then

$$0 = s_{\max}^2 - s_0^2 = \frac{\int s^2(s_{\max}^2 - s^2)\,dx}{\int s^2\,dx}$$

implies that $s(t,x) \in \{0, s_{\max}\}$ almost everywhere, contrary to the assumption that M_ϵ has a finite measure. ($\Rightarrow$) On the other hand suppose M_ϵ is empty for all $\epsilon > 0$, then s is either zero or $s_0 \le s \le s_{\max}$. Since the integrand in

$$0 = \int_\Omega s^2(s^2 - s_0^2)\,dx = \int_{\Omega\setminus M_0} s^2(s^2 - s_0^2)\,dx \ge 0,$$

is positive, this expression can only be zero if $s \in \{0, s_0\}$ almost everywhere, which implies $s_{\max} = s_0$.

□

4.1.3 Blow-Up of Solutions

Conservation of mass $\int_0^1 s(t,x)\,dx = 1$, non-negativity $s(t,x) \geq 0$, and uniqueness of solutions imply that solutions are bounded if the maximum is attained on a finite interval. In Figure 4.1 we showed an numerical example for such a behavior.

Suppose $s_i(x)$ is decreasing in x and $s_i(x)$ attains its unique maximum at $x = 0$. In this case the original problem can be mapped to an equivalent problem with decreasing initial data, as it is explained in the following remark.

Remark 4.1. Given an arbitrary $s \in C([0,1];\mathbb{R}^+)$ and for any $f \in C(\mathbb{R}^+)$ define $s(f) = \int_0^1 f\big(s(x)\big)dx$. We say s and $\bar{s} \in C([0,1];\mathbb{R}^+)$ are equivalent $s \sim \bar{s}$ if $s(f) = \bar{s}(f)$ for any $f \in C(\mathbb{R}^+)$. A decreasing $\bar{s}$ can be uniquely constructed as follows: Define $x(r) = \mu\big(y \in [0,1] : s(y) \geq r\big)$ and let $\bar{s}(x)$ be the largest decreasing, continuous function on $[0,1]$ with

$$\bar{s}\big(x(r)\big) = r. \tag{4.6}$$

The relation of this definition to the problem of replacing initial data by decreasing initial data can be easily understood in terms of step functions. Any solution $s(t,x)$ of (4.1) can be approximated by some step function $s^*(t,x)$, where s^* is still a solution of (4.1) with initial data replaced by a step function. By sorting the steps in decreasing order, one can uniquely construct a $s^{**}(t,x)$, for which $\max_\Omega s^* = \max_\Omega s^{**}$ and $s_0^* = s_0^{**}$, and more generally $s^*(f) = s^{**}(f)$.

There is no difference whether one first solves (4.1) for s^* and rearranges the steps then, or first rearrange the steps and then solves (4.1) for s^{**}. For continuous functions the rearrangement is performed formally using (4.6).

Even though the evolution of both systems is in some sense equivalent, the analysis will be less technical if we choose decreasing initial data s^{**}. Later on there will be an additional remark, what this ordering implies for self-similar solutions. $\diamondsuit$

In the following theorem it is shown that if the maximum $s_{\max}(0) = \max_{[0,1]} s_i(x)$ is only attained in a single point, then $s_{\max}(t)$ is unbounded. Recall that from this point on only decreasing initial data are considered; uniqueness implies that solutions are also decreasing then. Therefore define the set

$$P(t) = [0, p(t)] = \{x \in \Omega : s(t,x) \geq s_0(t)\}$$

and $N(t) = \Omega \setminus P(t)$ the complement of $P(t)$ in $\Omega = [0,1]$. Unboundedness of solutions can be proved as follows.

Theorem 4.2. *(Unboundedness of solutions)*
If the initial data (4.1c) *obeys* $s_i(0) > s_i(x)$ *for* $x > 0$*, then* $s_{max}(t)$ *is unbounded in time.*

Proof. Assume the converse is true, i.e., $s(t,0) \leq K$ for all times. Since s_0 and $s_{\max}$ are increasing (4.4c), monotone convergence implies that they converge; both functions must have the same limit $s_0 \to s_{\max} \to \bar{s} \leq K$ as $t \to \infty$. Suppose the limits are distinct, then the maximum cannot be bounded because the lower bound of $\dot{s}_{\max} = s_{\max}^2(s_{\max}^2 - s_0^2) > Cs_{\max}^2$ has an unbounded solution. Using the $P(t)$ and $N(t)$ volume conservation yields

$$1 = \int_\Omega s(t,x)\,dx \;\leq\; p(t)\,K + \int_{N(t)} s(t,x)\,dx. \tag{4.7}$$

Suppose $p(t)$ is bounded from below by $\delta > 0$, i.e., $s(t,x) \geq s_0(t)$ for all $x \leq \delta$. For every fixed $x \in P(T)$ and $0 \leq t \leq T$ the time-derivative $\dot{s}$ is an increasing function of $s(0,x)$, which implies that $s(t,0) - s(t,x)$ grows for all $x < \delta$. Then the inequality

$$s_{\max}(t) - s_0(t) \geq s(t,0) - s(t,\delta) \geq s_i(0) - s_i(\delta) > 0,$$

is a contradiction to convergence $s_0 \to s_{\max} \to \bar{s}$ showing that $p(t)$ must converge to zero. Analogously one finds $s(t,x) \to 0$ for any fixed $x \in N(t)$ as $t \to \infty$. Both terms on the right hand side of (4.7) go to zero. This contradiction to volume conservation finally shows that the assumption is wrong and $s_{\max}(t)$ must be unbounded. ☐

The time-dependent maximum $s_{\max}(t)$ is unbounded, if the maximal value of $s_i(x)$ is attained only in a single point. Unfortunately this proof does not produce any quantitative information about the speed of the blow-up. If more information about the initial data are available, in particular about the behavior near the maximum, one can compute an upper bound on the blow-up time explicitly. Suppose $s_i(x)$ is bounded from above near the maximum at $x = 0$ like

$$s_i(x) \leq s_i(0) - f(x),$$

where $f(x)$ is increasing with $f(0) = 0$. We are going to prove that $s_{\max}(t)$ is unbounded for some finite time if there exists an upper bound with $f(x) = Cx^n$ for some $C, n > 0$.

4.2 Thin-Film Rupture after Finite Time

In the introduction of this chapter we claimed that the finite time rupture is a qualitative feature, shared by many thin-film models. We observed this behavior for all solutions of the intertialess strong-slip equation. Now we need to check whether the simplified integro-differential equation also has this feature and whether the singularity develops at the same rate.

The strategy of our proof consists of two steps: First we consider a general bound $s_i(x) \leq s_i(0) - f(x)$ and define a time evolution for f such that

$$s(t,x) \leq s(t,0) - f(t,x).$$

For $x \in P(t)$ we estimate $f(t,x)$ from below.

Second, since $P(t)$ is decreasing, we should find an efficient estimate on $p(t)$ from below, i.e., $0 < \widetilde{p}(t) \le p(t)$. Then it holds that

$$s_{\max}(t) \ge s_{\max}(t) - s_0(t) \ge f\big(t, p(t)\big) \ge f\big(t, \widetilde{p}(t)\big).$$

If one expresses $\widetilde{p}(t)$ in terms of $s_{\max}(t)$ and t and integrates both sides of the inequality it turns out that the right hand side diverges after a finite time. Hence $s_{\max}(t)$ diverges after a finite time. For some parts of this proof we follow and generalize the ideas of Renardy [22].

The computation of a lower bound is quite simple; as before $s(t,x)$ denotes the exact solution of problem (4.1) and $s_0(t)$ is the functional defined in (4.1b). For any x with $s_i(x) \le s_i(0) - f(x)$ define $f(t,x) = s_{\max}(t) - \sigma(t)$, where $\sigma(t)$ is the solution of the ordinary differential equation

$$\dot\sigma = \sigma^2 \left(\sigma^2 - s_0^2(t)\right). \tag{4.8}$$

with initial data $s_i(0) - f(x)$. Uniqueness of solutions implies that $f(t,x)$ defines an upper bound in terms of $s(t,x) \le s_{\max}(t) - f(t,x)$. The following lemma gives an explicit lower bound for $f(t,x)$.

Lemma 4.3. *For any x in a small neighborhood of $x = 0$, let σ be a solution of Equation (4.8) with initial data $\sigma(0) = s_{max}(0) - f(x)$. Let $s(t,x)$ be decreasing in x and $s_0(t)$ given by (4.1b). Then the time-dependent bound*

$$f(t,x) = s_{max}(t) - \sigma(t)$$

can be estimated from below by the inequality

$$f(t,x) \ge f(x) \exp\left(\int_0^t s_{max}(t')^3 \, dt'\right) \qquad \forall\, x \in U(t). \tag{4.9}$$

Proof. We estimate the time derivative of σ by a series of steps:

$$\begin{aligned} \dot s_{\max}(t) - \dot f(t,x) &= (s_{\max} - f)^2 \left((s_{\max} - f)^2 - s_0^2\right) \\ &\overset{x\in P}{\le} s_{\max}^2 (s_{\max}^2 - s_0^2 - 2\tilde{f} s_{\max} + f^2) \\ &\overset{f \le s_{\max}}{\le} \dot s_{\max} - f s_{\max}^3. \end{aligned}$$

Now one can subtract $\dot s_{\max}(t)$ and the assertion follows after using Gronwall's lemma for $f(t,x)$. In the last step we used $f(t,x) \le s_{\max}(t)$, which follows again from positivity of σ in (4.8). When we simplified the ordinary differential equation and found an explicit expression for $f(t,x)$, we also reduced the size of the set where the bound is valid. At time t the inequality holds in $U(t) = U \cup P(t)$. □

Obviously one could improve that bound much more by using better estimates. But as we will see, this rough estimate suffices in order to show blow-up in finite time for a huge class of initial data. The following lemma provides the lower bound $\widetilde{p}(t) < p(t)$ that we need in order to prove the finite time blow-up.

Lemma 4.4. *Let the initial data be such that* $s_i(0) > s_0(0) > 1$, *then* $p(t)$ *is bounded from below by*

$$p(t) \geq C_1 \, (t + C_2)^{-2} s_{max}(t)^{-8}. \tag{4.10}$$

Proof. By property (6) there exists an $\epsilon > 0$ such that $|M_\epsilon| > 0$. Then the time-derivative is bounded by $\dot{s} \geq -s_0^2 s^2 \geq -s_{\max}^2 s^2$, which in turn implies

$$s(t,x) \geq \frac{1}{\epsilon^{-1} + t s_{\max}^2} \geq c_1 \, s_{\max}^{-2} (t + c_2)^{-1} \quad (t \geq 0, \forall x \in M_\epsilon). \tag{4.11}$$

where is was used that $\int_0^t s_{\max}(s) ds < t s_{\max}(t)$. Note that the size of the set $m(t) = |M_\epsilon|$ is an increasing function. Then use the integro-differential equation to bound $p(t)$ as follows

$$\begin{aligned} p(t) s_{\max}^4 &\geq p(t) \dot{s}_{\max} \, \geq \, \int_P \dot{s} \, dx \\ &= - \int_N \dot{s} \, dx \, \geq \, - \int_{M_\epsilon} \dot{s} \, dx \\ &\geq \int_{M_\epsilon} s^2 (s_0^2 - (s_0 - \epsilon)^2) \, dx \, \geq \, c_3 \int_{M_\epsilon} s^2 \\ &\geq m(0) \, c_3 \, \min_{M_\epsilon} s^2 \overset{(4.11)}{\geq} C_1 \, s_{\max}^{-4} (t + C_2)^{-2} \end{aligned}$$

which was to be shown. ☐

In the next lemma we combine both lemmas to show blow-up. It remains an open question, to which extent this proof can be extended if the maximum is unique but the solution is not bounded by such a power law, e.g., $s_i(x) = \alpha_n (e^{-1} - e^{-1/x^n})$ initial data (α_n is the normalization factor). For sufficiently large n the estimates in our proof do not suffice to show blow-up in a finite time.

Theorem 4.5. *Let* $s(t,x)$ *be a solution of* (4.51) *with non-negative, decreasing initial data* $s_i(x)$. *Suppose, in a small neighborhood* U *of* $x = 0$ *we have an upper bound*

$$s_i(x) \leq s_i(0) - C x^n$$

for some arbitrary $C, n > 0$. *Then* $s_{max}(t)$ *blows up after a finite time.*

Proof. First of all, volume conservation implies

$$p(t)s_0(t) \leq 1. \tag{4.12}$$

In Theorem 4.2 we showed that $s_{\max}(t)$ is unbounded. Suppose $s_0(t)$ is bounded, then the integro-differential equation immediately implies blow-up after a finite time. Suppose s_0 is unbounded, then (4.12) reveals that $P(t) \subset U$ holds after a finite time. Presume that this is already true initially at $t = 0$ and apply (4.9) from Lemma 4.3 with time-dependent $x = p(t)$. The upper bound $s_i(x) < s_i(0) - Cx^n$ implies $s_{\max} > s_0 > 1$ which makes the application of (4.10) from Lemma 4.4 possible. Thus we obtain the inequality

$$\begin{aligned}
s_{\max}(t) \geq & \qquad s_{\max}(t) - s(p(t), t) \geq f(t, p(t)) \\
\geq & \qquad f(p(t)) \exp\left(\int_0^t s_{\max}(t')^3 \, dt'\right) \\
\geq & \qquad f\left(C_1 s_{\max}^{-8}(t + C_2)^{-2}\right) \exp\left(\int_0^t s_{\max}(t')^3 \, dt'\right) \\
= & \qquad C\, C_1^n s_{\max}^{-8n}(t + C_2)^{-2n} \exp\left(\int_0^t s_{\max}(t')^3 \, dt'\right).
\end{aligned}$$

In order to rewrite this inequality in terms of a differential inequality, which is easier to deal with, define $q(t) = \int_0^t s_{\max}(t')^3 \, dt'$ and insert it into the previous estimate. This yields the differential inequality

$$(\dot{q})^{\frac{8n+1}{3}} \geq C C_1^n (t + C_2)^{-2n} \exp(q) \qquad \text{for} \quad t \geq 0,$$

with $q(0) = 0$. We end up with the following convenient expression after rescaling t and q with a finite but n dependent scale

$$\dot{q} \geq (t + c)^{-\alpha} \exp(q) \tag{4.13}$$

with $\alpha = \frac{6n}{8n+1} < 1$. By explicit integration we get

$$q(t) \geq -\log\left(1 - \frac{(t + c)^{1-\alpha} - c^{1-\alpha}}{1 - \alpha}\right), \tag{4.14}$$

which has a blow-up after a finite time. $\square$

The estimates that are used in this proof are quite rough. Therefore we check the leading order singular behavior of our estimate and compare with the expectation $h \sim (-h)^{1/3}$. Differentiating the lower bound

$$q(t) = -\log\left(1 - \frac{(t + c)^{1-\alpha} - c^{1-\alpha}}{1 - \alpha}\right) = -\log\bigl(w(t)\bigr),$$

with respect to time gives

$$s_{\max}(t)^3 \sim \dot{q}(t) = \frac{w'(0)}{t^* - t} + O(1),$$

which corresponds to the expected behavior $s_{\max}(t) \simeq C(t^* - t)^{-1/3}$; this result also justifies our rough estimates,

4.3 Jet Pinch-Off after a Finite Time

As it was mentioned earlier, basic ideas and notion of the previous proof are lend from the paper by Renardy on jet pinch-off in finite time [22]. In his proof Renardy assumed differentiability of the initial data and used an essential auxiliary lemma, which unfortunately turned out to be incorrect (see corrigendum of [22]).

We use (4.9) to estimate the upper bound. This approach different because it makes no use of the property used in Renardy's auxiliary lemma, and it's more general because no differentiability of initial data is required.

The same technique can be applied to the jet pinch-off model very easily, because the model differs only slightly from (4.51). Consider the following set of equations describing inertialess jet pinch-off of a liquid thread [19, 22]

$$\dot{s}(t,x) = s(t,x)^{3/2}\left(\sqrt{\frac{s(t,x)}{s_0(t)}} - 1\right), \tag{4.15a}$$

$$s_0^{1/2}(t) = \int_\Omega s(t,x)^2\,dx \Bigg/ \int_\Omega s(t,x)^{3/2}\,dx. \tag{4.15b}$$

As before initial data are non-negative, decreasing and normalized such that

$$\int_0^1 s_i(x)\,dx = 1. \tag{4.15c}$$

All properties of Lemma 4.1 can be carried over to (4.15). The computation of $\dot{s_0} > 0$ can be found in [22]. For jet pinch-off we compare solutions with solutions of the auxiliary ordinary differential equation

$$\dot{\sigma} = \sigma^{3/2}\left(\frac{\sigma^{1/2}}{s_0^{1/2}} - 1\right), \tag{4.16}$$

and obtain the following lemma.

Lemma 4.6. *Let $\sigma(t,x)$ be a solution of* (4.16) *and define $f(t,x) := s_{max}(t) - \sigma(t,x)$ for every $x \in U$. Then the following estimate holds:*

$$f(t,x) \geq f(x) \exp\left(\frac{1}{2}\int_0^t s_{max}(t')^{1/2}\,dt'\right), \qquad \forall x \in U \cap P(t). \tag{4.17}$$

Note that $P(t)$ is shrinking.

Proof. With the previous definition of σ and f the following steps are obvious:

$$\begin{aligned}
\dot{s}_{\max}(t) - \dot{f}(t,x) = \dot{\sigma} &= (s_{\max} - f)^{3/2}\left[\left(\frac{s_{\max} - f}{s_0}\right)^{1/2} - 1\right] \\
&\overset{x\in P}{\leq} s_{\max}^{3/2}\left[\left(\frac{s_{\max} - f}{s_0}\right)^{1/2} - 1\right] \\
&\leq s_{\max}^{3/2}\left[\left(\frac{s_{\max}}{s_0}\right)^{1/2}\left(1 - \frac{f}{2s_{\max}}\right) - 1\right] \\
&= \dot{s}_{\max} - \frac{f}{2}\frac{s_{\max}}{s_0{}^{1/2}}.
\end{aligned}$$

The assertion follows again after applying Gronwall's lemma to the differential inequality and using the initial data $f(0,x) = f(x)$. □

Similar to the previous theorem we need a lower bound to the size of $p(t)$.

Lemma 4.7. *If $s_{max}(0) > s_0(0) > 1$, then p is bounded by*

$$p(t) \geq C_1\, s_{max}^{-2}\,(t + C_2)^{-3} \qquad \text{for} \quad t \geq 0 \tag{4.18}$$

Proof. Analogous to proof of (4.10). □

Theorem 4.8. *Let $s(t,x)$ be a solution of (4.15) with non-negative, decreasing initial data $s_i(x)$. In an neighborhood of $x = 0$ we have*

$$s_i(x) \leq s_i(0) - Cx^n$$

for some $C, n > 0$. Then $s_{max}(t)$ blows up after a finite time.

Proof. Like in the proof for rupture in finite time we find

$$\begin{aligned}
s_{\max}(t) \geq s_{\max}(t) - s(p(t),t) &\geq f(t,x) \\
&\geq C\,(p(t))^n\, \exp\left(\frac{1}{2}\int_0^t s_{\max}(t')^{1/2}\,dt'\right) \\
&\geq C\,C_1^n\, s_{\max}^{-2n}(t + C_2)^{-3n}\, \exp\left(\frac{1}{2}\int_0^t s_{\max}(t')^{1/2}\,dt'\right).
\end{aligned}$$

and define $q(t) = \int_0^t s_{\max}(t')^{1/2}\,dt'$. For convenience we rescale q and t and obtain the differential inequality

$$\dot{q} \geq (t + c)^{-\alpha} \exp(q) \tag{4.19}$$

with $\alpha = \frac{3n}{4n+2} < 1$. Again this can be integrated explicitly and implies pinch-off after a finite time. $\square$

Analogous to the previous proof we find that the estimate reproduces the known leading order singular behavior $s_{\max}(t) \simeq C(t^* - t)^{-2}$ [15, 19].

Let us summarize what was proven in the first part of this chapter. The question of whether solutions blow-up after a finite time or whether they stay bounded depends very much on the local behavior of the initial data near the maximum. If the maximum is attained in a finite interval, then the solution stays bounded. In all other cases solutions are unbounded. In the special case where initial data are bounded from above like

$$s_i(x) \leq s_i(0) - Cx^n,$$

for some $C, n > 0$ we proved that the blow-up occurs after a finite time. The lower bound which we computed in the proof reproduces the known growth rates for jet pinch-off and the $(-t)^{1/3}$ behavior that we found in the previous chapter.

Slight changes of the initial data near the maximum of $s_i(x)$ can change the later behavior qualitatively. In the theory of Ostwald ripening self-similar solutions show a similar dependence on the initial data; this dependence is associated with the term *weak selection* [54]. For the remaining part of this chapter we explain how the local behavior of the initial data influences the emerging self-similar solutions for second-kind similarity solutions of (4.1).

4.4 Definition of Similarity Solutions

In Chapter 3 we performed a numerical analysis and found that the finite time rupture of the strong-slip equation evolves self-similar, computed similarity solutions and their similarity scales. Now the focus is the discussion of property ii), namely self-similarity in the simplified model. The main goal is to identify the similarity solutions of Chapter 3 within the set of similarity solutions of the simplified integro-differential equation.

In doing so we can show existence of exact self-similar solutions and convergence to self-similar solutions in some special cases. The following questions will be addressed:

- How can we identify the self-similar solution of the strong-slip equation?

- Are the self-similar solution of the integro-differential equation unique, or is there also a *weak selection* mechanism?
- Can we prove convergence to self-similar solutions is this simplified framework?

Therefore let us recall the integro-differential equation again. Let $s : [0, t^*) \times \Omega \mapsto \mathbb{R}_+$ be a solution of

$$\dot{s}(t,x) = s(t,x)^2 \big(s(t,x)^2 - s_0^2(t) \big), \tag{4.20a}$$

$$s_0^2(t) = \int_\Omega s(t,x)^4 \, dx \quad \Big/ \quad \int_\Omega s(t,x)^2 \, dx, \tag{4.20b}$$

defined in $\Omega = [0,1]$ for times $t \in [0, t^*)$. Initial data s_i are still non-negative and normalized, in addition assume that s_i is formally[1] continuously differentiable. The initial data are chosen such that $s(t,x)$ blows up after a finite time.

Working with self-similar solutions, one often finds that certain scale-transformations of $s(t,x)$ make it easier to characterize self-similar solutions of Equation (4.20). We will use the following two scale transformations

Definition 4.1. (similarity scaling) Let $a : \mathbb{R} \to \mathbb{R}^+$ be some a priori unknown continuous function and $s(t,x)$ is a solution of (4.20). Define the associated rescaled solution $\varphi(\tau, \eta)$ as follows:

$$\varphi(\tau,\eta) = \frac{s(t,x)}{s_{\max}(t)}, \qquad \tau = \ln\left(\frac{s_{\max}(t)}{s_{\max}(0)} \right), \qquad \eta = x\, a(\tau). \tag{4.21}$$

The function $a(\tau)$ is supposed to increase with time and $a(0) = 1$. One expects $a(\tau) \to \infty$ as $\tau \to \infty$. Two such scale transformations $a(\tau)$ and $\bar{a}(\tau)$ are said to be *equivalent*, if there exists a positive number C such that

$$\lim_{\tau \to \infty} \left(\frac{a(\tau)}{\bar{a}(\tau)} \right) = C.$$

The time τ is properly defined because it is continuous and strictly increasing in t. $\diamondsuit$

Definition 4.2. (height scaling) Alternatively, the solution $s(t,x)$ can be rescaled with respect the the maximum as follows

$$\psi(\tau,x) = \frac{s(t,x)}{s_{\max}(t)}, \qquad \tau = \ln\left(\frac{s_{\max}(t)}{s_{\max}(0)} \right). \tag{4.22}$$

This scaling is helpful if one discusses properties that are independent from a. $\diamondsuit$

---

[1] This is required in order to identify the limiting problem of self-similar solutions. For the time-dependent problem differentiability is not needed explicitly.

Both definitions are helpful in order to introduce self-similarity and establish uniqueness in a very simple and natural manner. In what follows we will heavily use that $s(t,x)$ in decreasing, which thereby also holds for ψ and φ, and that ψ and φ are continuous. Some consideration are more general. A definition of local self-similarity is given by the next lemma.

Lemma 4.9. *(local self-similarity) If there exists a similarity scaling $a(\tau)$, such that*

a) $\varphi(\tau,\eta) \to \bar{\varphi}(\eta)$ *pointwise in* η *as* $\tau \to \infty$*,*

b) $\bar{\varphi}(\eta) \to 0$ *as* $\eta \to \infty$*,*

c) $\bar{\varphi}(\eta)$ *maps onto* $(0,1]$ *and is continuous,*

then we say, the solution φ converges locally *to a* self-similar solution $\bar{\varphi}$ *characterized by the similarity scaling* $a(\tau)$*. The similarity scaling is unique up to equivalence.*

Proof. The first part is only definition. It remains to shown uniqueness of $a(\tau)$. In the proof it is used that $\varphi(\tau,\eta)$ converges uniformly, which we show later. Suppose φ_a and $\varphi_{\bar{a}}$ are two different limits obtained from one solution $s(t,x)$ by two non-equivalent scalings $a(\tau)$ and $\bar{a}(\tau)$ respectively. Furthermore, assume that $\varphi_a(\tau,\eta)$ converges to $\bar{\varphi}_a(\eta)$ as $\tau \to \infty$ (existence of a limit). For any two scalings the following identity holds

$$\varphi_{\bar{a}}(\tau,\eta) = \frac{s(t,\eta/\bar{a}(\tau))}{s_{\max}(t)} = \varphi_a\left(\tau, \tfrac{a(\tau)}{\bar{a}(\tau)}\,\eta\right).$$

From continuity and uniformity of the limit $\bar{\varphi}_a$ it follows that $\varphi_{\bar{a}}$ also converges locally to a self-similar solution, assuming that $a(\tau)/\bar{a}(\tau)$ converges to a finite, positive number C; the limit is given by $\bar{\varphi}_{\bar{a}}(\eta) = \bar{\varphi}_a(C\eta)$ then. In extended real numbers the limit might be $C = 0$ and $C = +\infty$ and the corresponding limits are

$$\lim_{\tau\to\infty} \varphi_{\bar{a}}(\tau,\eta) = 1, \tag{4.23a}$$

and

$$\lim_{\tau\to\infty} \varphi_{\bar{a}}(\tau,\eta) = \begin{cases} 1 & \eta = 0 \\ 0 & \text{otherwise} \end{cases} \tag{4.23b}$$

which can be understood from $\bar{\varphi}_{\bar{a}}(\eta) = \bar{\varphi}_a(C\eta)$ by using the formal rule $\infty \cdot 0 = 0$. However, these stationary limiting solutions are no self-similar solution because the solution corresponding to $C = 0$ does not obey property b), while the solution corresponding to $C = +\infty$ does not obey property c).

We still have to show that $\varphi_{\bar{a}}$ does not converge if $a(\tau)/\bar{a}(\tau)$ does not converge as $\tau \to \infty$. Suppose $a/\bar{a}$ does not convergence, then it has at least two distinct accumulation points $\alpha_1, \alpha_2 \geq 0$ (including infinity and zero) but $\varphi_{\bar{a}}$ converges locally to a self-similar solution. Due to uniform convergence we have $\varphi_a(\eta) = \varphi_{\bar{a}}(\alpha_1 \eta) = \varphi_{\bar{a}}(\alpha_2 \eta)$ for all η, which is only true if either $\alpha_1 = \alpha_2$ or if φ_a and $\varphi_{\bar{a}}$ are given by Equation (4.23). Where the first is a contradiction to the existence of distinct accumulation points, the second conjecture contradicts convergence of $\varphi_{\bar{a}}$ to a self-similar solution. ☐

Surely, this is not a general definition of self-similarity, rather it depends on the problem under consideration, e.g., we make heavy use of the assumption that solution decreases in x.

We stated that the choice of an appropriate scaling might simplify the discussion of similarity solutions considerably. The definition (4.21) has the advantage that we get rid of an additional s-scale. More generally, it is possible to consider to scale the function values $s(t,x)$ with an arbitrary time-dependent function $\phi(\tau,\eta) = b(\tau)s(t,x)$. But, since we want to resolve similarity solutions that describe the leading order singular behavior of the rupture, only scalings that are equivalent to (4.21) are reasonable.

In the definition of self-similarity continuity limiting properties, e.g., $\bar{\varphi}(\eta) \to 0$ (as $\eta \to \infty$), are required to ensure uniqueness. Let us clarify again why these properties are necessary. Say $a(\tau)$ is a scaling the yields a proper self-similar solution. Assume that only condition a) and b) of Lemma 4.9 are fulfilled. Then choose an arbitrary function $\bar{a}(\tau)$, such that $\bar{a}/a \to \infty$ as $\tau \to \infty$ and observe that

$$\varphi_{\bar{a}}(\tau,\eta) \to \begin{cases} 1 & \eta = 0 \\ 0 & \text{elsewhere} \end{cases} \tag{4.24}$$

which would also obey a) and b). However, this limit is trivial, it does not contain any information about the original solution, and hence should be excluded. On the other hand, if only a) and c) hold choose any $\bar{a}$ such $\bar{a}(t)/a(t) \to 0$ and find that $\varphi_{\bar{a}}(\tau,\eta) \to 1$ for all η. The limit obeys a) and c). Again this limit is trivial and should be excluded.

By the previous definition the study of self-similar solutions reduces to a study of similarity scalings $a(\tau)$. In some cases simple reasoning allows to determine $a(\tau)$ by scaling arguments; in these cases $a(\tau)$ is equivalent to $\exp(\tau\gamma)$ with a rational power $\gamma \in \mathbb{Q}$. For example, one might argue that $a(\tau)$ should be chosen such that the normalization $\|s(t,x)\|_{L^1}$ holds approximately for the limit $\bar{\varphi}$, i.e.,

$$\lim_{\tau\to\infty} \left[\int_0^1 s_{\max}(\tau)\, \bar{\varphi}(\, a(\tau)\, x \,)\, dx \right] = 1.$$

This implies $a(\tau) = s_{\max}(\tau) = \exp(\tau)$, i.e., $\gamma = 1$. However, convergence with $a(\tau) \simeq \exp(\tau)$ is commonly *not* observed in our numerical simulations. We continue with a discussion of possible scale transformations.

4.5 Similarity Equations and Solutions

The discussion of similarity solutions is much simpler, if all expressions and equations are rewritten in terms of the similarity scaling (4.21) or the height scaling (4.22). In order to transform the solution $s(t,x)$ to rescaled variables one has to assume that $a(\tau)$ and $\varphi(\tau,\eta)$ are differentiable with respect to τ and η. If the similarity scaling (4.21) is applied to solutions of (4.20), we obtain the following equation

$$\partial_\tau \varphi + (\partial_\tau \log a)\, \eta \partial_\eta \varphi = \frac{\varphi^4 - \varphi^2 \lambda}{1-\lambda} - \varphi \tag{4.25}$$

with $\lambda = s_0^2/s_{\max}^2$. The function $\lambda(\tau)$ is the rescaled version of $s_0(t)$ and ensures that the constraint

$$1 = \frac{s_{\max}(\tau)}{a(\tau)} \int_0^{a(\tau)} \varphi(\tau,\eta)\, d\eta.$$

is always fulfilled. Recall the definition $\eta = x\, a(\tau)$ and that the support of the solution increases with time.

We seek $a(\tau)$ such that $\varphi(\tau,\eta)$ approaches a stationary solution and hence we require that $(\log a)_\tau$ in (4.25) approaches a constant, say γ. Stationary solutions describe a self-similar limiting profiles as $\tau \to \infty$. Scale transformations with a constant γ are given by

$$a(\tau) = \left(\frac{s_{\max}(\tau)}{s_{\max}(0)} \right)^\gamma = \exp(\gamma\tau).$$

where the constant γ is the so-called *scaling dimension* of the self-similar solution. For what follows next we assume that the scale transformation is equivalent to a transformation with a constant γ. Using this scale transformation the integro-differential equation transforms into

$$\partial_\tau \varphi + \gamma\, \eta \partial_\eta \varphi = K(\tau)\big(\varphi^4 - \varphi^2\big) + \varphi^4 - \varphi = f\big(K(\tau), \varphi\big) \tag{4.26a}$$

with being $K(\tau)$ defined as

$$K(\tau) = \lambda\, (1-\lambda)^{-1} \tag{4.26b}$$

and

$$\lambda = \int_0^{a(\tau)} \varphi^4(\tau,\eta)\, d\eta \quad \Big/ \quad \int_0^{a(\tau)} \varphi^2(\tau,\eta)\, d\eta. \tag{4.26c}$$

Note that the value of $K(\tau)$ does not depend on a particular scaling, since it is defined as the quotient of two integrals. The domain of integration is the interval $[0, e^{\gamma\tau}]$ and $\lambda(\tau) \in (0,1]$. For every finite τ the integrals are well defined; since φ is in general not bounded by a measurable function it is not clear whether $K(\tau)$ converges, even though K might be well-defined for the limit. We will see that in most cases $\|\varphi\|_{L_1}$ is not bounded and in some cases even the second and fourth moments are unbounded as $\tau \to \infty$.

Remark 4.2. Note that the simplifying replacement of $(\log a)_\tau$ by a constant is not always justified. For example, if we compare two scalings

$$a(\tau) = \exp\bigl(\gamma\tau\bigr) \qquad \text{and} \qquad \bar{a}(\tau) = \exp\Bigl(\int_0^\tau \gamma(s)\, ds\Bigr),$$

with $\gamma(\tau) \to \gamma$ then we have $(\log\, a)_\tau \to \gamma$ for both scalings. However, both scalings are only equivalent if

$$\frac{a(\tau)}{\bar{a}(\tau)} = \exp\left(\int_0^\tau \bigl(\gamma - \gamma(s)\bigr)\, ds\right)$$

converges to a constant as $\tau \to \infty$, i.e., $\bigl(\int_0^\infty \gamma - \gamma(s)\, ds\bigr)$ is finite. This problem does not affect the discussion of exact similarity solutions, however, one should consider such scalings in the context of convergence. $\diamondsuit$

In any case, since the singularity is local we can infer that $\partial_\tau(\log a(\tau))$ converges to a positive constant $\gamma > 0$. Furthermore, in rescaled variables conservation of mass reads

$$\frac{\exp\bigl((\gamma - 1)\tau\bigr)}{s_i(0)} = \int_0^{e^{\gamma\tau}} \varphi(\tau, \eta)\, d\eta.$$

Now suppose φ converges to a self-similar solution, then the integral on the right hand side is bounded from below which in turn implies $\gamma \geq 1$.

One can also apply the height scaling (4.22) to any solution of the integro-differential equation. The height scaling will be helpful if we study properties which are independent from the choice of $a(\tau)$. The rescaled solution ψ solves the following differential equation

$$\partial_\tau \psi = f\bigl(K(\tau), \psi\bigr) \qquad \text{where} \qquad f(K, \psi) = K(\psi^4 - \psi^2) + \psi^4 - \psi \quad (4.27)$$

and with $K(\tau)$ defined as before. For all $\psi \in (0, 1)$ and $K \geq 0$ the function $f(K, \psi)$ is negative, with $f(K, \psi) = 0$ if $\psi \in \{0, 1\}$. Solution will ultimately run into the stable fixed point given by (4.24). Still this scaling will be useful, since we can write down an implicit solution formula for ψ. Before we discuss convergence to self-similar solutions, we first classify exact self-similar solutions of (4.26).

4.6 Exact Self-Similar Solution

In this section a characterization of exact similarity solutions will be given. These solutions will be compared to the known self-similar solutions of the strong-slip equation without inertia. Since there is a transformation between Eulerian and Lagrangian reference frames, we shall compute how similarity solutions in both systems are related to each other. In the previous chapter we found that $h(t,y)$ approaches a self-similar solution given by

$$(-t)^{-\alpha} h(t,y) = H(\tau,\eta) \overset{\tau\to\infty}{\to} H(\eta) \qquad \text{with } \eta = y\,(-t)^{-\beta}.$$

The transformation between variables related to x (Lagrangian) and y (Eulerian) variables by definition reads

$$y = \phi_t(x) = \int_0^x s(t,z)\,dz.$$

In order to compute the relationship between self-similar solutions in Eulerian and Lagrangian reference frames, suppose that $s(t,x)$ approaches locally a self-similar profile, i.e.,

$$s(t,x)/s_{\max}(t) = \varphi(\tau,\eta) \overset{\tau\to\infty}{\to} \bar{\varphi}(\eta) \qquad \text{with } \eta = x\, s_{\max}^{\gamma}(t).$$

Next, simply write both self-similar solutions in a common coordinate frame. Then the (outer) scale is fixed by requiring that the powers of $(-t)$ in

$$(-t)^{\alpha} H(\tau,\eta) = (s_{\max})^{-1} \frac{1}{\varphi(\tau,\eta)}$$

are equal, thus $s_{\max}(t) \to (-t)^{-\alpha}$. Similarly the (inner) scale can be determined by requiring that this is also true for the inner scale (the powers in front of η)

$$\begin{aligned} x\, s_{\max}^{\gamma} = x\,(-t)^{-\alpha\gamma} &= (-t)^{-\beta} \int_0^x s(t,z)\,dz \\ &= (-t)^{-\beta} x\, s(t,0) + o(x) \\ &= (-t)^{-\alpha-\beta} x\, \bar{\varphi}(0) \quad \Rightarrow \quad \gamma = \frac{\alpha+\beta}{\alpha}. \end{aligned}$$

At this point we refer to the results of the last chapter. We obtained values for the similarity scales α and β numerically, namely $\alpha = \frac{1}{3}$ and $\beta \approx 0.2489$; the former was determined by scaling arguments and the latter only numerically. Converting these numbers into the similarity scales of the integro-differential equation we compute the similarity scale $\gamma \approx 1.7468$.

First of all we define what we call an exact self-similar solution of (4.1).

Definition 4.3. (exact similarity solutions)
A continuous solution of

$$\gamma\eta\frac{d\bar{\varphi}}{d\eta} = f(K,\bar{\varphi}) \quad \text{with} \quad f(K,\bar{\varphi}) = K(\bar{\varphi}^4 - \bar{\varphi}^2) + \bar{\varphi}^4 - \bar{\varphi} \tag{4.28a}$$

$$K^* = \int_0^\infty \bar{\varphi}(\eta)^4 \, d\eta \quad \Big/ \quad \left(\int_0^\infty \bar{\varphi}(\eta)^2 - \bar{\varphi}(\eta)^4 \, d\eta\right), \tag{4.28b}$$

which solves the constraints $K^*\big(K,\gamma\big) = K$, $\bar{\varphi}(0) = 1$, and $\bar{\varphi}(\eta) \overset{\eta\to\infty}{\to} 0$ is called an *exact self-similar solution* of (4.1). In case the second moment of $\bar{\varphi}$ is infinite define $K^* = 0$. Setting $K^* = 0$ is motivated by the following propositions. ♢

Remark 4.3. Given a solution of (4.28a), the scaled function $\bar{\varphi}(c\eta)$ (for any $c > 0$) is a solution as well. The constraint $K^*(K,\gamma) = K$ is automatically fulfilled for scaled solutions because K^* does not change under such a transformation.

This is not surprising because those solutions correspond to equivalent self-similar solutions with scalings $\bar{a}/a \to c$, where the trivial solutions (4.23) with $c = 0$ and $c = \infty$ are excluded. ♢

The main difficulty regarding existence and uniqueness of self-similar solutions is to show that there exists solutions, such that the constraint $K^*(K,\gamma) = K$ holds true. Uniqueness is again up to equivalence of solution and for fixed γ, i.e., there exists a unique equivalence class of solutions for every $\gamma > 1$.

We set $K^* = 0$ if the second moment of $\|\bar{\varphi}^2\|_1$ is unbounded. This is is motivated by the following two propositions, which are simple consequences of convergence towards self-similar solutions.

Proposition 4.10. *(uniform convergence of solutions)*
Suppose $\varphi(\tau,\cdot)$ is a continuous mapping onto $[0,1)$ that decreases to zero as η goes to infinity, i.e., $\varphi(\tau,0) = 1$ and $\varphi(\tau,\eta) \overset{\eta\to\infty}{\to} 0$. If $\varphi(\tau,\eta)$ converges pointwise to a continuous limit $\bar{\varphi}$ as $\tau \to \infty$, then it even converges uniformly.

Proof. This property is a consequence of monotonicity and continuity which can be proven like this. For any given $\epsilon > 0$ choose a ordered set of points $\eta_i \in \mathbb{R}^+$ such that $\eta_1 = 0$, $\eta_i < \eta_{i+1}$, $|\bar{\varphi}(\eta_i) - \bar{\varphi}(\eta_{i+1})| < \epsilon/3$, and $\min_i \bar{\varphi}(\eta_i) < 2\epsilon/3$; one can always find a set with finitely many points $i \in \{1,...,m\}$. Pointwise convergence of φ at all $\{\eta_i\}$ implies that there exists a τ_0 such that $|\varphi(\tau,\eta_i) - \bar{\varphi}(\eta_i)| < \epsilon/3$ holds for all i and $\tau > \tau_0$. Then, for any $\eta_i \leq \eta \leq \eta_{i+1}$ $(i < m)$ we have

$$|\varphi(\tau,\eta) - \bar{\varphi}(\eta)| \leq |(\bar{\varphi}(\tau,\eta_i) + \epsilon/3) - (\bar{\varphi}(\eta_{i+1}) - \epsilon/3)| \leq \epsilon,$$

and for all $\eta \geq \eta_m$ we have $0 \leq \varphi(\tau, \eta) \leq \epsilon$ and $0 \leq \bar{\varphi}(\eta) \leq 2\epsilon/3$. Thus,

$$|\varphi(\tau, \eta) - \bar{\varphi}(\eta)| \leq \epsilon$$

uniformly as $\tau \to \infty$. □

Unfortunately this proposition does not help us to show convergence of $K(\tau)$ since the domain of integration is the unbounded. Uniform convergence is only helpful if $\varphi(\tau, \eta)$ has a finite support independently of τ. Nevertheless is serves as a good characterization of the limiting behavior. In one special case we can show convergence of $K(\tau) \to 0$ already.

Proposition 4.11. *Assume that $\varphi(\tau, \eta)$ converges to a self-similar solution and $\int_0^{e^{\gamma\tau}} \varphi^2 \, d\eta$ goes to infinity. Then*

$$\lim_{\tau \to \infty} K(\tau) = 0.$$

Proof. Divide the domain in a part $[0, \eta_0]$ and the remainder (η_0, ∞). The integrals in the first part are bounded, while they diverge in the second part. Since the denominator of the expression for K diverges much faster, K must converge to zero.

For any small $\epsilon > 0$ one can choose η_0 and τ_0 such that $\epsilon/2 < \varphi(\tau, \eta_0) < \epsilon$ (due to convergence) for all $\tau > \tau_0$. Using $K = \lambda/(1 - \lambda)$ we have

$$\begin{aligned}
\lambda(\tau) = \frac{\int_0^\infty \varphi^4 \, d\eta}{\int_0^\infty \varphi^2 \, d\eta} &\leq \frac{\int_0^{\eta_0} d\eta + \int_{\eta_0}^\infty \varphi^4 \, d\eta}{\int_0^{\eta_0} (\epsilon/2)^2 \, d\eta + \int_{\eta_0}^\infty \varphi^2 \, d\eta} \leq \frac{\eta_0 + \epsilon^2 \int_{\eta_0}^\infty \varphi^2 \, d\eta}{\eta_0 \epsilon^2/4 + \int_{\eta_0}^\infty \varphi^2 \, d\eta} \\
&\to \epsilon^2 \qquad \text{as } \tau \to \infty \text{ (integral is unbounded)} \\
&\to 0 \qquad \text{as } \epsilon \to 0
\end{aligned}$$

□

This proposition is the motivation to set $K^* = 0$ for exact self-similar solution, where $\int_0^\infty \bar{\varphi}(\eta)^2 \, d\eta$ is infinite. As this proposition shows, the case $K^* = 0$ might be simpler to handle. That is why we first consider this special case before we will prove a general theorem for the case $K^* \geq 0$.

4.6.1 Exact Self-Similar Solutions with $K = 0$

The reason to treat the case $K^* = 0$ separately is that one can integrate the ordinary differential equation explicitly and check explicitly if the integral constraint $K^*(\gamma, K) = K$ is fulfilled. Formal integration of $f^{-1}(K, \varphi)$ gives

$$H_K(s) := \int_q^s \frac{dr}{f(K, r)} \qquad \text{some } q \in (0, 1)$$

so that an implicit solution of (4.28) can be written

$$H_K(\varphi(y)) - H_K(\varphi_0) = \gamma^{-1} \log\left(\frac{\eta}{\eta_0}\right). \tag{4.29}$$

Observe the limiting properties of $H_K(s)$

$$H_K(s) = \begin{cases} -\infty & s \to 1 \\ \infty & s \to 0 \end{cases}.$$

When we set $K = 0$ the implicit expression reads

$$H_0(\varphi(y)) - H_0(\varphi_0) = \frac{1}{3} \log \left(\frac{s^3 - 1}{s^3} \right) \Bigg|_{\varphi_0}^{\varphi(y)}$$

which can be solved for $\varphi(\eta)$. Then, for $K = 0$, an explicit formula for the solution of (4.28a) is given by

$$\varphi(\eta) = \left(1 + C\eta^{3/\gamma}\right)^{-1/3} \qquad C = \eta_0^{-3\gamma} \left(\varphi_0^{-3} - 1\right). \tag{4.30}$$

The remaining free parameters of this solution are the constant of integration C, and the scaling dimension γ. Since the choice of C, which represents a scale transformation, does not affect K^*, we must vary γ to fulfill the constraint $K^* = K$. The solution above was derived under the assumption $K = 0$, and explicit integration of it yields

$$\lambda^*(K = 0, \gamma) = \begin{cases} 0 & \gamma \geq 2 \\ \frac{\Gamma(2/3)\,\Gamma(4/3-\gamma/3)}{3^{2/3}\,\Gamma(4/3)\,\Gamma(2/3-\gamma/3)} & \gamma < 2 \end{cases}$$

with $K^*(0, \gamma) = \lambda^*/(1 - \lambda^*)$. Accordingly, for $\gamma \geq 2$ the expression above produces valid solutions, which can be characterized by the asymptotic behavior $\bar{\varphi}(\eta) = 1 - C\eta^n$ near the maximum; the relation between n and γ is $n = 3/\gamma$.

4.6.2 Exact Self-Similar Solutions with $K > 0$

Setting $K = 0$ we found unique self-similar solutions for every $\gamma \geq 2$; obviously the self-similar solution of the strong-slip equation ($\gamma \approx 1.7468$) is not included in this set.

The strategy to show existence and uniqueness for $K > 0$ is twofold: First, existence of self-similar solutions with $K > 0$ is motivated by showing two numerical solutions of (4.28a). In these numerical example it is explained how the self-similar solution of the strong-slip equation is embedded into the set of self-similar solution of the integro-differential equation.

Second, existence and uniqueness of such K^* is proven for any $\gamma > 1$ rigorously.

In the special case $K = 0$ self-similar solution behave like

$$\bar{\varphi}(\eta) = 1 - C\eta^{3/\gamma} + o(\eta^{3/\gamma})$$

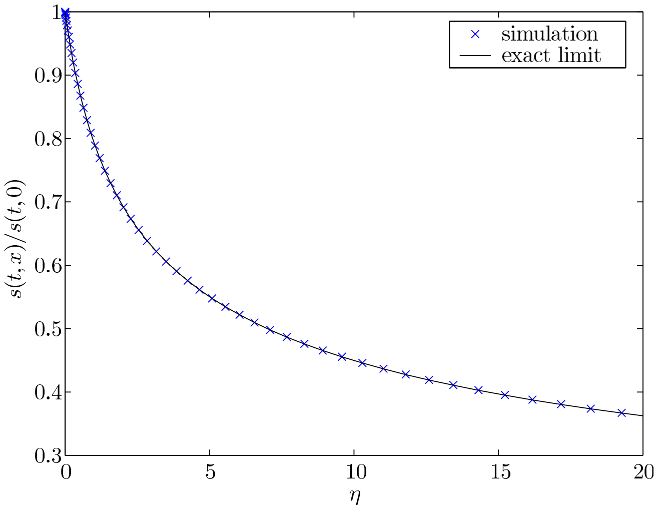

Figure 4.2: Comparison between the exact self-similar solution of (4.28) (full line, $n = 1$, $C = 1$) with a corresponding numerical solution of (4.20) using initial data $s_i(x) = 2(1 - x)$ (cross). The numerical solution is rescaled with respect to the maximum; η is chosen such that the rescaled solution always meets the exact solution at $\eta = 1$; and, the solution is shown at the instant when $s_{\max}(t) = 200$.

near zero. One can find a similar expression for $K > 0$ by formally expanding the solution $\bar{\varphi} = 1 - C\eta^n + o(\eta^n)$ $(C, n > 0)$ and inserting the leading orders into (4.28). To leading order this gives

$$\gamma n(-C\eta^n) = f(K,1) + f'(K,1)\big(-C\eta^n\big) = \big(2K+3\big)\big(-C\eta^n\big)$$

which in turn implies

$$\gamma n = 2K + 3. \tag{4.31}$$

This includes the expression $n = 3/\gamma$ as the special case $K = 0$. One can study exact self-similar solution and convergence to self-similar solution without using (4.31) at all. However, this equation is helpful to understand the relation between self-similar solutions of the integro-differential equation and of the strong-slip equation as follows.

Even though the integro-differential equation does not require differentiability of initial data, the presence of higher-order terms can enforce higher regularity of the solution of the strong-slip equation. Therefore, initial data of the integro-differential equation are expected to behave like $\varphi(0,\eta) = 1 - C\eta^n$ near the maximum, where $n \in \mathbb{N}$ is an even integer. When we derived the self-similar solution of the strong-slip equation in the last chapter we assumed that the solution is (locally) analytic with $H(\eta) = H_0 + H_2\eta^2 + \mathcal{O}(\eta^4)$. Most investigations of jet pinch-off and rupture of thin films mentioned before consider only self-similar solutions that are analytical at $\eta = 0$ and find that the only stable solution is the one corresponding to $n = 2$. The instability of $n > 2$ is due to the presence of surface tension.

The strategy to find the special solution is this:

- Set $n = 2, 4, 6, ...$ in (4.31)
- For each K and $\gamma = (2K+3)/n$ compute a (numerical) solution of the ODE (4.28a)
- Compute K^* and seek intersection points where $K = K^*(K, \gamma)$

Example 4.1. The resulting curve $K^*\big(K, (2K+3)/n\big)$ for $n = 2$ is shown in Figure 4.3. The exact self-similar solution is given by the bifurcation point of K with $K^*\big(\gamma(K), K\big)$; the numerical algorithm computes $K \approx 0.2467915$. Equivalently we have

$$\gamma = \frac{2K+3}{2} \approx 1.74679 \quad \Rightarrow \quad \beta \approx 0.248931,$$

which is in perfect agreement with the results in Table (3.5) and Table (3.6). ♢

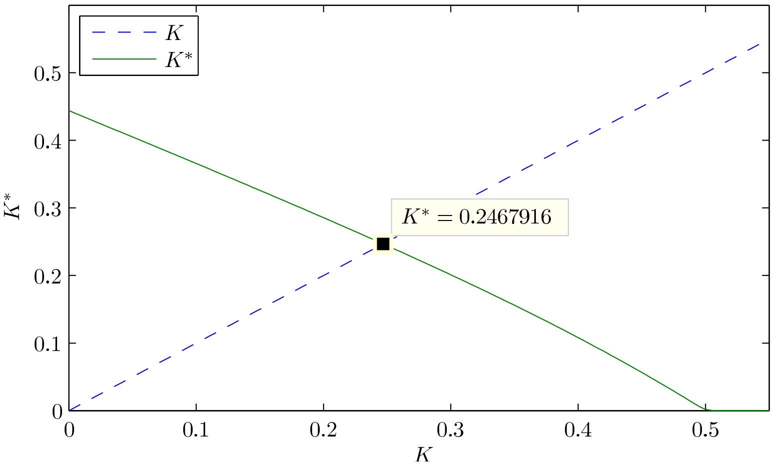

Figure 4.3: The curve $K^*(K)$ is obtained from a numerical simulation with $\bar{\varphi}(\eta) = 1 - \eta^2 + o(\eta^2)$; for $n = 2$ the full line shows $K^*(K)$ with $\gamma = (2K+3)/2$, while the dashed line shows K.

Example 4.2. The same analysis performed with $n = 4$ yields

$$K \approx 1.268220, \quad \gamma \approx 1.38411 \quad \text{and} \quad \beta \approx 0.128037,$$

which again verifies the results shown in the Tables (3.5,3.6). ♢

However, it is impossible to explain the stability of the $n = 2$ solution by considering the integro-differential equation alone. The integro-differential equation basically conserves the smoothness of initial data such that self-similar solutions are possible for any positive n. In order to explain this stability extra terms like surface tension have to be added to the equation again.

The numerical solution is computed using a $4th$ order Runge-Kutta scheme and adaptive η-stepping with $5th$ order error control. Integration starts at the point $\eta = \epsilon$ with the initial value $\bar{\varphi}(\epsilon) = 1 - \epsilon^2$ or $\bar{\varphi}(\epsilon) = 1 - \epsilon^4$ respectively. When K^* becomes zero, the results are numerically inaccurate because the integrals in K^* do not converge or converge only slowly.

4.6.3 Existence of Exact Self-Similar Solutions

Existence and uniqueness of self-similar solution with $K > 0$, which corresponds to the parameter range $1 < \gamma < 2$, will be addressed now. We proved that for each solution $s(t, x)$ of problem (4.20) there exists at most one class of scale transformations $a(\tau)$ for which we have local convergence to self-similar solutions $\varphi(\tau, \eta) \to \bar{\varphi}(\eta)$ as $\tau \to \infty$. Each of those scale transformation is characterized by a constant γ, such that $(\log a(\tau))_\tau$ converges to γ as $\tau \to \infty$.

Right now we are not concerned with convergence to self-similar solutions, but with exact self-similar solutions, i.e., the characterization of the relation between γ and $\bar{\varphi}(\eta)$. The following theorem establishes existence of exact self-similar solutions for $1 < \gamma < 2$; for $\gamma \geq 2$ we computed the solutions explicitly.

Theorem 4.12. *(existence and uniqueness of exact self-similar solutions) For any $\gamma \in (1, 2)$ there exists a solution of (4.28a) with $K^*(K, \gamma) = K$. Given any such solution $\bar{\varphi}$ define equivalent solutions by*

$$\bar{\varphi}_c(\eta) = \bar{\varphi}(c\eta) \qquad \Rightarrow \qquad \bar{\varphi}_c \sim \bar{\varphi}$$

for $c > 0$. Up to equivalence such solutions are unique.

In the proof, which is present in a moment, we approximate exact self-similar solutions. Before we prove the theorem, we introduce a notion of asymptotic equivalency which allows us to approximate solutions sufficiently precise.

Definition 4.4. (asymptotical equivalence)
Two functions $u(\eta)$ and $v(\eta)$ are *asymptotically equivalent at infinity*, if

$$\lim_{\eta \to \infty} \frac{u(\eta)}{v(\eta)} = 1.$$

We say the asymptotical equivalence is *strong*, if $\lim_{\eta \to \infty} \eta \big(u(\eta) - v(\eta) \big) = 0$ holds in addition. $\diamondsuit$

Remark 4.4. In fact, the requirement of being strongly asymptotically equivalent is only meaningful, if the functions do not approach zero faster than $1/\eta$. For example $u(\eta) = 1/\sqrt{\eta}$ and $v(\eta) = 1/\sqrt{\eta} - 1/\eta$ are asymptotically equivalent but not strongly asymptotically equivalent. For any two functions that approach zero faster than $1/\eta$, asymptotical equivalence implies strong asymptotical equivalence. ◇

The next lemma provides a tool to construct asymptotically equivalent solution (exact) self-similar solutions.

Lemma 4.13. *(equivalence of solutions) Suppose* $\varphi(\eta)$ *and* $\bar{\varphi}(\eta)$ *are solutions of*

$$\gamma\eta\varphi' = f(\varphi), \tag{4.32a}$$

$$\gamma\eta\bar{\varphi}' = \bar{f}(\bar{\varphi}), \tag{4.32b}$$

where f *and* $\bar{f}$ *are continuous, negative for all* $s \in (0,1)$, $f(0) = \bar{f}(0) = 0$, *and* $\bar{\varphi}, \varphi$ *are nontrivial in the sense that they are positive and* $\phi, \varphi \to 0$ *as* $\eta \to \infty$. *Furthermore assume that* f *and* $\bar{f}$ *are sufficiently close to each other at zero, which means that*

$$\left| \frac{\bar{f}(s) - f(s)}{f(s)\bar{f}(s)} \right|$$

is bounded as $s \to 0$. *Then, for any such* φ *there exists* a *solution* $\bar{\varphi}$ *of* (4.32b) *that is asymptotically equivalent to* φ *at infinity.*

Proof. We formally integrate both equations (4.32) and obtain

$$\int_q^{\varphi(\eta)} \frac{ds}{f(s)} = \frac{1}{\gamma}\log\frac{\eta}{\eta_0} \qquad \text{and} \qquad \int_{\bar{q}}^{\bar{\varphi}(\eta)} \frac{ds}{\bar{f}(s)} = \frac{1}{\gamma}\log\frac{\eta}{\bar{\eta}_0}$$

with initial data $\bar{\varphi}(\bar{\eta}_0) = \bar{q}$ and $\varphi(\eta_0) = q$. Comparing the two solutions φ and $\bar{\varphi}$ at the points where $\varphi(\eta) = \bar{\varphi}(\bar{\eta}) = r$ we write

$$\frac{1}{\gamma}\log\left(\frac{\eta/\eta_0}{\bar{\eta}/\bar{\eta}_0}\right) = C + \int_q^r \left(\frac{1}{f(s)} - \frac{1}{\bar{f}(s)}\right) ds = C + \int_q^r \frac{\bar{f}(s) - f(s)}{f(s)\bar{f}(s)}\, ds.$$

where $C = \int_{\bar{q}}^{q} 1/\bar{f}(s)\, ds$. By assumption the integrand is bounded and the integral exists for $r = 0$. Moreover, we see that there exists a finite initial value $\bar{\eta}_0$ such that $\eta/\bar{\eta} \to 1$ as $r \to 0$, which in turn implies that $\varphi(\eta)/\bar{\varphi}(\eta) \to 1$ as $\eta \to \infty$ then. Hence, both solutions are asymptotically equivalent at infinity. □

Lemma 4.13 enables us to construct lower and upper bounds of the exact solutions that are by construction asymptotically equivalent to each other, as one can see in the next lemma.

Lemma 4.14. *(asymptotically equivalent lower and upper bounds)*
Let $f, \bar{f}, \varphi, \bar{\varphi}$ *as in the previous lemma*[2] *and in addition* $f(s) \leq \bar{f}(s) \leq 0$ *for* $s < s_0$ *with some* s_0*. Assume* $\bar{\varphi}$ *obeys* $\lim_{\eta\to\infty} \bar{\varphi}(c\eta)/\bar{\varphi}(\eta) < 1$ *if* $c > 1$*. Then there exists an* $\bar{\eta} > 0$ *such that*

$$0 < \bar{\varphi}(\eta) \leq \varphi(\eta) \qquad \textit{for all } \eta \geq \bar{\eta}.$$

Proof. As both solutions tend to zero we can choose $\bar{\eta}$ such that $\varphi, \bar{\varphi} < s_0$ for $\eta \geq \bar{\eta}$. Now suppose $\bar{\varphi}$ is not a lower bound for large η, then there exists a $\eta_0 \geq \bar{\eta}$ where $\varphi(\eta_0) < \bar{\varphi}(\eta_0)$. Consequently there exists a $c > 1$ such that $\bar{\varphi}(c\eta_0) = \varphi(\eta_0)$ and therefore

$$\varphi(\eta) \leq \bar{\varphi}(c\eta) < \bar{\varphi}(\eta) \qquad \text{for } \eta \geq \eta_0.$$

The first inequality follows from $f \leq \bar{f}$ and the second from the monotonicity of $\bar{\varphi}$. In the next step we divide by $\bar{\varphi}(\eta)$ and use that $\bar{\varphi}(c\eta)/\bar{\varphi}(\eta) < 1$ in the limit. This is a contradiction to asymptotic equivalence of φ and $\bar{\varphi}$, which holds by definition. ☐

Corollary 4.15. *With* $\bar{f}(s) \leq f(s)$ *and using* $\lim_{\eta\to\infty} \varphi(c\eta)/\varphi(\eta) < 1$ *for in the proof, we similarly obtain an asymptotic upper bound*

$$0 < \varphi(\eta) \leq \bar{\varphi}(\eta).$$

Proof. Analogous to the last lemma. ☐

The preceding proofs show abstract results for asymptotic equivalent solutions of ordinary differential equations of a certain type. In the next lemma, which is the essential step of the existence and uniqueness proof, we compute explicit upper and lower bounds.

Lemma 4.16. *For a suitable constant c, the solution* $\varphi_c(\eta)$ *of* (4.28a) *is asymptotically equivalent to* $\bar{\varphi}(\eta) = 1/\eta^{1/\gamma}$ *at infinity. This equivalence is strong, and* $\bar{\varphi}$ *is a lower bound of* φ*.*

Proof. The first statement follows from the equivalence lemma by using $\bar{f}(s) = -s$, which is also a lower bound of φ because of the lower bound lemma. Using $\bar{\bar{f}}(s) = -s - Ks^2$ we find an upper bound $\bar{\bar{\varphi}} = 1/(\eta^{1/\gamma} - K)$. For $\gamma < 2$ this equivalence is strong, because upper and lower bound are strongly asymptotically equivalent.

$$|\eta \cdot (\varphi - \bar{\varphi})| < |\eta \cdot (\bar{\bar{\varphi}} - \bar{\varphi})| \sim \eta^{1-2/\gamma} \to 0 \qquad \text{if } \gamma < 2$$

☐

Lemma 4.17. *For fixed* $\gamma \in (1, 2)$ *the function* $K^*(K, \gamma)$ *depends continuously on* K*.*

---

[2] In particular φ and $\bar{\varphi}$ are asymptotical equivalent at infinity

Proof. Apply dominated convergence theorem to $K^*(K_n, \gamma)$. Integrable upper bounds for the integrands in K^* are given by powers of $\bar{\bar{\varphi}}$ (valid for $\gamma \in (1,2)$) from the previous lemma. $\square$

Now we prove the main theorem.

Proof of existence and uniqueness. By using a continuity argument we first prove the existence part of the theorem, i.e., for any fixed $\gamma \in (1,2)$ there exists a solution with $K^*(K,\gamma) = K$. As a byproduct of the special case $K = 0$ and $\gamma < 2$ we already found an explicit expression showing $K^*(0,\gamma) > 0$. In addition, we will show that $K^*(K,\gamma) < K$ for sufficiently large K. Then the intermediate value theorem implies existence of a fixed point with $K^*(K,\gamma) = K$. What remains to be shown now is that $K^*(K,\gamma) < K$ for sufficiently large K.

Integrate (4.28a) over the finite interval $(0,x)$ and apply integration by parts to obtain

$$\left(\gamma\eta\varphi(\eta)\Big|_0^x + (1-\gamma)\int_0^x \varphi(\eta)\,d\eta\right) \Big/ \left(\int_0^x \varphi^4(\eta) - \varphi^2(\eta)\,d\eta\right) = K - K^*(x). \tag{4.33}$$

with

$$K^*(x) = \int_0^x \varphi^4(\eta)\,d\eta \Big/ \left(\int_0^x \varphi^2(\eta) - \varphi^4(\eta)\,d\eta\right)$$

and $K^*(x) \to K^*$ as $x \to \infty$. Now $K^*(K,\gamma) < K$ is equivalent to

$$\gamma\eta\varphi(\eta)\Big|_0^x + (1-\gamma)\int_0^x \varphi(\eta)\,d\eta < 0 \tag{4.34}$$

for large K, fixed $\gamma \in (1,2)$, and with $x \to \infty$. This expression is easier to handle because it contains φ only linearly. The problem with this expression is, however, that both expression on the left side of the inequality are unbounded as $x \to \infty$; hence, we can not simply evaluate the expression at infinity.

Our strategy is to find lower bounds for the second integral such that the singularities of the first and the second term cancel. In order to compute good lower bounds $\tilde{\varphi}$, we divide the domain $[0,\infty)$ into 3 parts.Then the lower bounds are computed separately in each domain by using the previous theorems in the following way:

- Lower bound in $(1,\infty)$: Choose a solution φ_c of (4.28a) which is asymptotically equivalent to $\bar{\varphi}(\eta) = K^{-1}\eta^{-1/\gamma}$. Lemma 4.16 tells us that this is possible. In fact, $\bar{\varphi}$ is a lower bound to the solution φ_c. The bound is valid as long as $0 \le \bar{\varphi} < (K/(K+1))^{1/2}$. Suppose that $K > 4/3$, then we just need the bound until $\bar{\varphi}$ approaches $\bar{\varphi} = K^{-1}$ from below; this happens to be at $\eta = 1$.

- Lower bound in $(\eta_{1/2}, 1)$: The exact solution φ is bounded from below by solutions of $\gamma\eta\,\bar{\varphi}' = -\frac{K}{2}\bar{\varphi}^2$ with final data $\bar{\varphi}(1) = K^{-1}$ as long $\bar{\varphi} \leq 1/2$.
$$\bar{\varphi} = \frac{2\gamma}{2K\gamma + K\log\eta}$$
and $\bar{\varphi}(\eta_{1/2}) = 1/2$ at
$$\eta_{1/2} = \exp\left(-2\gamma\frac{K-2}{K}\right). \tag{4.35}$$
- Lower bound in $(0, \eta_{1/2})$: The constant function $\bar{\varphi} = 1/2$ suffices.

Assuming $K > 4/3$ and $\gamma \in (1, 2)$, we plug these approximations into (4.34) and obtain

$$\begin{aligned}
&\gamma\eta\varphi(\eta)\Big|_0^x + (1-\gamma)\int_0^x \varphi(\eta)\,d\eta \\
\leq\;& \gamma x\varphi(x) + (1-\gamma)\left(\int_0^1 \varphi\,d\eta + \int_1^x \bar{\varphi}\,d\eta\right) \\
\leq\;& \gamma x\varphi(x) + (1-\gamma)\left(\int_0^1 \varphi\,d\eta + \frac{\gamma}{\gamma-1}\,K^{-1}\eta^{\frac{\gamma-1}{\gamma}}\Big|_1^x\right) \\
&\overset{x\to\infty}{=} (1-\gamma)\int_0^1 \varphi\,d\eta + \frac{\gamma}{K}
\end{aligned}$$

All the work in the preceding lemmas, in particular the construction of a strongly asymptotically equivalent lower bound $\bar{\varphi}$, was necessary in order to cancel out the singularities in the last step. From (4.35) we conclude

$$\int_0^1 \varphi(\eta)\,d\eta > \int_0^1 \widetilde{\varphi}(\eta)\,d\eta > \tfrac{1}{2}\,\eta_{1/2} > \tfrac{1}{2}\exp(-2\gamma),$$

and so we see

$$0 > \frac{\gamma}{K} - \frac{\gamma-1}{2}\exp(-2\gamma) > \gamma\eta\varphi(\eta)\Big|_0^x + (1-\gamma)\int_0^x \varphi(\eta)\,d\eta.$$

which shows that, depending on γ, for sufficiently large K the inequality (4.34) is true.

Uniqueness follows by an analogous, but shorter indirect argument. Therefore suppose φ_1 and φ_2 are two different solutions with $K_1 = K^*(K_1, \gamma)$ and $K_2 = K^*(K_2, \gamma)$ respectively. Since both have the same γ, we can select solutions φ_1 and φ_2 which are strongly asymptotically equivalent to each other[3]. Subtracting the two expressions in (4.33) from each other and using

---

[3] Mind the difference between asymptotic equivalence and equivalence of self-similar solutions.

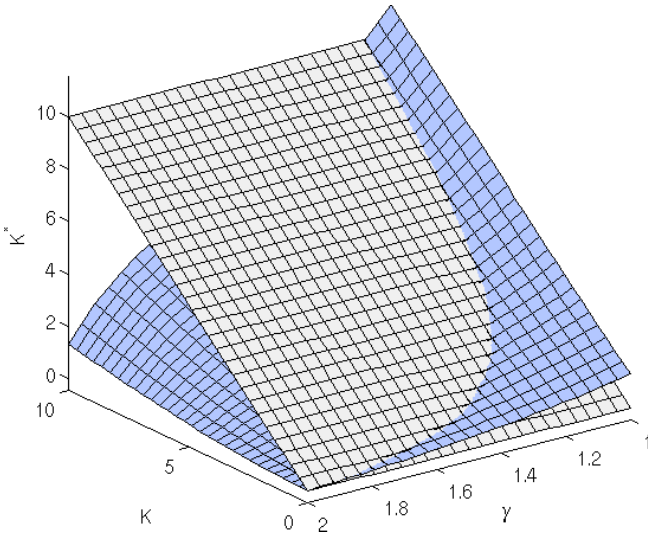

Figure 4.4: $K^*(K,\gamma)$ surface (dark) and K plane (bright); Exact self-similar solutions with $\gamma \in (1,2)$ lie on the intersection curve of both surfaces. As usual, we obtain the surface $K^*(K,\gamma)$ by numerical quadrature.

strong equivalence of Lemma 4.16 we conclude

$$\begin{aligned} 0 &= \gamma\eta(\varphi_1-\varphi_2)\Big|_0^x + (1-\gamma)\int_0^x (\varphi_1(\eta)-\varphi_2(\eta))\,d\eta \\ &\overset{x\to\infty}{=} (1-\gamma)\int_0^x (\varphi_1(\eta)-\varphi_2(\eta))\,d\eta \end{aligned}$$

If $K_1 > K_2$ we have $f(K_1,s) < f(K_2,s)$ and thereby $\varphi_1 > \varphi_2$ (or vice versa), which immediately produces a contradiction to the expression above for $\gamma > 1$. □

For numerical solutions this prediction is shown in Figure 4.4, where one can see the point where $K^*(K,\gamma)$ and K meet and a global solutions exists. In fact, for any γ there is only one unique intersection point in the $K-\gamma$ plane visible.

We proved that for every $1 < \gamma$ there exists exactly one self-similar solution of (4.28). Earlier in this section we introduced the relation $\gamma n = 2K+3$ between the similarity scale γ and n, where n characterizes the behavior of the exact self-similar solution at $\eta = 0$. Since we would like to introduce an relation between the behavior of the initial data at $\eta = 0$ and the self-similar limiting solution, it is desired to prove also existence and uniqueness for every n. In the next corollary we present a simple argument that there is also one unique self-similar for every $n > 0$.

Corollary 4.18. *For every positive $n \in \mathbb{R}$ there exists a unique solution $\varphi(\eta)$ of Equation* (4.28) *with the property that $\varphi(\eta) = 1 - C\eta^n + o(\eta^n)$ $(C > 0)$.*

Proof. For $\gamma \geq 2$ we have $K = 0$ and $n = 3/\gamma$, which implies existence of a unique solution for every $0 < n \leq 3/2$. Then, for $K > 0$ we have $n = (2K + 3)/\gamma > 3/2$. We already showed that for every γ with $1 < \gamma < 2$ there exists a unique K with $K^*(K, \gamma) = K$. Figure 4.4 shows that K^* *decreases* with γ for fixed K, which in turn implies that $n = (2K^*(\gamma) + 3)/\gamma$ is invertible. $\square$

4.7 Convergence to Self-Similar Solutions

So far finite-time blow-up of time-dependent solutions and existence of exact self-similar solutions was shown in this chapter. Up to equivalence there exists exactly one exact self-similar solution for every $\gamma > 1$ or equivalently for every $n > 0$.

Now we address the question whether there exist solutions of the time-dependent problem that converge to an exact self-similar solution. For a certain class of initial data where $K(\tau) \to 0$ we rigorously prove convergence, whereas in the general situation we have to assume that $K(\tau)$ converges to some K^* sufficiently fast. We derive conditions for the scaling $a(\tau)$, for which no self-similar solution can exist. We supplement our theorems by examples for convergence and no-convergence. First we introduce a helpful implicit solution formula.

4.7.1 Solution Formula

In the previous part the function H_{K^*} already played some role and in the context of convergence to self-similar solution this expression will again be very useful. Therefore consider a solution of (4.20) which is rescaled with respect to height according to Equation (4.22). The resulting rescaled solution $\psi(\tau, x) : [0,\infty) \times [0,1] \to [0,1]$ solves the integro-differential equation

$$\partial_\tau \psi(\tau, x) = f\big(K(\tau), \psi(\tau, x)\big) \qquad \text{where} \tag{4.36a}$$

$$K(\tau) = \int_0^1 \psi(\tau, x)^4 \, dx \Big/ \int_0^1 \left(\psi(\tau, x)^2 - \psi(\tau, x)^4\right) \, dx. \tag{4.36b}$$

As before define

$$H_{K^*}(\psi) = \int_q^\psi \frac{ds}{f(K^*, s)} \qquad \text{for some } q \in (0,1)$$

and use this expression to obtain an implicit solution formula as follows. Insert the solution ψ into H_{K^*} and differentiate with respect to τ. One obtains the evolution law

$$\frac{d}{d\tau} H_{K^*}(\psi(\tau, x)) = \frac{\partial_t \psi}{f(K^*, \psi)} = \frac{f\big(K(\tau), \psi(\tau, x)\big)}{f\big(K^*, \psi(\tau, x)\big)}.$$

This expression can be integrated with respect to time such that

$$\begin{aligned} H_{K^*}\big(\psi(\tau, x)\big) - H_{K^*}\big(\psi(0, x)\big) &= \tau + \int_0^\tau \left(\frac{f\big(K(t), \psi(t, x)\big)}{f\big(K^*, \psi(t, x)\big)} - 1 \right) dt \\ &= \tau + \int_0^\tau \big(K(t) - K^*\big) g\big(\psi(t, x)\big) \, dt \qquad (4.37) \end{aligned}$$

with g defined as

$$g(s) = \frac{s(s+1)}{1+(K^*+1)s(s+1)}.$$

Note that g is independent of $K(\tau)$; in the integral it appears only in the factor in front of g. It is convenient to study convergence to self-similar solution in this formulation, because convergence of $K(\tau) \to K^*$ and the behavior of solutions near $x = 0$ are encoded separately in the integral over $(K - K^*)g$ and in H_{K^*} respectively. If for fixed x the integral converges as $\tau \to \infty$ then the evolution of ψ for large times is approximately given by

$$H_{K^*}\big(\psi(\tau, x)\big) = H_{K^*}\big(\psi(0, x)\big) + \tau + C$$

and convergence properties are related to properties of H_{K^*}.

Given some solutions $\psi(\tau, x)$ in the height scaling (4.22), the corresponding solution in the similarity scaling (4.21) fulfills

$$x = y\,\exp(-\gamma\tau) \qquad \text{and} \qquad \psi(\tau', x) = \varphi\big(\tau', x\exp(\gamma\tau')\big)$$

and one can easily verify

$$\psi(\tau', x) = \varphi\big(\tau', ye^{\gamma(\tau'-\tau)}\big).$$

Substituting this expression into (4.37) we obtain an equivalent implicit solution formula in similarity scaling

$$\begin{aligned} H_{K^*}\big(\varphi(\tau, y)\big) &= \tau + H_{K^*}\big(\varphi(0, ye^{-\gamma\tau})\big) + ... \\ ... &+ \int_0^\tau \big(K(t) - K^*\big)g\big(K^*, \varphi(t, y\, e^{(t-\tau)\gamma}\big)\, dt. \end{aligned} \tag{4.38}$$

Equation (4.37) and (4.38) are implicit solution formulas for the $\psi(\tau, x)$ solution in the height scaling and solution $\varphi(\tau, y)$ in the similarity scaling; the implicit dependence is due to the dependence on $K(\tau)$ and $\varphi(t, \cdot)$ (or $\psi(t, \cdot)$) of the integral.

Note that no differentiability with respect to the spatial coordinate is needed in order to make this formula well-defined.

4.7.2 Convergence of $K(\tau)$ to Zero

An important issue in the proof of convergence to a self-similar solution is establishing convergence of $K(\tau)$. Even though $K(\tau)$ is computed from $\varphi(\tau, y)$, its actual value is independent of a scaling $a(\tau)$ since $K(\tau)$ is the quotient of two such integrals. Therefore one can treat the question of convergence of $K(\tau) \to K^*$ independently.

Assume for a moment that $\varphi(\tau, y)$ converges to a self-similar solution and $K(\tau)$ converges to K^*. By Proposition 4.10 we know that convergence to self-similar solutions is uniform. Therefore one might guess that K^* is given by expression for K evaluated at the limit. Of course this is generally wrong because the support of φ is $\mathbb{R}^+$ and uniform convergence is insufficient to conclude convergence of the integral, i.e.,

$$K^* = \lim_{\tau\to\infty} \frac{\|\varphi(\tau,\cdot)^4\|_1}{\|\varphi(\tau,\cdot)^2 - \varphi(\tau,\cdot)^4\|_1} \neq \frac{\|\bar{\varphi}^4\|_1}{\|\bar{\varphi}^2 - \bar{\varphi}^4\|_1}$$

where $\bar{\varphi} = \lim_{\tau\to\infty}\varphi(\tau,\cdot)$. One could try to use dominated convergence to insure convergence of $K(\tau) \to K^*$, but there are exact self-similar solutions where $\|\bar{\varphi}(y)^2\|_1$ is infinite and this is impossible. Nevertheless, in this case we already know that $K(\tau) \to 0$ due to Proposition 4.11.

In the next proof we provide a condition which ensures convergence $K(\tau) \to 0$, in addition we show that convergence is exponentially fast, i.e., $K(\tau) = \mathcal{O}(e^{-\alpha\tau})$ for some $\alpha > 0$ as $\tau \to \infty$.

Theorem 4.19. *(fast convergence of $K(\tau)$ to zero)*
Assume $\psi(0,x) \le 1 - cx^n$ for some $c > 0$ and $0 < n < 3/2$. Then $K(\tau) \to 0$ as $\tau \to \infty$, and the speed of convergence is exponentially fast.

Proof. Consider the solution $\psi(\tau,x)$ of the integro-differential equation

$$\partial_\tau\psi(\tau,x) = K(\tau)\big(\psi(\tau,x)^4 - \psi(\tau,x)^2\big) + \psi(\tau,x)^4 - \psi(\tau,x) \qquad \forall x \in [0,1]$$

with $K(\tau) = \int_0^1 \psi(\tau,x)^4\,dx \Big/ \int_0^1 \big(\psi(\tau,x)^2 - \psi(\tau,x)^4\big)\,dx$. A generic upper bound $\bar{\psi}$ to ψ is given by

$$\bar{\psi}(\tau,x) = \left(1 + \frac{1-\psi(0,x)^3}{\psi(0,x)^3}\,e^{3\tau}\right)^{-1/3},$$

which is the solution of the integro-differential equation with $K = 0$. We have conservation of volume $\int_0^1 \psi(\tau,x)\,dx = e^{-\tau}$ and hence Cauchy-Schwarz inequality yields

$$\int_0^1 \psi(\tau,x)^2\,dx \ge \left(\int_0^1 \psi(\tau,x)\,dx\right)^2 = e^{-2\tau}.$$

Thus the following estimates hold

$$\psi^4(\tau,x) \le \bar{\psi}^4(\tau,x) \le \big(1 + (1-\psi_0(x)^3)\,e^{3\tau}\big)^{-4/3} \le \big(1 + 3cx^n\,e^{3\tau}\big)^{-4/3}.$$

Hence, λ is bounded from above by

$$\lambda(\tau) \le \frac{\int_0^1 \big(1 + 3cx^n\,e^{3\tau}\big)^{-4/3}\,dy}{e^{-2\tau}} < C\,\exp\big(\tau(2 - \tfrac{3}{n})\big).$$

In the last step the integrand was estimated from above by 1 on the interval $[0, e^{-3\tau/n}]$ and estimated from above by $(6cx^n e^{3\tau})^{-4/3}$ in the complement in $[0,1]$. Exponentially fast convergence $\lambda(\tau) \to 0$ implies the same property for $K(\tau) = \lambda(\tau)/\big(1 - \lambda(\tau)\big)$. □

This theorem enables us to show convergence to a self-similar solution in a simple way, because we can estimate the integral in the solution formula easily.

Unfortunately, convergence $K(\tau) \to K^*$ could not be established yet and remains an open problem. Nevertheless suppose that, similarly to Theorem 4.19, $K(\tau) \to K^*$ converges. We expect that one can show convergence using monotonicity of $\psi(0,x)$ and some regularity property of $\psi(0,x)$ at (near) $x = 0$.

4.7.3 Convergence to Self-Similar Solutions

Now we are going to present examples and our results regarding convergence to self-similar solutions. For $\psi(t,x) \leq 1 - cy^n$ with $0 < n < 3/2$ and $c > 0$ we explicitly know that $K(\tau) \to 0$ exponentially fast, otherwise we assume that initial data are such that $K(\tau)$ converges to some $K^* \geq 0$. In our first convergence theorem we only use the following two basic properties of H_{K^*}

- boundedness of g:
$$g(K^*, s) \in \left[0, \frac{1}{K^* + 3/2}\right],$$
- and the leading-order singular behavior of $H_{K^*}(\psi)$ as $\psi \to 1$:

$$\begin{aligned} 0 &< \frac{1}{2K^*+3}\log(1-\psi) - H_{K^*}(\psi) \\ &= \int_q^\psi \frac{3 + s(s+2) + K^*(2 + s(s+2)}{(3+2K^*)s(1+(K^*+1)s(s+1))}\,ds \\ &< \frac{4K^*+5}{2K^*+3}\log\left(\frac{\psi}{q}\right) \overset{\psi\to 1}{<} C. \end{aligned} \tag{4.39}$$

The latter expression can be directly obtained by estimating the integrand $1/f$ in the definition of H_{K^*}. In this theorem we prove a negative convergence result, that is to say, supposing $K(\tau)$ converges and given some initial data which are bounded from above or from below by some power law behavior, i.e., $\psi(0,x) \leq 1 - cx^n$ or $\psi(0,x) \geq 1 - cx^n$, we show that a solution does not converge to self-similar solution for a certain range of γ.

Theorem 4.20. *Consider a solution $s(t,x)$ of (4.20) and assume $K(\tau) \to K^*$. Furthermore let $\varphi(t,y)$ be defined as in (4.21) with the scaling $a(\tau) = e^{\gamma\tau}$.*

1. *If the initial data satisfy*
$$\varphi(0,y) \geq 1 - \alpha y^n \qquad \alpha, n > 0$$
near zero and $\gamma n > (2K^* + 3)$, then $\varphi(\tau,y) \to 1$ for all $y \geq 0$.

2. *Conversely, if the initial data satisfy*

$$\varphi(0,y) \leq 1 - \alpha y^n \qquad \alpha, n > 0$$

near zero and $\gamma n < (2K^* + 3)$, *then* $\varphi(\tau, y) \to 0$ *for all* $y > 0$.

Hence, both conditions define intervals, for which the scaling associated with γ *does not produce a self-similar solution.*

Proof. 1. Using the last proposition yields

$$H_{K^*}(\varphi(\tau,y)) \leq \ldots$$

$$\frac{1}{2K^*+3}\log\left(1-\varphi(0,ye^{-\gamma\tau})\right) + \tau + \int_0^\tau (K-K^*)g\,ds + C_1(K^*,q)$$

$$\leq \tau\left(1 - \frac{n\gamma}{2K^*+3}\right) + \int_{\tau_0}^\tau (K-K^*)g\,ds + C_2(K^*,q,y,n,\tau_0)$$

$$\leq \tau\left(1 - \frac{n\gamma}{2K^*+3} + \frac{\sup_{\tau>\tau_0}|K-K^*|}{K^*+3/2}\right) + C_2(K^*,q,y,n,\tau_0)$$

Since $K \to K^*$ we can make the $|K-K^*|$ term arbitrarily small, so that

$$\tau\left(1 - \frac{n\gamma}{2K^*+3} + \epsilon\right) + C_2 \to -\infty \qquad \text{as} \quad \tau \to \infty$$

which holds for all $y > 0$ and so $\varphi(\tau,y) \to 1$ as $\tau \to \infty$.

2. Analogous to 1. show

$$H_{K^*}(\varphi(\tau,y)) \geq \tau\big(1 - \frac{n\gamma}{2K^*+3} - \frac{\sup_{\tau>\tau_0}|K-K^*|}{K^*+3/2}\big) + \ldots$$

$$\ldots + C_3(K^*,q,y,n,\tau_0)$$

and

$$\tau\left(1 - \frac{n\gamma}{2K^*+3} - \epsilon\right) + C_3 \to \infty \qquad \text{as} \quad \tau \to \infty,$$

where C_3 is finite and does not depend on τ.

□

This theorem can be used to contain the similarity in the following way.

Example 4.3. Consider the class of initial data

$$\psi(0,x) = 1 - x^n \qquad 0 < n < 3/2.$$

Then Theorem 4.19 implies $K(\tau) \to 0$ and Theorem 4.20 implies that for $a(\tau) = \exp(\gamma\tau)$ convergence can only take place for $\gamma = 3/n$. ♢

But it is still open whether $\varphi(\tau, x)$ converges for this initial data. Using the stronger knowledge, namely that $K(\tau)$ converges exponentially fast, the following theorem provides a sufficient condition for convergence to a self-similar solution.

Definition 4.5. (power-law behavior)
A function $\psi(y)$ is said to behave like a *power-law* with power n at zero, if there exists a $c \neq 0$ such that $\psi(y) = cy^n + o(y^n)$ as $y \to 0$. ♢

Theorem 4.21. *Let $s(t, x)$ be a solution of (4.20) and assume $K(\tau)$ converges exponentially fast to K^*. Furthermore let $\varphi(\tau, y)$ as in (4.21) with $a(\tau) = \exp(\gamma\tau)$ and with continuous initial data. Then $\varphi(\tau, y)$ converges to a self-similar solution, if and only if $1 - \varphi(0, \cdot)$ behaves like a power-law with power n at zero and $\gamma n = (2K^* + 3)$.*

Proof. Exponentially fast convergence of $K(\tau)$ and boundedness of g ensure that the integral in (4.38) converges for every fixed y as $\tau \to \infty$. It remains to show $\tau + H_{K^*}\big(\varphi_0(ye^{-\gamma\tau})\big)$ converges, if and only if $\varphi(0, y)$ has a power-law behavior. We rely on the fact that the leading order singular behavior of H_{K^*} as $\varphi \to 1$ is given by (4.39), namely

$$H_{K^*}(\varphi) = \frac{1}{2K^* + 3} \log(1 - \varphi) + C(K^*, \varphi, q),$$

where $C(K^*, \varphi, q)$ is continuous and bounded for $0 < \epsilon \leq \varphi \leq 1$. An explicit expression for C is not needed. Thus convergence to a self-similar solution is equivalent to convergence of

$$\lim_{\tau\to\infty} \left[\frac{\log\big(1 - \varphi(0, ye^{-\gamma\tau})\big)}{2K^* + 3} + \tau \right]. \tag{4.40}$$

$\Rightarrow$ Let $\varphi(0, y) = 1 - cy^n + o(y^n)$, then the expression above can be transformed to

$$\lim_{\tau\to\infty} \left[\frac{cy^n e^{-n\gamma\tau} + o(e^{-n\gamma\tau})}{e^{-(2K^*+3)\tau}} \right]$$

which converges to a positive limit for $\gamma n = 2K^* + 3$ as $\tau \to \infty$ and is continuous. Property b) and c) of Lemma (4.9) are also satisfied in the limit, which one can easily see by estimating the integral in (4.38) properly.
$\Leftarrow$ Conversely assume the limit (4.40) exists. Convergence of the difference of (4.40) evaluated at τ and $\tau + T$ with $\psi = 1 - \varphi(0, \cdot)$ implies that for any $\epsilon > 0$ exists a τ_0 such that

$$\left| \frac{\psi(y\, e^{-\gamma(\tau+T)})}{e^{-(2K^*+3)T}\psi(y\, e^{-\gamma\tau})} - 1 \right| < \epsilon \qquad \forall T > 0, \tau > \tau_0$$

Define $\hat{y} = ye^{-\gamma\tau}$, $\lambda = e^{-\gamma T}$, and $\psi(y) = y^n g(y)$ then the condition that must hold is

$$\left|\frac{g(\hat{y}\lambda)}{g(\hat{y})} - 1\right| < \epsilon \tag{4.41}$$

with $n = (2K^*{+}3)/\gamma$ for any sufficiently small $\hat{y}, \lambda$. For fixed λ this condition is related to *slow variation* [55, 56]. However, condition (4.41) is stronger because it is supposed to hold uniformly for small λ, y. Continuity of $\varphi(0, y)$ and the condition above imply that g is continuous and $g(0) > 0$ (since $\varphi(0, y)$ is decreasing). Therefore we can conclude

$$\varphi(0, y) = 1 - y^n\, g(y) = 1 - y^n g(0) + o(y^n),$$

which is what we wanted to show. □

The previous theorem establishes a correspondence between initial data where $1 - \varphi(0, \cdot)$ behaves like a power-law and convergence to a self-similar solution. In the next example we show that even though $K(\tau)$ converges exponentially fast, and the initial data *almost* behave like a power-law, there is no convergence to a self-similar solution. With almost power-law be mean the functions of *slow variation* or functions of *regular variation* [33, 55, 56] (as introduced by Karamata). First let us define the term regular variation.

Definition 4.6. (regular variation) A measurable function $g : (0, \infty) \to (0, \infty)$ is $\big($or equivalently on $(0, a]\big)$ is called *regularly varying* at zero with index n ($n \in \mathbb{R}$) if

$$\lim_{x\to 0^+} \frac{g(\lambda x)}{\lambda^n g(x)} = 1 \qquad \forall \lambda > 0. \tag{4.42}$$

For $n = 0$ the property is called *slowly varying at zero.* ♢

Example 4.4. Functions which are (are not) regularly varying

- $1 + x^n$ is slowly varying at zero
- x^n is regularly varying at zero with index n
- $-x^n/\log(x)$ is regularly varying at zero with index n
- the Cantor-function is not regularly varying at zero
- $\exp(-1/x)$ is not regularly varying at zero ♢

Now consider the following counter-example to convergence with $a(\tau) = e^{\gamma\tau}$.

Example 4.5. The idea of this counterexample goes back to Remark 4.2 where it was explained that it can be insufficient to rescale the solution using a constant similarity scale γ, i.e., $a(\tau) = e^{\gamma\tau}$. We use the representation of solutions in terms of H_{K^*} in (4.37) with the leading order singular behavior (4.39). Consider the initial data

$$\varphi_0(y) = 1 - y\,\frac{\log\bigl(1/2\bigr)}{\log\bigl(y/2\bigr)}$$

the function $1-\varphi_0$ is regularly varying with index $n=1$ and bounded from above by $\varphi_0(y) \leq 1 - cy^{1+\alpha}$ for any $0 < \alpha < 1/2$ and some $c > 0$. Using Theorem 4.19, this implies exponentially fast convergence of the integral in (4.38) supposedly we set $K^* = 0$. Due to Theorem 4.20 with $K^* = 0$ and $n = 1$, convergence to a self-similar solution can only take place for $\gamma = 3$. Nevertheless, if we plug φ_0 into (4.38) we get

$$H\bigl(\varphi(t,y)\bigr) = t + H\bigl(\varphi_0(ye^{-\gamma t})\bigr) + \int_0^t K(\tau)g(\cdot)\,d\tau = \tfrac{t(3-\gamma)-\log(\gamma t)}{3} + C,$$

where $C = C(q,y,t)$ has a finite limit as $t \to \infty$. For $\gamma = 3$ the linear leading-order term vanishes, but the logarithmic correction goes to minus infinity and thus $\varphi(t,y) \to 1$ for all y. This contradicts convergence towards a self-similar solution. There might be a self-similar solution, but one cannot obtain this self-similar solution by scaling that is equivalent to $a(t) = e^{3t}$. ♢

4.7.4 Beyond a Constant γ

After introducing a counter-example for which there is no convergence to a self-similar solution using a simple power-law $a(\tau) = e^{\gamma\tau}$, we show how one can use the generalization of power-law behavior, i.e., regular variation, to establish convergence to self-similar solution for a wider class of initial conditions. Therefore we consider the counter-example Example 4.5 again and show how to establish convergence in this case. Afterwards we indicate a generalization and provide a "real" counter-example for convergence in the general situation. Still we assume that $K(\tau) \to K^*$ exponentially fast.

Definition 4.7. Define a scale transformation of the form

$$a(\tau) = \exp\Bigl(\int_0^\tau \gamma(t)\,dt\Bigr),$$

i.e., γ is now time-dependent. Still one should have that $\gamma(\tau)$ converges as $\tau \to \infty$. By using (4.37) one can simply generalize (4.38) to

$$H_{K^*}\bigl(\varphi(\tau,y)\bigr) = \tau + H_{K^*}\left(\varphi_0\left(\tfrac{y}{a(t)}\right)\right) + \int_0^\tau \bigl(K(t) - K^*\bigr)\; g\Bigl(\varphi\left(t, y\tfrac{a(t)}{a(\tau)}\right)\Bigr)\,dt. \tag{4.43}$$

Now the problem can be stated as follows:

> For given initial data seek $a(\tau)$ such that $\tau + H\bigl(...\bigr)$ in (4.43) converges pointwise in y. This idea can be used to extend self-similar solution beyond those with a power-law behavior. ♢

Example 4.6. Example 4.5 shows that the solution $\varphi(t,y)$ of Equation (4.38) with initial data

$$\varphi(0,y) = 1 - y\frac{\log 1/2}{\log y/2} \tag{4.44}$$

does not converge to a self-similar solution for any constant $\gamma \in \mathbb{R}$. Now consider the scale transformation

$$\widetilde{a}(\tau) = e^{3\tau}/\tau, \tag{4.45}$$

which is somewhat similar but not equivalent to the familiar choice $a(\tau) = e^{3\tau}$ that corresponds to $\gamma = 3$; recall $\gamma = 3$ is the generic choice for regularly varying initial data with index $n = 1$ and $K^* = 0$. Anyway, using (4.45) we have

$$\begin{aligned}\tau + H\left(\varphi\left(0, \tfrac{y}{\widetilde{a}}\right)\right) &= \frac{1}{3}\log\left(\frac{y}{e^{-3\tau}\,\widetilde{a}\log\frac{y}{2\widetilde{a}}}\right) + C(q,y,\tau)\\ &\overset{\tau\to\infty}{=} \frac{1}{3}\log\bigl(y\log(2)\bigr) + C(q,y),\end{aligned}$$

where $C(q,y) = \lim_{\tau\to\infty} C(q,y,\tau)$. Indeed we find convergence to a self-similar solution and by using the identity $\gamma(\tau) = \partial_\tau\bigl(\log a(\tau)\bigr)$ we find $\gamma(\tau) = 3 - 1/\tau$, i.e., $\gamma(\tau) \overset{\tau\to\infty}{\to} 3$ as expected. ◊

Finally, we construct a counter-example for which no $a(\tau)$ exists such that (4.43) converges.

Example 4.7. Let $c(y)$ the Cantor-function and consider $\varphi(\tau,y)$ a solution of Equation (4.38) with initial data $\varphi(0,\tau) = 1 - c(y)$.

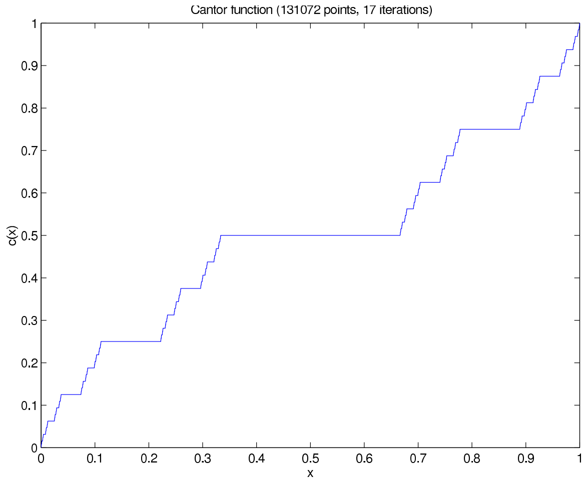

Figure 4.5: Numerical approximation of the Cantor-function with 17 recursive iterations (2^{17} points)

One can easily check $1 - c(y) \leq 1 - 3y/4$, thus $K(\tau) \to 0$ exponentially fast. In order to compute an approximate $a(\tau)$ choose $y_0 = 1/2$ and a sequence τ_n such that $\exp(-3(\tau_{n+1} - \tau_n)) = 1/2$ and $\tau_0 = 0$. This implies $\tau_n = n(\log(2)/3)$ for $n \in \mathbb{N}$.

By the way the sequence is constructed it is immediately clear that $a(\tau_n) = 3^n$ ensures

$$\frac{1 - \varphi(0, y_0/a(\tau_n))}{\exp(-3\tau_n)} = 1$$

for all $n \in \mathbb{N}$. In a similar manner one can construct $a(\tau)$ such that this expression identically holds other sequences τ_n with $y_0 = 1/2$. We performed this procedure with an approximation of the Cantor-function consisting of 2^{17} points. The resulting scale transformation is shown in Figure 4.6. The figure shows that the scale transformation oscillates around $a(\tau) = e^{3\tau \log 3/\log 2}$, where the period of oscillation is $\Delta\tau = \log(2)/3$.

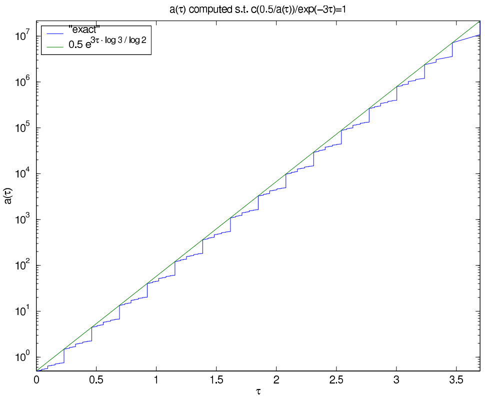

Figure 4.6: Scale transformation $a(\tau)$ that ensures convergence for any sequence where $y_0/a(\tau)$ is one of these lattice points (crinkly line). One can easily compute $a(\tau_n) = 3^n = \exp(3\tau_n \log 3/\log 2)$ for the sequence $\tau = n\log(2)/3$ (full straight line)

Now we need to check whether (4.43) converges also for $y \neq y_0$; we simply compute

$$\frac{1 - \varphi(0, y_{0,1,2}/a(\tau))}{\exp(-3\tau)}$$

for y_0 and $y_1 = 1/4$, $y_2 = 3/4$. The resulting curves are shown in Figure 4.7.

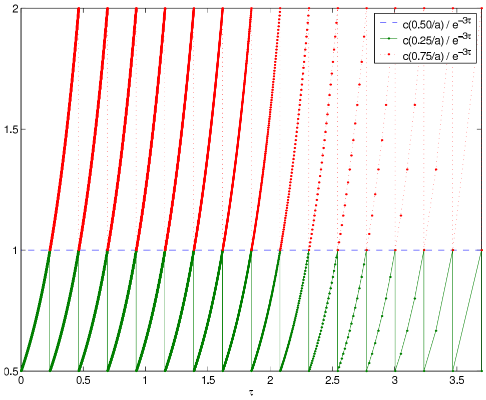

Figure 4.7: Expression in the solution formula (4.43) for different values of y. Apparently the expression does not converge but rather oscillates.

In our example there is no convergence due to oscillations. $\diamondsuit$

4.8 Summary

Starting from the strong-slip equation, one will observe similarity solution of this integro-differential equation with $n = 2$ if the Reynolds number is zero, whereas for nonzero Reynolds number only the singularity studied by Vaynblat et al. is stable.

By passing to Lagrangian coordinates, we simplified the strong-slip equationto an integro-differential equation. If the initial data of the integro-differential equation are bounded by

$$s_i(x) = s_i(0) - Cx^n$$

for some $C, n >$ in an arbitrary small neighborhood of $x = 0$, then solutions blow up after a finite time. The strong requirement that the initial data are decreasing in x allows us to conclude uniqueness of self-similar solutions, i.e., up to equivalence there is a unique scaling $a(\tau)$ by which one finds convergence to a self-similar solution. It was motivated why it is always possible to restrict to decreasing initial data.

The equivalence class of scalings is defined by $a \sim \bar{a}$ if $\frac{a}{\bar{a}}$ converges to a finite, positive number as $\tau \to \infty$. First we focussed on similarity scalings of the form $a(\tau) = e^{\gamma\tau}$ with $\gamma > 1$. We characterized all exact self-similar solutions for $\gamma > 1$ and proved existence and uniqueness, in particular:

> For every $\gamma > 1$ there exists a unique self-similar solution, which solves the similarity equation and the constraint $K^*(K, \gamma) = K$.

In contrast to the common conception scale transformations with corrections from plain power-laws play a role if one wishes to prove convergence to self-similar solutions. That is the case for our model — especially if no further information about the regularity of initial data $1 - \varphi(0, y)$ is known for y being close to zero.

This is quite different compared to similarity solutions of first kind where one usually works with plain power laws and where the similarity scales are a priori known. In this case convergence takes place only if the initial data fit to the concept of a plain power law without corrections.

We established a characterization of initial data for which $K(\tau) \to 0$ exponentially fast; that happens for $\varphi_0 \leq 1 - cy^n$ with $c > 0$ and $0 < n < 3/2$. For the general case, when $K(t) \to K^*$ sufficiently fast, we established that the property "$1 - \varphi_0(y)$ has a power-law behavior" ensures convergence to self-similar solution.

It is insufficient to study only scale transformations such as $a(\tau) = e^{\gamma\tau}$ in order to determine all self-similar solutions. We presented an example where this is not sufficient and showed that a modified scale transformation $a(\tau) = \exp\bigl(\int_0^\tau \gamma(t')dt'\bigr)$ can do the job. We also provided an example of continuous initial data where $K(\tau)$ converges but no convergence to a self-similar solution is possible (Cantor function).

However the proof of convergence $K(t) \to K^*$ is still an open issue, in particular how the speed of convergence depends on the initial data.

4.9 Motivation

In many different models of thin liquid films the formation of interface singularities has common features. Two such features are:

i) Singularities occur already after a finite time, i.e.,

   there exists a finite time $0 < t^* < \infty$, such that the quantity

$$\frac{1}{\min h(t,x)}$$

   is unbounded as the time t approaches t^*.

ii) Singularities evolve *locally self-similar*.

It's both mathematically challenging and physically meaningful to study the origin of these properties. Where the former is a subject of this chapter, the physical justification to study the self-similar structure is that it directly produces universal numbers, the scaling exponents, that one can also measure in experiments and which are determined by the driving forces of the singularity formation process. Even though the 2-dimensional model studied here is slightly unrealistic, the techniques that we employ also work for more realistic 3-dimensional models.

To address property i) and ii) this chapter is divided into two parts: In the parts 4.1-4.4 we study property i) for two models that describe two physical processes: *Rupture* of a liquid film on a flat solid substrate and jet *pinch-off* of a liquid thread. Neglecting inertia, one can simplify both models and transform them into sets of integro-differential equations. For both models we prove blow-up in finite time, which is equivalent to rupture or pinch-off in the original formulation, whereby we focus on *rupture* in finite time. The existing results by Renardy [22] are extended.

Then, in 4.5-4.9 features of ii) are proven. As a motivation we show convergence to self-similar solutions in a simple numerical scheme, the limit is characterized, and some results regarding convergence to self-similar solutions are proven. In a special case we can fully characterize exact similarity solutions and convergence to these solutions and point out how to prove convergence in the general case. Finally we shortly summarize the main results of this chapter in 4.10.

The main motivation to study a simplified integro-differential equation is that it still contains important properties of the singularity formation, e.g., we still find $h \sim (-t)^{1/3}$ as $t \to 0$ and the self-similar solution with similarity scales of Table (3.6).

4.10 Simplification of the Strong-Slip Model

Before we address i) and ii) we motivate the simplification of the strong-slip equation. In the previous chapter we argued that only Trouton-viscosity, van der Waals force, and the mass balance are the leading order terms of the strong-slip equation in the vicinity of the rupture; vicinity means being close to the point and close to the time of the rupture incident.

First, we neglect all other terms that are of a smaller magnitude in the partial differential equation and obtain a well-posed problem. In the second step we transform the observer's point of view from the Eulerian to a Lagrangian reference frame. This allows to transform the system of partial differential equations into a system of integro-differential equations, for which we can prove things more easily. Another motivation to study these integro-differential equations is that similar equations turn up in LSW (Lifshitz, Slyozov, Wagner) models for particle growth in solids [33–35, 57], which is further explained in the outlook 5.3.

Once more consider the strong-slip model[4]

$$\begin{aligned} \dot{h} + (hu)_y &= 0, \\ \Re(\dot{u} + uu_y) &= \frac{4}{h}(hu_y)_y + (h_{yy} - \phi(h))_y - b^{-1}\frac{u}{h}, \end{aligned}$$

where $y \in [0, L] = \Omega$. At $y = 0$ and $y = L$ we impose boundary conditions $u = 0$ and $h_y = 0$. The scaling exponents in Table (3.6) suggest that only Trouton viscosity and van der Waals forces are relevant. We neglect all other terms and obtain

$$\dot{h} + (hu)_y = 0, \tag{4.46a}$$

$$\frac{4}{h}(hu_y)_y - \phi(h)_y = 0, \tag{4.46b}$$

together with the van der Waals potential $\phi(h) = h^{-3}$. Equation (4.46) describes transport of fluid particles and acceleration due to van der Waals forces, which in turn are equal to dissipating viscous forces due to the Trouton viscosity term. The major difference to the strong-slip equation is that this model only requires initial data $h(0, y) = h_0(y)$; the value of $u(0, y)$ must be computed such that it solves the algebraic differential equation (4.46b) with the boundary conditions $u = 0$ at $y = 0$ and $y = L$. Properties of this equation will be studied in the remainder of this chapter.

Remark 4.5. The velocity $u(t, y)$ can be written like

$$u(t, y) = \int_0^y \left(\frac{C(t)}{h(t, s)} - \frac{3}{8h(t, s)^3} \right) ds$$

---

[4] We changed notation slightly and refer to a point in space by (y, z) $\big($previously $(x, z)\big)$, so that we can use the Lagrangian coordinate x later.

where $C(t)$ such that $u(0, L) = 0$ holds consistently. But we use a different approach. ♢

It is easy and instructive to address existence, uniqueness, and qualitative features such as i) and ii) in the Lagrangian formulation of the strong-slip model. Before we proceed to simplify (4.46), a definition and explanation for the transformation from the Eulerian to the Lagrangian reference system is given.

Basically, the strong-slip equation is written down for an observer in the Eulerian reference system, who measures velocities at some fixed point in space, say $y \in \Omega$. In the Lagrangian system, on the other hand, the observer follows particles on their trajectories $\phi_t(x) \in \Omega$. The points x are elements of a so-called reference coordinate system, which we denote by Ω_{ref}. The reference coordinate system is often identified with Ω at some time t_0. Elements y of Ω correspond to positions in space, while each element x in Ω_{ref} corresponds to a particle with trajectory[5] $y(t) = \phi_t(x)$.

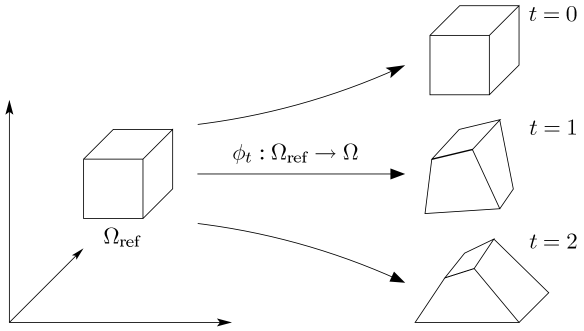

Figure 4.8: Illustration of the mapping ϕ_t. The trajectory of a particle in the Lagrangian reference frame is, by definition, constant in $x \in \Omega_{\text{ref}}$. In the corresponding Eulerian reference frame the trajectory of the same particle is defined by $y(t) = \phi_t(x) \in \Omega$. Such a transformation ϕ_t is supposed to be smooth, injective and conserve the orientation, i.e., $\partial_x \phi_t(x)$ is non-negative.

Both observer measure the same velocities at the same points, i.e.,

$$u\big(t, y(t)\big) = \dot{\phi}_t(x) \qquad \forall x \in \Omega_{\text{ref}}. \tag{4.47}$$

For given initial values $\phi_{t_0}(x)$ this relation can be seen as a definition of $\phi_t : \Omega_{\text{ref}} \to \Omega$. Usually one has $\Omega_{\text{ref}} = \Omega$ and $\phi_{t_0=0} = \text{id}_\Omega$, however, this restriction is not essential. In one spatial dimension the transformation of the strong-slip equation from Eulerian to Lagrangian reference frames works as follows:

---

[5] Note that the "t" refers to the parameter time and is not the partial derivative w.r.t. time.

Definition 4.8. Assume (h, u) is a solution of (4.46) (or strong-slip equation) and ϕ_{t_0} is a one-to-one mapping between $\Omega_{\text{ref}} = [0, 1]$ and $\Omega = [0, 1]$ and $\partial_x \phi_t > 0$. Then define the transformed solution $(\bar{h}, \bar{u})$ in the Lagrangian reference system by

$$\bar{h}(t, x) = h(t, y), \tag{4.48a}$$

$$\bar{u}(t, x) = u(t, y), \tag{4.48b}$$

With $s(t, x) = \partial_x \phi_t(x)$ we denote the so-called stretching of ϕ_t. We assume that ϕ_t preserves the orientation, i.e., $s(t, x) \geq 0$. The assumption $\Omega_{\text{ref}} = \Omega = [0, 1]$ is equivalent to the condition $\phi_t(1) = \int_0^1 s(t, x)\, dx = 1$. ♢

One can immediately check that derivatives of $\bar{u}$ and $\bar{h}$ transform as follows:

$$\begin{aligned} \dot{\bar{h}}(t, x) &= \dot{h}(t, y) + u(t, y)\, \partial_y h(t, y), \\ \partial_x \bar{h}(t, x) &= \partial_y h(t, y)\, s(t, x), \\ \partial_x \bar{u}(t, x) &= \dot{s}(t, x). \end{aligned}$$

If one replaces the derivatives of h and u in the simplified strong-slip equation (4.46a) by derivatives of $\bar{h}$ and $\bar{u}$ respectively, one obtains the following differential equation

$$\partial_t(\bar{h}(t, x)\, s(t, x)) = 0. \tag{4.49}$$

This equation shows that $\bar{h}s$ is constant along characteristic curves, where the constant can depend on x, i.e., $c(x) = \bar{h}(t, x)s(t, x)$. If one integrates (4.46b) once more with respect to y and applies the transformation rules (4.48b), then one ends up with

$$\frac{s_t(t, x)}{s(t, x)} = \frac{3}{8}\left(\frac{1}{\bar{h}(t, x)^3} - \frac{C(t)}{\bar{h}(t, x)}\right). \tag{4.50}$$

The usual approach is to choose $\phi_{t_0} = \text{id}_{[0,1]}$ and thus $c(x) = 1/h(t_0, x)$, which can be used to eliminate the dependence on $h(t, x)$ in (4.50). Leaving the equation like that the remaining dependence on $h(t_0, x)$ would be very inconvenient to deal with. So, given arbitrary initial data, we choose $\phi_{t_0}(x) = \int_0^x C_1/\bar{h}(t_0, s) ds$ and C_1 such $\phi_{t_0}(1) = 1$, which allows us to rewrite (4.50) to

$$\dot{s}(t, x) = s(t, x)^2\big(s(t, x)^2 - C(t)\big). \tag{4.51a}$$

All remaining constants are absorbed in the definition of $C(t)$ and the timescale. Since we solve the problem in the domain $\Omega_{\text{ref}} = \Omega = [0, 1]$, the time-dependence of $C(t)$ is fixed by the constraint $\phi_t(1) = 1$, or equivalently $\int_0^1 \dot{s}(t, x) dx = 1$, thus

$$C(t) = \int_0^1 s(t, x)^4\, dx \;\Big/\; \int_0^1 s(t, x)^2\, dx. \tag{4.51b}$$

Chapter 5

Summary and Outlook

5.1 Summary

With the intention to provide a fresh look on different aspects of thin-film rupture, we constructed various thin film models with slippage, we introduced a numerical scheme to investigate the nonlinear behavior of thin-film rupture, and finally we proved some properties of thin-film rupture for a simplified model.

Recent experimental data strongly suggest that the no-slip boundary condition is invalid at microscopic length scales, and, hence, more sophisticated models allowing slippage at solid–liquid interfaces are required. This effect is very pronounced for complex, hydrophobic fluids. So-called spinodal dewetting is induced in our models by inclusion of attractive van der Waals forces.

We discussed the so-called free-slip, weak-slip, intermediate-slip, and strong-slip equation, each of them corresponding to a certain scaling in the Navier-Stokes equations. Since it is possible to obtain free-slip and intermediate-slip model in the limit $b \to \infty$ and $b \to 0$ of the strong-slip equation, we only study numerical solution of the strong-slip equation. Similar studies of suggest that the interfacial singularities of thin films evolve locally self-similarly. Using $\mathcal{O}(1)$ initial data and various values of the Reynolds number, slip-length, and domain sizes, we are able to identify three different similarity regimes.

For zero Reynolds number, i.e., without inertial, the similarity solutions of the (inertialess) strong-slip equation are of second kind, which was so far only known for inertialess jet pinch-off. We computed the similarity scales of all those similarty solution with a high numerical precision. With the choice of parameters $0 < \Re, b \ll 1$ it was possible to observe all three regimes in a single (numerical) solution.

The role of slippage is to select which similarity solution dominates the first stages of the rupture.

Afterwards we focus on the inertialess strong-slip equation with similarity solutions of the second kind. The corresponding partial differential equation allows an essential simplification if we neglect inertia, surface tension, and slippage. Transforming the partial differential equation to Lagrangian coordinates, we obtain an integro-differential equation that has a finite-time singularity and the same similarity solutions as the inertialess strong-slip equation. Finally, we could even prove convergence to self-similar solutions in the simplified model for some class of initial data. Similar results were previously known for LSW models, however, not all of these results can be applied to second-kind similarity solutions. Further work is required to prove convergence to self-similar solutions rigorously.

5.2 Thin Films on Elastic Substrates

Up to now we studied nonlinear models of liquid films on solid substrates with van der Waals interactions between the liquid and the solid phase. The effect of slippage on these models was one of our major concerns. Now we introduce a possible extension of such research, to be specific we discuss the dynamics of a thin liquid film on a *viscoelastic* substrate.

This investigation is a part of the *DFG Priority Program SPP 1164 Nano- and Microfluidics*, which is partly concerned with the mathematical analysis of thin films and droplets on rigid and viscoelastic substrates [36]. The goal of mathematical modeling is to incorporate slippage into these models and to understand the influence of the microscopic setting onto those models.

Therefore consider a multiphase system consisting of a gaseous, a liquid, a viscoelastic solid, and a solid phase; however, we only model the dynamical behavior in the liquid and the viscoelastic phase. The role of the other two phases is to impose a free-slip boundary condition on the gas–liquid and a no displacement boundary condition on the viscoelastic solid-solid interface. Suppose that the complex liquid can be described by the incompressible Navier-Stokes equations with the stress tensor of an ideal Newtonian liquid — the complex fluid is characterized by van der Waals forces and wall slippage between liquid and viscoelastic solid phase. The geometric setup of the domains is shown in Figure 5.1. First studies of such models were performed by Matar in [58, 59] or will appear in [60].

Accordingly we examine an incompressible Navier-Stokes equation with van der Waals force $\mathbf{f}_{\text{ext}}$ coupled to a Kelvin-Voigt model of a viscoelastic, isotropic solid

$$\begin{aligned}
\rho_l(\dot{\mathbf{u}} + \mathbf{u}\cdot\boldsymbol{\nabla}\mathbf{u}) - \boldsymbol{\nabla}\cdot\boldsymbol{\sigma}_l &= \mathbf{f}_{\text{ext}} && \text{in } \Omega_l, && (5.1\text{a})\\
\boldsymbol{\nabla}\cdot\mathbf{u} &= 0 && \text{in } \Omega_l, && (5.1\text{b})\\
\rho_s\ddot{\mathbf{s}} - \boldsymbol{\nabla}\cdot\boldsymbol{\sigma}_s &= \mathbf{0} && \text{in } \Omega_s, && (5.1\text{c})\\
\boldsymbol{\nabla}\cdot\mathbf{s} &= 0 && \text{in } \Omega_s. && (5.1\text{d})
\end{aligned}$$

The stress tensors in the liquid phase (Newtonian fluid) and in the solid phase (Kelvin-Voigt material) are given by

$$\boldsymbol{\sigma}_l(\mathbf{u},p_l) = -p_l\mathbb{I} + \mu_l\left(\boldsymbol{\nabla}\mathbf{u} + (\boldsymbol{\nabla}\mathbf{u})^\top\right), \tag{5.1e}$$

$$\boldsymbol{\sigma}_s(\mathbf{s},p_s) = -p_s\mathbb{I} + G\left(\boldsymbol{\nabla}\mathbf{s} + (\boldsymbol{\nabla}\mathbf{s})^\top\right) + \mu_s\left(\boldsymbol{\nabla}\dot{\mathbf{s}} + (\boldsymbol{\nabla}\dot{\mathbf{s}})^\top\right). \tag{5.1f}$$

With μ_s and μ_l we denote dynamic viscosities in the solid and liquid phase, G is the shear modulus of the solid, $\mathbf{u}$ is the velocity in the liquid phase, and $\mathbf{s}$ is the deformation of the viscoelastic solid. Unlike in conventional elastic materials, the deformation stress tensor of viscoelastic materials depends on the rate of deformation $\boldsymbol{\nabla}\dot{\mathbf{s}}$.

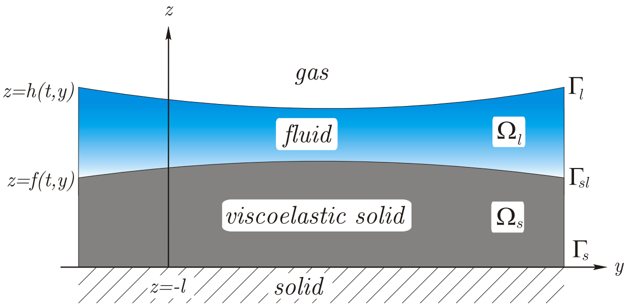

Figure 5.1: Geometry of the experiment with a (complex) liquid on a viscoelastic solid in the (y, z)-plane. The domain of the liquid and viscoelastic solid are denoted by Ω_l and Ω_s and the interfaces between with gas–liquid, liquid–viscoelastic solid, and viscoelastic solid–solid by Γ_l, Γ_{sl}, and Γ_s respectively. Boundaries are parametrized by $z = h(t, y)$, $z = f(t, y)$, and $z = -l$ as shown in the picture.

Both models are coupled due to the requirement that the forces onto the liquid–solid interface Γ_l are in equilibrium. The time-dependent domains Ω_s and Ω_l are defined as follows

$$\begin{aligned}\Omega_l &= \big\{(y,z) \in \mathbb{R}^2 : f(t,y) \le z \le h(t,y)\big\},\\ \Omega_s &= \big\{(y,z) \in \mathbb{R}^2 : -l \le z \le f(t,y)\big\}.\end{aligned}$$

On the interface between the gaseous and the liquid interface we require an equilibrium of forces; between tangential stresses of both phases and between normal stresses of both phases together with the normal surface tension force. To state the interface condition we will need the normal and tangential vectors on Γ_l and Γ_{sl}, which are defined as

$$\begin{aligned}\mathbf{n}_l &= \begin{pmatrix}-h_y\\ 1\end{pmatrix}(1+h_y^2)^{-1/2}, & \mathbf{t}_l &= \begin{pmatrix}1\\ \partial_y h\end{pmatrix}(1+h_y^2)^{-1/2},\\ \mathbf{n}_{sl} &= -\begin{pmatrix}-f_y\\ 1\end{pmatrix}(1+f_y^2)^{-1/2}, & \mathbf{t}_{sl} &= \begin{pmatrix}1\\ f_y\end{pmatrix}(1+f_y^2)^{-1/2}.\end{aligned}$$

On the air–liquid interface we have a balance of shear stresses and surface tension together with the kinematic boundary condition

$$\begin{aligned}\mathbf{n}_l \cdot \boldsymbol{\sigma}_l(\mathbf{u}, p) &= \gamma_l\, \kappa_l\, \mathbf{n}_l && \text{on } \Gamma_l,\\ \dot{h}(t,y) &= w - u(\partial_y h) && \text{on } \Gamma_l,\end{aligned}$$

where we used the components of the velocity vector $\mathbf{u} = (u, w)^\top$, and the mean curvature of the gas–liquid interface Γ_l is κ_l. The kinematic boundary condition expresses that the velocity $\mathbf{u}$ is equal to the speed of the interface. Like it was said in the discussion of boundary conditions in the introductory modeling chapter, it suffices to define this relation for the normal component of $\mathbf{u}$.

The conservation laws on the liquid–viscoelastic solid interface are slightly more complex. On this interface we impose conservation of mass[1], Navier-slip boundary conditions, and surface tension

$$\begin{aligned} \mathbf{n}_{sl}(\dot{\mathbf{s}} - \mathbf{u}) &= 0 && \text{on } \Gamma_{sl}, \\ \frac{b}{\mu_l}\mathbf{t}_{sl} \cdot \boldsymbol{\sigma}_l \mathbf{n}_{sl} + \mathbf{t}_{sl} \cdot (\dot{\mathbf{s}} - \mathbf{u}) &= 0 && \text{on } \Gamma_{sl}, \\ \mathbf{n}_{sl} \cdot (\boldsymbol{\sigma}_l - \boldsymbol{\sigma}_s) - \gamma_{sl}\, \kappa_{sl}\, \mathbf{n}_{sl} &= 0 && \text{on } \Gamma_{sl}. \end{aligned}$$

Note that the Navier-slip condition looks much simpler on planar interfaces, i.e., $b\partial_z u = u$, than on curved interfaces. The general definition, which was already given in the first chapter, is that the tangential stress if proportional to the tangential part of the slip $\mathbf{u}-\mathbf{v}$ past the interface. The mean curvature on Γ_{sl} is noted by κ_{sl} and γ it thesurface tension coefficient.

On the interface between solid and viscoelastic solid Γ_s the viscoelastic solid is undeformed, i.e.,

$$\mathbf{s} = \mathbf{0} \qquad \text{on } \Gamma_s.$$

The signed mean curvature of a height profile implicitly defined by $z = h(t, y)$ is

$$\kappa_l = \frac{h_{yy}}{(1 + h_y^2)^{3/2}}.$$

An analogous expression exists for κ_{sl}, one only needs to replace $h(t, y)$ by $f(t, y)$. The system of equations above is the complete model of a thin film coupled to a viscoelastic solid. Since this model is far to complex, we use a long-wavelength approximation to derive a simpler model.

5.2.1 Model reduction

In the first chapter we showed how to employ a lubrication or long-wavelength approximation in order to simplify a higher-dimensional Navier-Stokes equation. Similarly one can apply this technique to simplify the model of a viscoelastic solid coupled to a non-Newtonian liquid. We use the conservative van der Waals force $\mathbf{f}_{\text{ext}} = (0, \phi')$, where different implementations of the interaction potential ϕ can be found in [3]. Using components of the deformation field are $\mathbf{s} = (s, r)$ we introduce the scales

$$\begin{aligned} &z = H\,\widetilde{z}, && h = H\,\widetilde{h}, && b = H\,\widetilde{b}, && y = L\,\widetilde{y}, \\ &u = U\,\widetilde{u}, && w = \epsilon\, U\,\widetilde{w}, && t = (\epsilon\, U)^{-1} H\,\widetilde{t}, && p_l + \phi' = P(\widetilde{p} + \widetilde{\phi}'), \\ &s = D\,\widetilde{s}, && r = \epsilon\, D\,\widetilde{r}, && p_s = P\,\widetilde{p}_s, && f = H\,\widetilde{f}, \end{aligned}$$

---

[1] For the multiphase system this implies that the normal component of liquid velocity $\mathbf{u}$ is equal to the normal component of the deformation speed $\dot{\mathbf{s}}$.

where the small scale is defined by $\epsilon = H/L$. At this points let us restrict to a scaling that is similar to the one of the weak-slip regime, i.e.,

$$D = \epsilon^3 \frac{\gamma_l}{G} \qquad U = \epsilon^3 \frac{\gamma_l}{\mu_l} \qquad P = \frac{G}{\epsilon^2} \qquad H = \epsilon^4 \frac{\gamma_l}{G},$$

whereby one ends up with the following leading order problem in fluid phase Ω_l

$$\begin{aligned} (p_l + \phi)_y - u_{zz} &= 0, \\ (p_l)_z &= 0, \\ u_y + w_z &= 0. \end{aligned}$$

These equations are basically equal to the leading order equation of the weak-slip equation. In addition this equation is coupled to the solid phase Ω_s by the following leading order problem

$$\begin{aligned} -(p_s)_y + s_{zz} + \left(\frac{\mu_s}{\mu_l}\right) s_{tzz} &= 0, \\ (p_s)_z &= 0, \\ s_y + r_z &= 0. \end{aligned}$$

On the air–liquid interface Γ_l the solution solves

$$\begin{aligned} u_z &= 0, \\ p_l + h_{yy} &= 0, \\ h_t - w + u h_y &= 0, \end{aligned}$$

which represents an equilibrium of forces (surface tension and normal stress) and mass conservation (kinematic boundary condition). The leading order problem on the viscoelastic solid–liquid interface Γ_{sl} is more complex because, due to the Navier-slip boundary condition, the momentum transfer between Ω_l and Ω_s depends linearly on the difference between the tangential part of $(\mathbf{u} - \mathbf{s})$

$$\begin{aligned} u_z - (s_z + \left(\frac{\mu_s}{\mu_l}\right) s_{tz}) &= 0, \\ p_s - p_l + \left(\frac{\gamma_{sl}}{\gamma_l}\right) f_{yy} &= 0, \\ f_t - w + u f_y &= 0, \\ (s_t - u) + b u_z &= 0. \end{aligned}$$

There are no deformations on the viscoelastic solid–solid interface Γ_s, thus $s = 0$ and $r = 0$. In the non-dimensionalized formulation of the leading order problem we replace the remaining parameters by $\lambda = \mu_s/\mu_l$ and $\Lambda =$

γ_{sl}/γ_l. Next, we integrate the leading order equations in the viscoelastic and the liquid phase and obtain the following equations for $h(t,y)$ and $f(t,y)$

$$\begin{aligned}\partial_t(h-f) =& -\partial_y\Big[\left(\frac{1}{3}(h-f)^3+b(h-f)^2\right)(h_{yyy}-\phi_y)...\\ &\quad ...+(h-f)\dot{s}\Big|_{z=f}\Big], \qquad (5.3\text{a})\\ \lambda\partial_t f =& -\partial_y\Big[\frac{1}{3}(f+l)^3(h_{yyy}+\Lambda f_{yyy})...\\ &\quad ...+\frac{1}{2}(h-f)(f+l)^2(h_{yyy}-\phi_y)-I(t,y)\Big]. \qquad (5.3\text{b})\end{aligned}$$

In addition to the obvious coupling, the equations for h and f are coupled by the functions $s(t,y)$ and $I(t,y)$, where I can be computed from s. The auxiliary function s is the solution of an ordinary differential equation that is solved simultaneously with the equation for f and h and stores intrinsic information about the deformation of the viscoelastic solid. The functions $I(t,y)$ and $s(t,y)$ are defined by

$$I(t,y)=(f+l)s_1(t,y)+\frac{1}{2}(f^2-l^2)s_2(t,y)+\frac{1}{3}(f^3+l^3)s_3(t,y) \qquad (5.3\text{c})$$

$$\dot{s}(t,y)\Big|_f=\dot{s}_1(t,y)+f(t,y)\,\dot{s}_2(t,y)+f^2(t,y)\,\dot{s}_3(t,y) \qquad (5.3\text{d})$$

and the auxiliary functions s_i are solutions of the ordinary differential equation

$$s_1(t,y)+\lambda\,\dot{s}_1(t,y)=\frac{l}{2}\Big((2h+l)h_{yyy}+(2f+l)\Lambda f_{yyy}+2(f-h)\phi_y\Big), \qquad (5.3\text{e})$$

$$s_2(t,y)+\lambda\,\dot{s}_2(t,y)=hh_{yyy}+\Lambda ff_{yyy}+(f-h)\phi_y, \qquad (5.3\text{f})$$

$$s_3(t,y)+\lambda\,\dot{s}_3(t,y)=-\frac{1}{2}(h_{yyy}+\Lambda f_{yyy}). \qquad (5.3\text{g})$$

A numerical scheme of this equation should solve the initial value problem for

$$\big(h(t,y),f(t,y),s_1(t,y),s_2(t,y),s_3(t,y)\big).$$

Initial data for h represent the shape of the liquid interface, while f and the s_i's represent the initial shape and deformation of the viscoelastic solid. For a similar problem, but without slippage, Omar et al. derived a model, made a linear stability analysis of flat liquid films, and computed numerical solutions using a interaction potential with a long ranged attraction and possibly a short ranged repulsion term

$$\phi(h)=\frac{A_1}{h^3}, \qquad \text{or} \qquad \phi(h)=\frac{A_1}{h^3}-\frac{A_2}{h^4},$$

where $A_1, A_2 > 0$. We perform a similar linear stability analysis and some preliminary numerical results of thin film dewetting on viscoelastic substrates will be presented. In corporation with the DFG Priority Program SPP 1164 it will be possible to compare those results (qualitatively and quantitatively) with real experiments, i.e., dewetting of thin liquid films (polystyrene) on viscoelastic solid substrates (PDMS/PMMA). By including an repulsive term we are not only interested in the short-time behavior but also the long-time behavior of thin liquid films, i.e., later stages of dewetting. In the introduction we mentioned to motion of liquid rims and formation of liquid droplets. Recent studies for the coarsening dynamics of the strong-slip model are performed by Kitavtsev et al. [61]. In the next section we catch a glimpse of the coarsening dynamics of liquid rims and their final stage (liquid droplet) on an viscoelastic substrate.

5.2.2 Linear stability

First, we verify the model by comparing a linear stability analysis with the previous work by Kumar and Matar [58] and show some numerical results similar to the ones in [59].

Assume that initially the fluid and the viscoelastic solid are flat, i.e., $h = 1$, $f = 0$, and $s_i = 0$ $(i = 1, 2, 3)$. Now consider perturbations of the flat solution which have the form

$$h = 1 + \delta h, \qquad f = 0 + \delta f \qquad s_i = 0 + \delta s_i.$$

with δf, δh, and δs_i as usual

$$\delta h = \hat{h}\, e^{iky+\gamma t}, \qquad \delta f = \hat{f}\, e^{iky+\gamma t}, \qquad \delta s_i = \hat{s}_i\, e^{iky+\gamma t}.$$

For simplicity use the abbreviation $c(w) = (w^3/3 + bw^2)$ and the potential without the short ranged repulsion, i.e., $\phi = A_1(h-f)^{-3}$. Then the linearized system is simply

$$\begin{aligned}
\partial_t(\delta h - \delta f) &= -c(1)\Big(\delta h_{yyyy} - \phi'(1)(\delta h_{yy} - \delta f_{yy})\Big) - \partial_{ty}^2 \delta s_1, \\
\lambda \partial_t \delta f &= -\tfrac{l^3}{3}(\delta h_{yyyy} + \Lambda \delta f_{yyyy}) - \tfrac{l^2}{2}(\delta h_{yyyy} + \phi'(1)(\delta h_{yy} - \delta f_{yy})) + \delta I_y, \\
\delta s_1 + \lambda \delta \dot{s}_1 &= \frac{l}{2}\Big((2+l)\delta h_{yyy} + l\Lambda \delta f_{yyy} - 2\phi'(1)(\delta h_y - \delta f_y)\Big), \\
\delta s_2 + \lambda \delta \dot{s}_2 &= \delta h_{yyy} - \phi'(1)(\delta h_y - \delta f_y), \\
\delta s_3 + \lambda \delta \dot{s}_3 &= -\frac{1}{2}\left(\delta h_{yyy} + \Lambda \delta f_{yyy}\right), \\
\delta I &= l\, \delta s_1 - \frac{l^2}{2}\, \delta s_2 + \frac{l^3}{3}\, \delta s_3.
\end{aligned}$$

Plugging the sinusoidal perturbations into this equation one can easily compute the growth rate γ as a function of the wave-number k, the so-called inverse dispersion relation, and compare with the linear stability analysis of Matar and Kumar [58]. For the ease of presentation we only present explicit expressions for the following two special cases of unstable modes: $l = 0$ and $\lambda = 0$.

- without viscoelastic substrate ($l = 0$)

  $$\gamma(k) = \frac{1}{3}\big(3A - k^2\big)k^2(3b+1)$$

  This is the usual dispersion relation of the weak-slip equation with slippage and qualitatively coincides with the expression given in (3.8).

- solid is elastic but not viscous ($\lambda = 0$)

$$\gamma = \frac{4(1+3b)k^2\big(3k^2 - k^6 l^3 \Lambda - 3A(3 + k^4 l^3(1+\Lambda))\big)}{3\big(12 + k^8 l^4 \Lambda - 3Ak^2 l(12 + k^4 l^3(1+\Lambda)) + 4k^4 l(3 + l(3 + l + l\Lambda))\big)}$$

Alternatively, in Figure 5.2 we show the growth rates for different substrate thicknesses l and for $\Lambda = 1$, $\lambda = 1$, $b = 0$; the results agree with [58] (page 585, Figure 2).

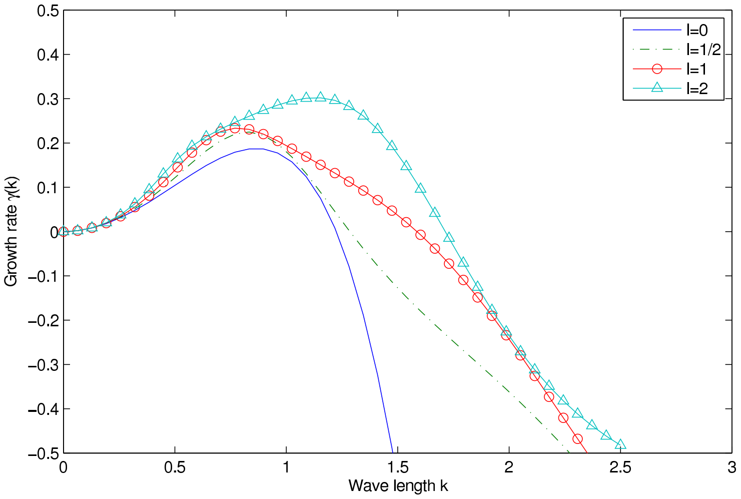

Figure 5.2: Growth rate $\gamma(k)$ for perturbation $h = 1 + \delta h$, $f = 0 + \delta f$; we show $\gamma(k)$ for $\Lambda = \lambda = 1$, $A_1 = 1/2$, and $b = 0$. Different curves differ in the thickness of the viscoelastic substrate l

In any of those cases depicted in Figure 5.2 exist a range of wave numbers for which the flat film is unstable. The maximal growth rate and the size of the unstable interval increase with larger l. Based on the algorithm presented in Chapter 2, a numerical scheme that solves problem (5.3) was created and we show and discuss some numerical solutions.

5.2.3 Numerical solutions

In the previous section we presented a model that is part of ongoing research; the model is an extension of the work by Matar for two reasons: First, the lubrication equations are integrated and thus written in a more compact and convenient form, and, second and more importantly, the effect of slippage between molecules of the viscoelastic solid and the fluid phase is added.

Now we show some preliminary numerical results and compare with experimental results. Our first example is rupture of a thin liquid film on a viscoelastic solid. Since this phenomenon is observed on very fast timescales no experimental data exists. experimental data. However, if we consider the model with repulsive forces $\phi = A_1/(h-f)^3 - A_2/(h-f)^4$ we can study longtime behavior, i.e., traveling waves and dewetting fronts, and compare with experimental results. Being part of the outlook, this is supposed to give a flavor which additional physical effects are important in microfluidics and how more complex and realistic model might look like.

As the first example consider the numerical solution of Equation (5.3) with initial data $h(0,y) = 1 - \frac{1}{5}\cos\bigl(\frac{2\pi}{L}(y - L/2)\bigr)$, $f(0,y) = s(0,y) = 0$. We use the parameters $A_1 = 1$, $A_2 = 0$ (no repulsion), $\Lambda = \lambda = 1$, $b = 1$, and $l = 10$.

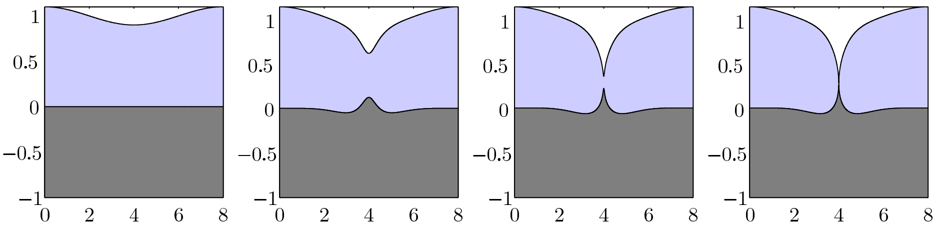

Figure 5.3: Rupture of thin liquid film with slip on an elastic substrate with attractive forces only; the panel shows the domain occupied by the liquid layer (light shaded area) and the elastic substrate (dark shaded area) at different time steps

For rupture of a thin film the film thickness became singular after a finite time; for this model the relative height $h - f$ goes to zero after a finite time. The absolute positions $h(t,y)$ and $f(t,y)$ are more or less arbitrary and it is reasonable to look for self-similar behavior of $h - f$. We skip a detailed discussion at this point and show and only show the dependence of $(h - f)$ on the remaining time until rupture.

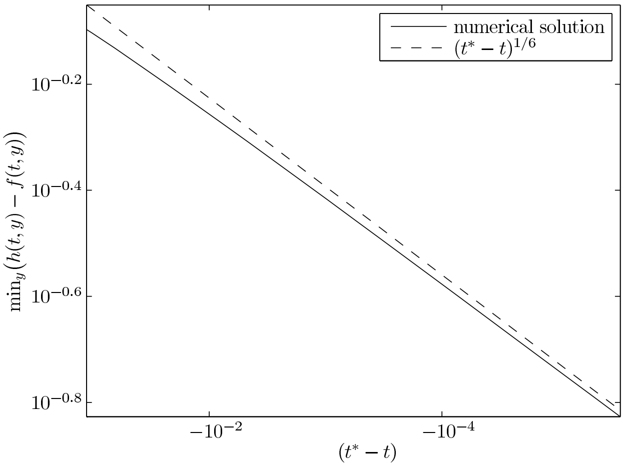

Figure 5.4: The graph shows the critical fluid layer thickness $\min_y(h - f)$ versus the time until rupture $(t^* - t)$ compared to the $(t^* - t)^{1/6}$ law (inferred from self-similar solutions of the weak-slip equation).

As one might have already expected, the numerical solution suggests the relationship $\min_y(h(t, y) - f(t, y)) = C(t^* - t)^{1/6}$, which we found is typical for self-similar solutions of weak-slip equation.

The second example shows the solutions when a repulsive force is active, i.e., $A_2 > 0$. As it turns out, the strong repulsive force prevents rupture from happening and thus the numerical solution is well defined for all times.

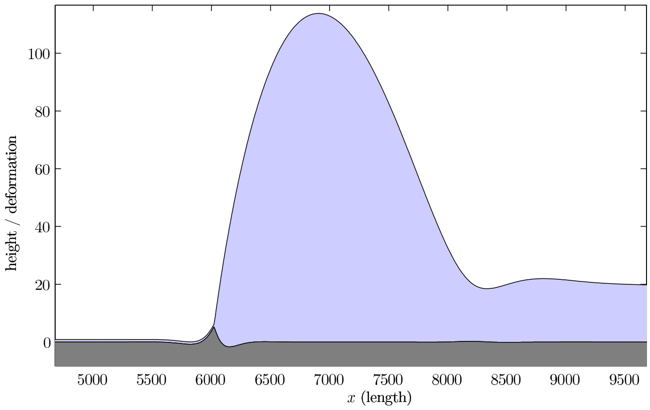

Figure 5.5: Dewetting in a late stage; thin liquid film with slip on an elastic substrate and repulsive term $A_2 > 0$

Even though the simulation is just 2-dimensional, translational symmetry along the remaining axis is a good approximation of traveling-waves if the wave has traveled sufficiently far. The height profile looks similar to the experimental data, while the deformation of the viscoelastic looks qualitatively different.

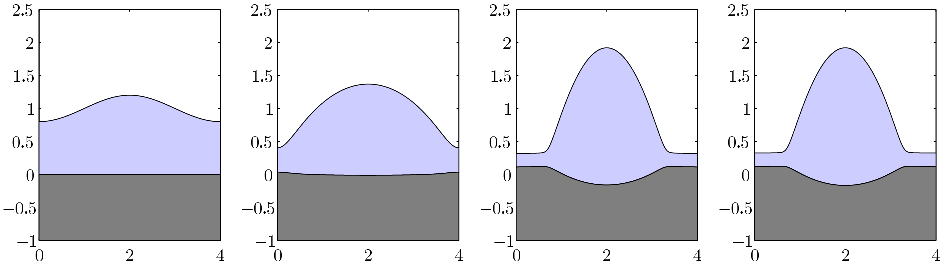

Figure 5.6: Time-dependent solution with initial data $h(0, y) = 1 + 0.2\cos(\pi x/L)$ and $f = s_i = 0$ $(i = 1, 2, 3)$ with $\lambda = b = l = A_1 = 1$, $\Lambda = 5$, $A_2 = 0.2$ on $\Omega = [0, 4]$. Simulation was performed with 1024 mesh points and $h_y = h_{yyy} = f_y = f_{yyy} = 0$ boundary conditions. The region occupied by the liquid is shaded with a light color, while the region occupied by the viscoelastic substrate is shaded with a darker color.

5.2.4 Stationary and Solutions

Finally, we observed that solutions $h(t, y)$ and $f(t, y)$ become stationary as $t \to \infty$ and that h has the typical shape of a droplet. We shortly derive the equation for stationary solution $h(y)$ and $f(y)$, and we point out the relation to the usual droplet solution. Whereby, we set the velocity and all time derivatives to zero and obtain the two equations

$$h_{yy}(y) + f_{yy}(y) - \phi(h(y)) = C_1, \tag{5.4}$$

$$h_{yy}(y) + (1 + \Lambda)f_{yy}(y) = C_2, \tag{5.5}$$

where $\phi(h) = A_1 h^{-3} - A_2 h^{-4}$ (we replaced $h - f$ by h) and with some unknown constants of integration C_1, C_2. Suppose the fluid film is flat away from a droplet with thickness $h_{\min}$, then the constants are simply $C_1 = -\phi(h_{\min})$ and $C_2 = 0$. Under this condition the equation can be simplified further to

$$\frac{\Lambda}{\Lambda + 1} h_{yy} = \phi(h) + C_1, \tag{5.6}$$

$$f = a + by - \frac{h}{1 + \Lambda}, \tag{5.7}$$

where constants a and b are fixed by the initial conditions. This equation can be integrated in the usual manner, i.e.,

$$\frac{\Lambda}{2(\Lambda + 1)} \left(\frac{dh}{dy}\right)^2 = \psi(h) - \psi(h_{\min}) + C_1(h - h_{\min})$$

where $\psi'(h) = \phi(h)$. Basically h is the usual droplet solution known for lubrication models, and f will be proportional to $-h$.

5.2.5 Comparison with Experiments

In the following part a comparison with experimental results of Konstantina Kostourou and Ralf Seemann, who work at the Max Planck Institute for Dynamics and Self-Organization in the Department Dynamics of Complex Fluids of Professor Herminghaus. The results shown here are a part of the SPP 1164s research and are shown with the kind permission of Konstantina Kostourou.

The picture below shows a droplet of fluid polystyrene on an elastic rubber-like substrate.

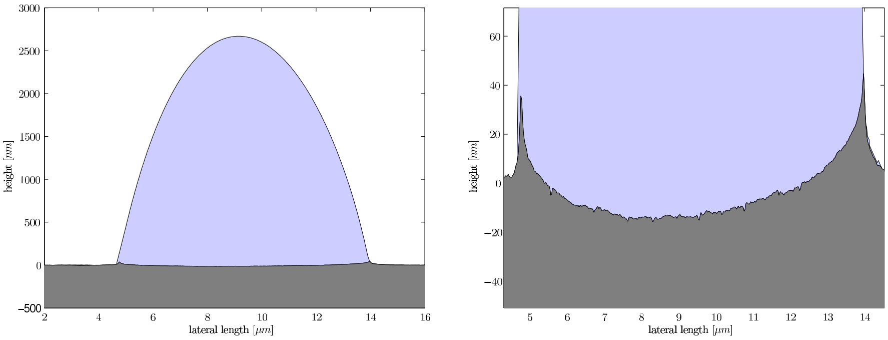

Figure 5.7: AFM image of an stationary liquid droplet of polystyrene (PS(18k)) at $T = 120°$ Celsius on a rubber-liker substrate prepared with SG186 (Sylgard) with elastic modulus $E = 1.7\,M\,Pa$.

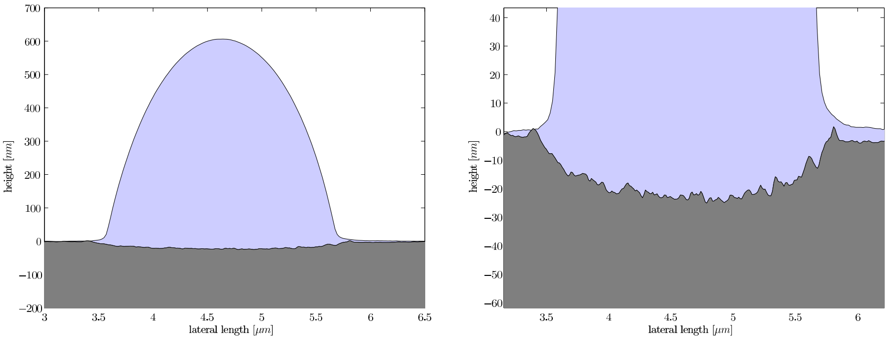

Figure 5.8: AFM image of an stationary liquid droplet of polystyrene (PS(18k)) at $T = 120°$ Celsius on a rubber-liker substrate prepared with SG186 (Sylgard) with elastic modulus $E = 4.1\,M\,Pa$.

Most interestingly, notice the different characteristic shapes of the deformation at the liquid–solid–air contact zone. While the substrate in Figure 5.7 has an additional kink in the deformation profile, the result in Figure 5.8

looks similar to the prediction of our model shown in Figure 5.6.

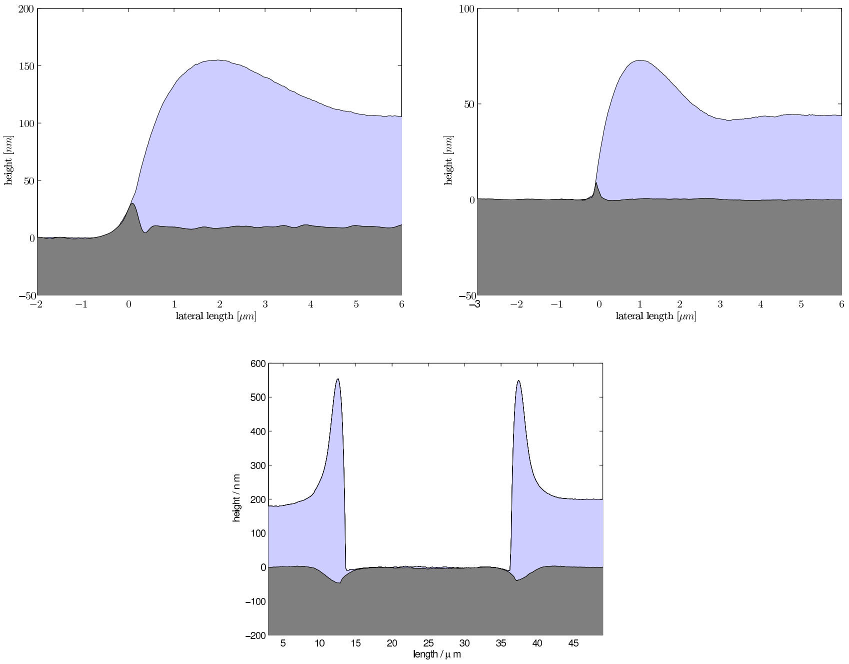

Figure 5.9: AFM image on dewetting rims; (upper left) PS18K on PMMA at 160° Celsius; (upper right) PS100K on PMMA at 160° Celsius; (lower) PS18K on SG186 at 120° Celsius

In particular the results of polystyrene on a PMMA substrate in Figure 5.9 qualitatively fit to the signature shown in Figure 5.5. However, the theory for thin-film dynamics on elastic substrates is still work in progress and there are many open questions regarding validation and predictions of the model (5.3).

A more detailed derivation and discussion of such models can be found in the upcomming paper by Wagner et al. [60].

5.3 Extension to LSW Models

In the previous chapter we already indicated that the integro-differential equation actually is related to LSW models. In order understand this relation suppose that a solution of the simplified model of thin-film rupture

$$\begin{aligned} \dot{s}(t,x) &= s^2(s^2 - s_0^2), \\ s_0^2 &= \int_\Omega s^4\,dx \quad \Big/ \quad \int_\Omega s^2\,dx, \end{aligned}$$

with $x \in \Omega = [0,1]$ is strictly decreasing and maps the domain Ω onto the interval $[0,1]$, i.e., the mapping $s(t,x)$ is invertible for every fixed t. Let $\phi(t,s)$ be its inverse such that $\phi\big(t, s(t,x)\big) = x$ holds for every t. Hence,

$$\frac{d\phi}{dt} = \dot{\phi} + \partial_s c\, \partial_t s = \dot{\phi} + \big(s^2(s^2 - s_0^2)\big)\partial_s \phi = 0. \tag{5.8}$$

In the new variables s_0 is now computed via

$$s_0^2(t) = \int_\omega \partial_s\phi(t,s)\, s^4 ds \Big/ \int_\omega \partial_s\phi(t,s)\, s^2 ds.$$

Note that the domain $\omega = \big[0, \sigma(t)\big]$ grows in time according to $\dot{\sigma} = \sigma^2(\sigma^2 - s_0^2)$. In order to compare with LSW models we write the partial differential equation in terms of $c = \partial_s\phi$. We differentiate (5.8) with respect to s and find that $c(t,s)$ solves

$$\dot{c}(t,s) = -\partial_s \left[\Big(s^2\big(s^2 - s_0^2(t)\big)\Big)\, c(t,s)\right]$$

on $\omega = [0,\sigma]$ with $s_0^2 = \int s^4 c\, ds / \int s^2 c\, ds$. Such models play a central role in the theory of coarsening of dilute alloys, or supersaturated solutions, such as in the models by Lifshitz, Slyozov [34], Wanger [35], and Todes, Khrushchev [62], i.e., so-called LSW models. They consider general models of the form

$$\begin{aligned}\dot{c}(t,s) &= -\partial_s\big(v(t,s)\, c(t,s)\big)\\ v(t,s) &= a(s)\big(u(t) - s^{-1/\nu}\big)\end{aligned}$$

where $u(t)$ corresponds to our s_0 and is defined such that the integral over c is conserved, i.e., $\int \dot{c}(t,s)\, ds = 0$. Hence,

$$u(t) = \int_0^\infty s^{-1/\nu} a(s) c(t,s)\, ds \Big/ \int_0^\infty a(s) c(t,s)\, ds.$$

At some given time t, the quantity $c(t,s)$ represents the probability density that spherical clusters containing s particles exist, and $v(t,s)$ is the average speed by which clusters grow; usually $a(s)$ is of the form $a(s) = \lambda^\beta$. Note that this equation differs from the simplified rupture model by the definition of $v(t,s)$ (it contains negative powers of s), and correspondingly by the definition of $u(t)$.

Since the pioneering works mentioned above it was clear that solutions of the LSW equations posses self-similar solutions. Rigorous mathematical studies of self-similar solutions were done by Carr and Penrose [57], and Niethammer and Pego [33], each of them for a different choice of β and ν.

It is well known that such models also posses a intriguing dependence on initial data, a phenomenon called weak-selection [54]. On approach to cure the problem of weak selection that is discussed in the community is inclusion of particle density fluctuactions, which yields higher-order terms in the LSW equation [63]. A similar phenomenon occurs in our simplified strong-slip equation. Even though surface tension is negligible near the singularity, the presence of this higher-order term is very likely the reason that only the self-similar solution with $n = 2$ solution is stable.

The possibility of second-kind similarity solutions was not raised so far for LSW models. Thus, this discussion of similarity solution might enrich the discussion of LSW models, if it is found that self-similarity of second-kind plays a role. Convergence of self-similar solution of second kind in the context of the integro-differential equation or the LSW equation will be studies further on [64].

Constants, Scales, and Symbols

symbol	name	SI unit	magnitude/SI units
A'	Hamaker constant	$kg \cdot m^2 \cdot s^{-2}$	10^{-20}
b	slip-length	m	10^{-8}
γ_l	surface tension liquid–gas	$kg \cdot s^{-2}$	10^{-2}
G	elasitc modulus of viscoelastic body	$kg \cdot m^{-1} \cdot s^{-1}$	10^6
h	typical thickness of thin film	m	10^{-7}
L	typical lateral scale	m	10^{-6}
μ	liquids' (dynamic) viscosity	$kg \cdot m^{-2} \cdot s^{-1}$	10^7
ρ	liquids' density	$kg \cdot m^{-3}$	10^3

symbol	name	value
Plank constant	$\hbar$	$1.05 \cdot 10^{-34}\, kg \cdot m^2 \cdot s^{-1}$
speed of light	c	$3.00 \cdot 10^8\, m \cdot s^{-1}$

symbol	description	
$\mathbb{R}^+$	nonnegative real numbers	
$(\mathbf{u})_{x_j}$	jth component of vector $\mathbf{u}$	$\mathbf{u} \cdot \mathbf{e}_{x_j}$
h_{x_j}	partial derivative of scalar w.r.t. x_j	$\partial_{x_j} h$
∇h	scalar spatial gradient	$\nabla h = (\partial_x h, \partial_z h)^\top$
$\nabla \mathbf{u}$	vector gradient	$(\nabla \mathbf{u})_{ij} = \partial_{x_i} (\mathbf{u})_{x_j}$
$\operatorname{div} \mathbf{u} = \nabla \cdot \mathbf{u}$	divergence of a vectorfield	$\operatorname{div}\mathbf{u} = \sum_j \partial_{x_j} (\mathbf{u})_{x_j}$
$\operatorname{div} \boldsymbol{\sigma} = \nabla \cdot \boldsymbol{\sigma}$	divergence of a tensorfield	$\operatorname{div} \boldsymbol{\sigma}_{x_i} = \sum_j \partial_{x_j} (\mathbf{u})_{x_i, x_j}$
$\mathbf{v} \cdot \nabla \mathbf{u}$	directional derivative of $\mathbf{u}$ along $\mathbf{v}$	$\sum_j \mathbf{v}_{x_j} \partial_{x_j} \mathbf{u} = \mathbf{v} \cdot (\nabla \mathbf{u})$
$\dot{\mathbf{u}}, \dot{h}$	time derivative	$\partial_t \mathbf{u}, \partial_t h$
$A : B$	Frobenius inner product	$\sum_{ij} A_{ij} B_{ij}$
$\\|u\\|_p$	L^p norm $(p \in (0, \infty)$ $(\int_\Omega u^p \, dx)^{1/p}$	

Bibliography

[1] Steve Granick, Yingxi Zhu, and Hyunjung Lee. Slippery questions about complex fluids flowing past solids. *nature materials*, 2:221–227, 2003.

[2] K. Jacobs, R. Seemann, and H. Kuhlmann. Trendbericht Mikrofluidik. *Nachrichten aus der Chemie*, 53:300–304, 2005.

[3] Alexander Oron, Stephen H. Davis, and S. George Bankoff. Long-scale evolution of thin liquid films. *Rev. Mod. Phys.*, 69(3):931–980, Jul 1997. doi: 10.1103/RevModPhys.69.931.

[4] Stephan Herminghaus, Karin Jacobs, Klaus Mecke, Jörg Bischof, Andreas Fery, Mohammed Ibn-Elhaj, and Stefan Schlagowski. Spinodal Dewetting in Liquid Crystal and Liquid Metal Films. *Science*, 282 (5390):916–919, 1998. doi: 10.1126/science.282.5390.916.

[5] P. G. de Gennes. Wetting: statics and dynamics. *Rev. Mod. Phys.*, 57 (3):827–863, Jul 1985. doi: 10.1103/RevModPhys.57.827.

[6] Andrea L. Bertozzi, Michael P. Brenner, Todd F. Dupont, and Leo P. Kadanoff. Singularities and similarities in interface flows. In *Trends and perspectives in applied mathematics*, volume 100 of *Appl. Math. Sci.*, pages 155–208. Springer, New York, 1994.

[7] Francisco Bernis and Avner Friedman. Higher order nonlinear degenerate parabolic equations. *J. Differential Equations*, 83(1):179–206, 1990. ISSN 0022-0396.

[8] Eric Lauga, Michael P. Brenner, and Howard A. Stone. Microfluidics: The no-slip boundary conditin. *Handbook of Experimental Fluid Dynamics*, pages 1219–1240, 2007.

[9] Andreas Münch, Barbara Wagner, and Thomas P. Witelski. Lubrication models with small to large slip lengths. *Journal of Engineering Mathematics*, 53:359–383, Dec 2005. doi:10.1007/s10665-005-9020-3.

[10] P. Gilberto López, S. George Bankoff, and Michael J. Miksis. Non-isothermal spreading of a thin liquid film on an inclined plane. *Journal*

of Fluid Mechanics Digital Archive, 324(-1):261–286, 2006. doi: 10.1017/S0022112096007914.

[11] Günter Reiter. Dewetting of thin polymer films. *Phys. Rev. Lett.*, 68 (1):75–78, Jan 1992. doi: 10.1103/PhysRevLett.68.75.

[12] A. Sharma and G. Reiter. Instability of thin polymer films on coated substrates: Rupture, dewetting and drop formation. J. Colloid Interface Sci., 178:383–389, 1996.

[13] R. Fetzer, A. Münch, B. Wagner, M. Rauscher, and K. Jacobs. Quantifying Hydrodynamic Slip: A Comprehensive Analysis of Dewetting Profiles. *Langmuir*, 23(21):10559–10566, 2007. ISSN 0743-7463.

[14] Ralf Seemann, Stephan Herminghaus, Karin Jacobs, Stefan Schlagowski, Neto Chiara, Podzimek Daniel, Renate Konrad, and Hubert Mantz. Dynamics and structure formation in thin polymer melt films. *Journal of Physics: Condensed Matter*, 17:267–290, 2005. doi: 10.1088/0953-8984/17/9/001.

[15] Jens Eggers. Nonlinear dynamics and breakup of free-surface flows. *Rev. Mod. Phys.*, 69(3):865–930, Jul 1997. doi: 10.1103/RevModPhys.69.865.

[16] Jens Eggers and Marco A. Fontelos. A catalogue of singularities, 2007.

[17] Jens Eggers. Universal pinching of 3d axisymmetric free-surface flow. *Phys. Rev. Lett.*, 71(21):3458–3460, Nov 1993. doi: 10.1103/PhysRevLett.71.3458.

[18] William Strutt Rayleigh. *Proc. London Math. Soc.*, 4, 1878.

[19] Demetrios T. Papageorgiou. On the breakup of viscous liquid threads. *Phys. Fluids*, 7(7):1529–1544, 1995. ISSN 1070-6631.

[20] Grigory Isaakovich Barenblatt. *Scaling, self-similarity, and intermediate asymptotics*, volume 14 of *Cambridge Texts in Applied Mathematics*. Cambridge University Press, Cambridge, 1996. ISBN 0-521-43516-1; 0-521-43522-6. With a foreword by Ya. B. Zeldovich.

[21] Michael P. Brenner, John R. Lister, and Howard A. Stone. Pinching threads, singularities and the number $0.0304\cdots$. *Phys. Fluids*, 8(11):2827–2836, 1996. ISSN 1070-6631.

[22] Michael Renardy. Finite time breakup of viscous filaments. *Z. Angew. Math. Phys.*, 52(5):881–887, 2001. ISSN 0044-2275.

[23] Michael Renardy. A comment on self-similar breakup for inertialess Newtonian liquid jets. *IMA J. Appl. Math.*, 70(3):353–358, 2005. ISSN 0272-4960.

[24] Martine Prévost and Dominique Gallez. Nonlinear rupture of thin free liquid films. *The Journal of Chemical Physics*, 84(7):4043–4048, 1986. doi: 10.1063/1.450065.

[25] Thomas Erneux and Stephen H. Davis. Nonlinear rupture of free films. *Physics of Fluids A: Fluid Dynamics*, 5(5):1117–1122, 1993. doi: 10.1063/1.858597.

[26] Michael P. Ida and Michael J. Miksis. Thin film rupture. *Appl. Math. Lett.*, 9(3):35–40, 1996. ISSN 0893-9659.

[27] Dimitri Vaynblat, John R. Lister, and Thomas P. Witelski. Symmetry and self-similarity in rupture and pinchoff: a geometric bifurcation. *European J. Appl. Math.*, 12(3):209–232, 2001. ISSN 0956-7925. The dynamics of thin fluid films.

[28] A. L. Bertozzi and M. Pugh. The lubrication approximation for thin viscous films: regularity and long-time behavior of weak solutions. *Comm. Pure Appl. Math.*, 49(2):85–123, 1996. ISSN 0010-3640.

[29] Raymond E. Goldstein, Adriana I. Pesci, and Michael J. Shelley. Instabilities and singularities in Hele-Shaw flow. *Phys. Fluids*, 10(11): 2701–2723, 1998. ISSN 1070-6631.

[30] Kai-Seng Chou and Ying-Chuen Kwong. Finite time rupture for thin films under van der Waals forces. *Nonlinearity*, 20(2):299–317, 2007. ISSN 0951-7715.

[31] Josephus Hulshof and Andrey E. Shishkov. The thin film equation with $2 \leq n < 3$: finite speed of propagation in terms of the L^1-norm. *Adv. Differential Equations*, 3(5):625–642, 1998. ISSN 1079-9389.

[32] D. Slepčev and M. C. Pugh. Selfsimilar blowup of unstable thin-film equations. *Indiana Univ. Math. J.*, 54(6):1697–1738, 2005. ISSN 0022-2518.

[33] Barbara Niethammer and Robert L. Pego. Non-self-similar behavior in the LSW theory of Ostwald ripening. *J. Statist. Phys.*, 95(5-6):867–902, 1999. ISSN 0022-4715.

[34] I. M. Lifshitz and V. V. Slyozov. The kinetics of precipitation from supersaturated solid solutions. *J. Phys. Chem. Solids*, 19(1-2):35–50, 1961.

[35] C. Wagner. Theorie der Alterung von Niederschlägen durch Umlösen. *Z. Electrochem.*, 65:581–591, 1961.

[36] For information about DFG Priority Program SPP 1164 Nano- and Microfluidics check out the website `http://www.softmatter.de`.

[37] J Marsden and Hughes T.J.R. *Mathematical Foundations of Elasticity.* Prentice-Hall, 1983.

[38] Konstantin Afanasiev, Andreas Münch, and Barbara Wagner. Landau-Levich problem for non-Newtonian liquids. *Physical Review E (Statistical, Nonlinear, and Soft Matter Physics)*, 76(3):036307, 2007. doi: 10.1103/PhysRevE.76.036307.

[39] Claude Louis Marie Henri Navier. Mémoire sur les lois du mouvement des fluides. *Memoires de l'Académie Royale des Sciences de l'Institut de France*, 6:389–440, 1823.

[40] George Gabriel Stokes. *Mathematical and Physical Papers*, chapter Report on Recent Researches in Hydrodynamics, pages 185–187. Cambridge University Press, 1880. freely available under `http://www.archive.org`.

[41] J.-T. Cheng and N. Giordano. Fluid flow through nanometer-scale channels. *Phys. Rev. E*, 65(3):031206, Mar 2002. doi: 10.1103/PhysRevE.65.031206.

[42] Willem Hendrik Keesom. *Leiden Comm. Suppl.*, 1912.

[43] Peter Joseph William Debye. Die van der Waalsschen Kohäsionskräfte. *Physikalische Zeitschrift*, 1920.

[44] S. C. Wang. *Physik Z.*, 1927.

[45] Fritz London. The general theory of molecular forces. *Transactions of the Faraday Society*, 33:8–26, 1937.

[46] I.E. Dzyaloshinskii, E.M. Lifshitz, and L.P. Pitaevskii. General theory of van der Waals' forces. *Soviet Physics Uspekhi*, 4(2):153–176, 1961.

[47] J. Thomas Beale. The initial value problem for the Navier-Stokes equations with a free surface. *Comm. Pure Appl. Math.*, 34(3):359–392, 1981. ISSN 0010-3640.

[48] J. T. Beale. Large-time regularity of viscous surface waves. *Arch. Rational Mech. Anal.*, 84(4):307–352, 1983/84. ISSN 0003-9527.

[49] Dimitri Vaynblat, John R. Lister, and Thomas P. Witelski. Rupture of thin viscous films by van der Waals forces: Evolution and self-similarity. *Physics of Fluids*, 13(5):1130–1140, 2001.

[50] Thomas P. Witelski and Andrew J. Bernoff. Stability of self-similar solutions for van der Waals driven thin film rupture. *Physics of Fluids*, 11(9):2443–2445, 1999.

[51] Wendy W. Zhang and John R. Lister. Similarity solutions for van der Waals rupture of a thin film on a solid substrate. *Phys. Fluids*, 11(9): 2454–2462, 1999. ISSN 1070-6631.

[52] Thomas P. Witelski and Andrew J. Bernoff. Dynamics of three-dimensional thin film rupture. *Phys. D*, 147(1-2):155–176, 2000. ISSN 0167-2789.

[53] Günther Grün and Martin Rumpf. Nonnegativity preserving convergent schemes for the thin film equation. *Numer. Math.*, 87(1):113–152, 2000. ISSN 0029-599X.

[54] Boaz Giron, Baruch Meerson, and Pavel V. Sasorov. Weak selection and stability of localized distributions in ostwald ripening. *Phys. Rev. E*, 58(4):4213–4216, Oct 1998. doi: 10.1103/PhysRevE.58.4213.

[55] J. Galambos and E. Seneta. Regularly varying sequences. *Proc. Amer. Math. Soc.*, 41:110–116, 1973. ISSN 0002-9939.

[56] N.H. Bingham, C.M. Goldie, and J.L. Teugels. *Regular Variation*, volume 27. Encyclopedia of Mathematics and its Applications, 1989.

[57] J. Carr and O. Penrose. Asymptotic behaviour of solutions to a simplified Lifshitz-Slyozov equation. *Phys. D*, 124(1-3):166–176, 1998. ISSN 0167-2789.

[58] Omar K. Matar and Satish Kumar. Dewetting of thin liquid films near soft elastomeric layers. *Journal of Colloid and Interface Science*, 273: 581–588, 2004.

[59] Omar K. Matar, Vasileios Gkanis, and Satish Kumar. Nonlinear evolution of thin liquid films dewetting near soft elastomeric layers. *Journal of Colloid and Interface Science*, 286:319–332, 2005.

[60] Andreas Münch, Dirk Peschka, and Barbara Wagner. Dewetting of a liquid film from an elastomer. *to appear*, 2008.

[61] Georgy Kitavtsev, Barbara Wagner, and Lutz Recke. Coarsening dynamics of slipping droplets. *In Preparation*, 2008.

[62] O.M. Todes and V.V. Khrushchev. Theory of coagulation and particle growth in sols. *Zhur. Fiz. Khim*, 21:301–312, 1947.

[63] B. Niethammer and J. J. L. Velázquez. On screening induced fluctuations in Ostwald ripening. *J. Stat. Phys.*, 130(3):415–453, 2008. ISSN 0022-4715.

[64] Dirk Peschka, Barbara Niethammer, and Andreas Münch. Self-similar rupture. *to appear*, 2008.

Selbständigkeitserklärung

Hiermit versichere ich, meine Dissertation *Self-Similar Rupture of Thin Liquid Films with Slippage* selbständig und ohne unerlaubte Hilfsmittel erstellt zu haben.

Die verwendete Literatur und die Hilfsmittel sind in der Arbeit angegeben. Die Promotionsordnung der Mathematisch-Naturwissenschaftlichen Fakultät II ist mir bekannt. Ich habe mich nicht anderwärts um einen Doktorgrad beworben und ich besitze noch keinen Doktorgrad im Promotionsfach.

Berlin, den 16. Juli 2008